OPTICAL CHARACTERISATION OF HIGH PRESSURE DIESEL FUEL INJECTORS

DARLINGTON ONYEWUCHI NJERE

A thesis submitted in partial fulfilment of the requirements of the University of Brighton, in collaboration with Ricardo UK Ltd., for the degree of Master of Philosophy

April 2015

Abstract

The main combustion by-products of an automotive diesel engine are carbon-dioxide (CO_2), particulate matter (PM) and oxides of nitrogen (NO_x). Engine designers are challenged by the legal limits for PM and NO_x reductions, especially as options are limited. Exhaust after- treatment devices are being used as a means to meet emission legislations. Another option, optimising the combustion process itself, has potential for improved efficiency as well as reducing the regulated emission species. Studies have confirmed this, by demonstrating that the in-cylinder flow conditions, which are driven by fuel spray and piston bowl interaction, are critical for the combustion event. Achieving emission reductions without compromising engine efficiency requires improved understanding of fuel/gas mixing and pollutant formation mechanisms. This improved understanding of the combustion system can be obtained through mechanical, electrical/electronic and optical techniques. Optical techniques are often preferred due to their non-intrusive nature.

In the present work, direct imaging diagnostics were applied to an optical research engine (Proteus) to study fuel/ambient interactions, without impingement (spray/piston bowl interaction). The use of high speed image acquisition equipment with Mie scatter and shadowgraph techniques were developed and optimised around the Proteus, to visualise in- cylinder spray penetration through successive regimes of tests. These tests allowed for the determination of the influence that the injection parameters (injection pressure and nozzle geometry) and in-cylinder thermodynamics variable (pressure) had on the penetration of diesel spray, under evaporative (non-combusting) conditions. The conditions for the work are non-reactive.

The results suggest that increase in injection pressure induces increase in momentum which controls the transient injection stage of liquid spray penetration up to the liquid length.

During the steady state injection, which starts from the liquid length, the increase in injection pressure has no effect on liquid tip penetration. For liquid spray, the high energy provided by the increased injection pressure is compensated by an equivalent increase in air entrainment, and hence evaporation. An expected trend is also observed for vapour penetration, which increases with increase in injection pressure. The effect of nozzle geometry is based on the k- factor. The higher the k-factor: the greater the conicity, the lesser the cavitation and the longer the spray penetration.

These results are used to complement the spray data for the validation of spray models used in diesel engine combustion modelling for emission reduction. Another application of the results is in analysing in-cylinder spray penetration, which is very useful in determining the geometric design of high speed diesel engine combustion chambers with direct injection. For these systems, the understanding gained from this work provides clear indication on what parameters to vary in conducting impingement studies, and how. In addition, the generated spray data which quantifies in-cylinder spray behaviour can be transformed into usable statistics. Although the measurements were performed for high-speed diesel engine applications, the results may be transferable to other applications. It therefore follows that, the experimental methodology which effectively combined high-speed laser visualization and continuous recording can be employed to study the conditions of the in-cylinder spray for qualitative and/or quantitative data acquisition.

Contents

List of tables

List of figures

Acknowledgements

I would like to express my sincere gratitude to my supervisors: Dr. Cyril Crua, Dr. Rob Morgan and Dr. Guillaume de Sercey for their support and understanding. The assistance rendered by the technical staff of Sir Harry Ricardo Laboratories, at the University of Brighton, towards the research, is very well appreciated.

My special thanks to: my colleagues at the office for their guidance, and the visiting researchers and student interns that I worked with, for their support.

I am also indebted to all other persons, who contributed in one way or the other to the success of this work. My family members and friends are well acknowledged: especially, my Angel, for her love, sacrifices and belief in me. I am grateful to Rev. (Fr.) Anthony Ekendu Onyeocha for being a wonderful "Father" to me. I would be remiss if I do not acknowledge the financial and technical support provided by Ricardo UK Limited throughout the course of this study. More thanks are due to Mr. Roscoe Sellars and other members of the Team than can be expressed here.

Above all, I render my deepest gratitude, though unfortunately inadequate, to God Almighty. TO HIM IS ALL THE GLORY!

Declaration

I hereby certify that this thesis is my own work except where otherwise indicated. All sections of the text and results which have been obtained from other workers/sources are fully referenced. The thesis has not been previously submitted to this or any other university for a degree, and does not incorporate any material already submitted for a degree.

Signed: Date:

NOMENCLATURE

Symbols

A.....Numerical constant for nozzle geometry, $A = 3 + 0.28\ (\frac{l_n}{d_n})$

d_n……...Nozzle diameter [m],
Number of droplets
D_d……...……Droplet diameter [m]
l_n……..……Nozzle length [m]
Oh..... Ohnesorge number, ratio between viscous drag and surface tension
θ.....Spray angle, $\text{Tan}\frac{\theta}{2} = \frac{1}{A}4\pi\sqrt{\rho^*}\frac{\sqrt{3}}{6}$ [°]

σ.....Surface tension [N/m]
ρ…….....Density [kg m^{-3}]

ρ*.....Density ratio, $\rho^* = \frac{\rho_a}{\rho_l}$

Re.....Reynolds number, Re = $\frac{\rho_a V_{inj} d}{\mu}$

S.....Spray penetration length, $S = 3.07 \cdot (\frac{294}{T_g})^{0.25} \cdot \sqrt{\sqrt{\frac{\Delta P}{\rho_g}} \cdot d_n \cdot t}$ [m]

SMD.....Sauter mean diameter, $SMD = \left(\int D_d^3 d_n\right) \Big/ \left(\int D_d^2 d_n\right)$ [m]

t.....Time of start of injection [s]
T_L.....Leidenfrost temperature [^oC]
.....Nukiyama temperature [^oC]
T_W.....Wall temperature [^oC]

V_{inj}.....Injection velocity, $V_{inj} = C_d\sqrt{\frac{2(P_{inj}-P_{cyl})}{\rho_f}}$ [m/s]

We.....Weber number, We = $\frac{\rho_a V_{inj}^2 d}{\sigma}$

ΔP.....Difference between injection pressure and chamber pressure [bar]

Subscripts

a.....Air (or ambient)
cyl.....Chamber (or cylinder)
d.....Orifice coefficient (or diameter)
f.....Fuel
g.....Gas (or ambient air)
in.....Inlet orifice diameter
inj.....Injection
l.....liquid fuel
n.....Number of droplets (nozzle)
out.....Outlet orifice diameter

Acronyms

ASI.....After Start of Injection
CAE.....Centre for Automotive Engineering
CCD.....Charge-Coupled Device
CFD.....Computational Fluid Dynamics
CHG.....Greenhouse Gas
CMOS.....Complementary Metal-Oxide Semiconductor
CO.....Carbon monoxide
CO_2.....Carbon dioxide
CPF.....Constant-Pressure Flow
CR.....Compression Ratio
CRS.....Common-Rail System
CVL.....Copper-Vapour Laser
CVP.....Constant-Volume Pre-burn
DC.....Direct Current
DI.....Direct Injection
DOC..... Diesel Oxidation Catalyst
DPF.....Diesel Particulate Filters
ECN.....Engine Combustion Network
ECU.....Electronic Control Unit
EGR.....Exhaust Gas Re-circulation
fps……frames per second
HC.....Hydro-carbon
HCCI.....Homogeneous Charge Compression Ignition
HeNe.....Helium Neon
HP.....High Pressure
HSDI.....High Speed Direct Injection
HSV.....High Speed Visualisation
ICE.....Internal Combustion Engine
ICP.....In-Cylinder Pressure
IR.....Infra-Red
ISFC……..……..Indicated specific fuel consumption
K-fact.....Nozzle conicity
LP.....Low-Pressure
LTC.....Low Temperature Diesel Combustion
MK.....Modulated Kinetics
NO_x.....Oxides of Nitrogen
PCCI.....Premixed Charge Compression Ignition
PIV.....Particle Imaging Velocimetry
PM.....Particulate Matter
RCCI.....Reactivity Controlled Compression Ignition
RCM.....Rapid Compression Machine
SCR.....Selective Catalytic Reduction
T.....Temperature
TDC.....Top Dead Centre
TKE.....Turbulence Kinetic Energy
TMAN.....Intake Manifold Temperature
TP.....Test Point
uH.....unburned Hydro-Carbon
U.....Ultra Violet

1 INTRODUCTION

1.1 Background

Amongst all the prime movers in today`s global transportation infrastructure, the diesel engine stands out as the most reliable. It is set to maintain this position even in the foreseeable future. For example, diesel engine has advantages over the petrol engine that include: higher efficiency due to higher compression ratio and reduced negative work, higher torque capacity and durability (Takeda et al., 1994; Pierpont et al., 1995; Bergstrand et al., 2002; Fang et al., 2005). Nevertheless, diesel engine continues to undergo constant improvement, which was initially driven by reliability and performance until later, when exhaust gas emissions and fuel consumption started commanding the attention. The by- products of automotive diesel, which include: carbon dioxide (CO_2), particulate matter (PM) and oxides of nitrogen (NO_x), are known to have adverse effects on the environment and health. Even though CO_2 is non-toxic, its effect as a greenhouse gas (CHG) on climate change is a significant concern. A cap on its emission is imminent. On the other hand, PM is a probable carcinogen and harmful to human health (Kennedy, 1997), while NO_x contributes to acid rain formation (Pidwirny, 2006).

The concern generated by these pollutants is an on-going challenge for different environmental protection groups. On its part, the European Union (EU) has, amongst other things, particularly regulated automotive NO_x and PM emissions. Since 1992, the EU has been rolling-out these regulations designed to become more stringent every year for different classes of vehicles. Figure 1-1 shows EU regulations for category M_1 cars (with maximum mass of not more than 3.5 tons). Current limits for this class of vehicle must conform to Euro 5, whilst preparing for Euro 6 that will take effect from 2014.

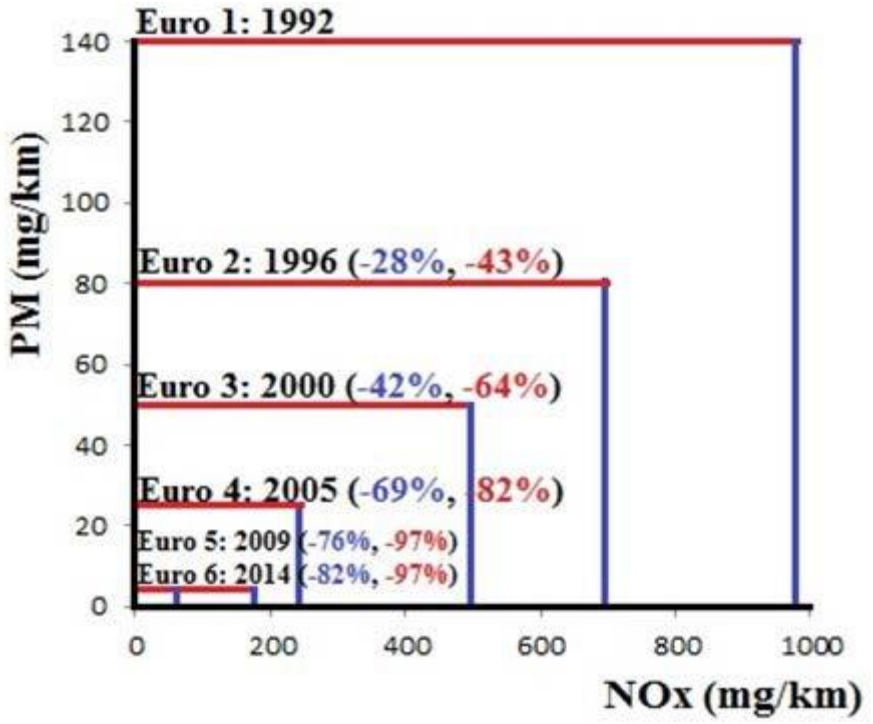

Figure 1-1: EU emission standards for category M_1 diesel passenger cars (adapted from DieselNet)

In order to comply with these regulations, and remain competitive, automotive manufacturers use emission reduction schemes. These schemes are broadly classified as either combustion control or exhaust cleaning. Combustion control includes the use of direct and high pressure injection, the application of exhaust gas re-circulation (EGR), and even the development of advanced combustion modes. While exhaust cleaning schemes, which are commonly referred to as after-treatment devices, include: diesel particulate filters (DPF), diesel oxidation catalyst (DOC), selective catalytic reduction (SCR) and NO_x traps. After-treatment devices are mainly associated with high cost of parts and maintenance, even though they are effective in reducing tailpipe emission (Tao et al., 2008). Whereas the combustion control schemes, which are not only cheaper, can improve engine performance as well.

Combustion control for diesel engine drives many research investigations because the combustion process, which is strongly affected by in-cylinder spray behaviour,

offers significant potentials for optimisation. Diesel combustion process occurs in four phases (Khair, 2010), which are: ignition delay, premixed combustion, mixing-controlled combustion (or quasi-steady diffusion) and the late combustion (Figure 1-2). Most of the heat-release happens during the quasi-steady diffusion combustion stage. This is therefore an important phase for conventional diesel combustion with respect to pollutant formation.

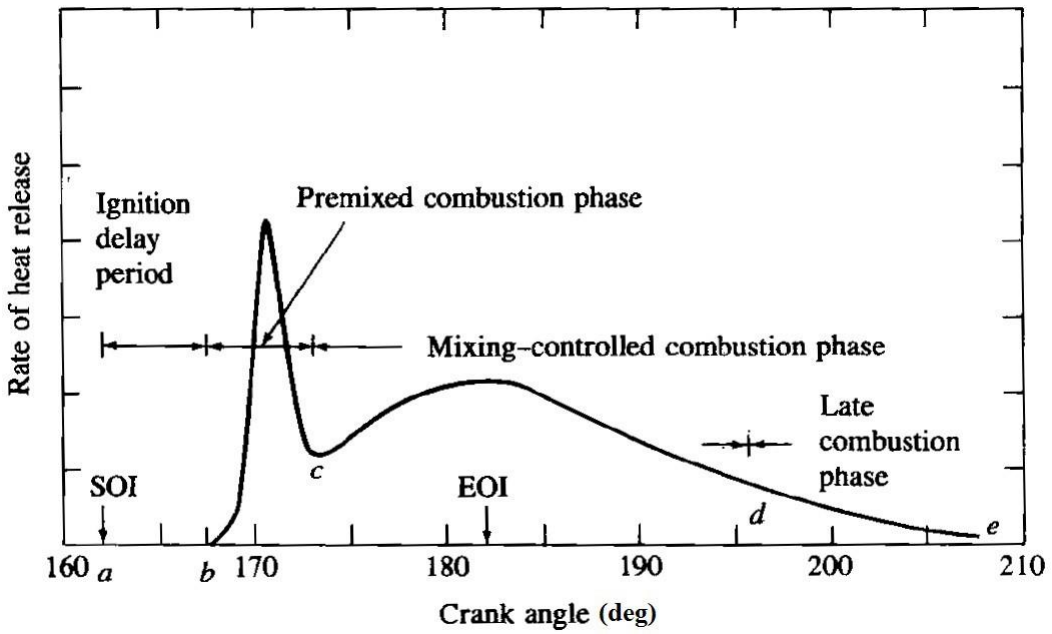

Figure 1-2: Phases of diesel combustion (Block, 2007)

Investigations, such as conceptual model (Dec, 1997) and extended mechanism (Heywood, 1988), have improved the understanding of combustion. These studies have shown that diesel combustion is heterogeneous due to non-uniform fuel distribution and the consequent non- stoichiometric combustion mixture. As a result, NO_x is formed at the high temperature region, while PM is emitted at the rich region (Khalid' A. et al., 2009). The reverse relationship between the two pollutants has made it difficult to simultaneously effect their reductions. Since common strategies used to reduce PM tend to increase NO_x, and vice versa (Wickman DD et al., 2001; Genzale et al., 2006). However, diesel combustion investigations have led to the development of

high speed direct injection (HSDI) diesel engine. In HSDI, combustion is controlled with improved combustion chamber design, the use of adequate high pressure injection system and EGR. This allows the efficient reduction of engine-out emissions. As consumer expectations (on fuel economy and performance) rise, in spite of the challenging emission laws, meeting these demands is a continuous target for the auto- industry. Further attempts to improve HSDI combustion led to the development of advanced combustion strategies.

Low temperature diesel combustion (LTC) is one of the strategies, and it achieves simultaneous reduction of NO_x and PM emissions by using high EGR rate to suppress combustion temperature, and premixing fuel with the in-cylinder charge before ignition. The reduced oxygen content of the charge produces longer ignition delays; this gives more mixing time and leads to lower equivalence ratios in the jet section. Wall wetting and operating range are some of the key challenges. Combustion systems that operate on LTC include; premixed charge compression ignition (PCCI), modulated kinetics (MK), homogeneous charge compression ignition (HCCI) and reactivity controlled compression ignition (RCCI) (Tree et al., 2007; Dec, 2009).

Here in University of Brighton, the Centre for Automotive Engineering (CAE) is dedicated to optimising control of in-cylinder diesel combustion. To sustain this position, the available facility includes an optical research engine (Ricardo Proteus). With this engine, it is possible to visualise in-cylinder events, such as spray development and interaction, and combustion, with little or no interference. It is essentially a single cylinder reciprocating, rapid compression machine (RCM). The optical access to the combustion chamber is provided by three removable glass windows. Visualisation (or optical) techniques on the optical engine are carried out with a light source (e.g. high speed laser) and a high speed camera. The number of these components may differ between techniques. However, optical techniques have

been very invaluable in providing useful information on the critical parameters of the in-cylinder event(s) under study, and their influences on the performance and quality of real engine combustion.

In one of the studies by CAE diesel group, conducted on a conventional light duty diesel fired research engine (Ricardo Hydra), it was established that a slight change in piston bowl geometry resulted to a significant emission reduction. This observation highlighted the inadequate understanding of the interaction between diesel fuel spray and surfaces. From the observation, it can be suggested that rather than discard a piston bowl for non-performance, which is usually the practice, its performance can be improved by altering the geometry. The present research is thus motivated; as part of a wider research aim of providing further understanding by visualising the interaction using optical techniques and analysing the emission profile with respect to change in bowl geometry. Other combustion control investigations (Timoney. D.J., 1985; Arcoumanis et al., 1991; Shundoh et al., 1991; Espey et al., 1995; Bruneaux, 2005; Tao et al., 2008; Bruneaux et al., 2011) have also inspired this work, by identifying the need for more insight into the mechanisms that drive in-cylinder spray behaviour. The compact nature of the modern HSDI for passenger vehicles, which introduces extensive impingement of the fuel sprays on to the piston bowl walls, has also stimulated this research.

In this report, the understanding of in-cylinder diesel fuel spray behaviour under different conditions was developed, using visualisation techniques on the optical engine. The first step involved the characterisation of free spray using high speed imaging technique to study liquid length penetration. Secondly, free spray was characterised by using high-speed laser shadowgraph technique to study vapour penetration. The results of these experiments showed the effects of some critical parameters, such as: high

injection pressure, in-cylinder pressure and nozzle geometry on spray penetration. Essentially, the results conformed to the current understanding in the research area, and hence confirm the reliability of the experimental methodology employed for this work. In addition, the insight on the effects of the identified critical parameters will provide the necessary guidance for further investigations on impingement.

1.2 Objectives

The objective of this research is to provide an insight into in-cylinder free spray behaviour, as part of a broader research aim of understanding the interaction between high pressure diesel fuel spray and piston bowl geometry, in order to improve the control of pollutant emissions. Experiments were performed on the Proteus, using optical techniques and under conditions that represent real engine operation. These conditions reflect the changes in key parameters such as temperature and pressure.

The methodology for this research is the use of optical technique to visualize in-cylinder spray penetration in the absence of a piston bowl, according to the following main steps:

- High speed liquid spray visualization (Mie scattering technique)
- Vapour spray visualization using high-speed laser shadowgraph

In order to achieve the objective, these steps would provide the answers to the following research questions:

- What is/are the key parameter(s) that drive(s) in-cylinder spray behaviour?
- What is/are the effect(s) of the parameter(s)?

1.3 Report structure

This report has three parts. In the first part, current understanding on spray and piston

bowl interaction was reviewed (Chapter 2). This review focused on spray development, bowl design, spray/bowl interaction and optical technique. In the second part (Chapters 3 and 4), the methodology was defined for spray characterisation and results. The last part (Chapter 5) concludes with recommendation for future works. Additional information about chapters 3 and 4, were attached as appendices at the end of this report.

2 LITERATURE REVIEW

2.1 Introduction

As stringent emission laws continue to challenge the design of present and future diesel engines, research investigations seeking means of controlling the combustion process are rapidly proceeding on all fronts. It has therefore become possible for knowledge in this area to advance by building on previous results in creating models/scope for optimisation. Yet, reduction of the soot emissions from in-cylinder combustion to effectively balance with the reduction of overall emission, without compromising efficiency, remains a major concern. The present trend of applying high injection pressure in excess of 2000 bar, to improve air/fuel mixing in order to optimise in-cylinder combustion, significantly encouraged investigations into spray/bowl interaction. It is an indication that for combustion in diesel, the process of emission formation relies heavily on fuel distribution and the change of this distribution with time.

Insights gained from spray behaviour have provided very fascinating and dynamic information on the entire combustion process. This has been possible through numerical, theoretical and experimental studies. Numerical studies have made more progress mainly through: the successful establishment of Computational Fluid Dynamics (CFD) for Internal Combustion Engine (ICE) simulations; and, hence, the use of mathematical models, as well as development of codes to incorporate vital parameters. Theoretical studies assume ideal situations in defining combustion to be complete. Even though this is often far from typical scenarios, it does help in framing perspectives for benchmarking. Experimental studies can be in forms of local, global or visualisation. Local studies use methods to identify and focus on a

particular interest for a detailed outcome. Global studies present overall information. On the other hand, visualisation, which will be used in this work, involves optical techniques.

Challenges for these types of study are varied. The main challenges for numerical studies are extensive computations and time consumption. Over simplification to arrive at results that did not draw from typical situations is the problem with theoretical studies. Experimental studies are characterised by huge outlay in terms of equipment modification, process re-definition and physical damages. Nevertheless, they are often reliable, especially for the purposes of validating concepts and results generated from all other types of studies. Research investigations are always stymied when experimental validations are not available in a particular study area. However, optimisation by numerical technique has brought a measure of compensation. The particular advances with CFD codes and the use of high performance computers have tremendously overcome the limitations of experimental studies. Contemporary analyses and wide parametric studies can now be embarked upon with relative ease. These advances have made theoretical, numerical and experimental studies to be complementary in providing useful guidance for present and future engine designers. In the next sections, literatures that applied these forms of studies will be reviewed.

The aim of this review is to understand the critical parameters that affect spray penetration and interaction, and the application of appropriate optical techniques to spray studies. For this purpose, the next sections will cover works on: spray characteristics, piston bowl design, spray/bowl interaction and optical techniques. At the end of the chapter, the review will be concluded to underscore relevance to present study.

2.2 Diesel spray characteristics

The development of in-cylinder diesel spray starts as soon as the liquid fuel is injected in an ambient with a certain pressure and temperature. The fuel mixes with the ambient gases and momentum is transferred to the ambient in the combustion chamber (Lefebvre, 1989). Spray interaction with the ambient (heating, evaporation and impingement) leads to fuel vaporisation, and ultimately combustion. As shown in Figure 2-1, the key parameters of spray are: spray-tip penetration, break-up length, spray angle and droplet size distribution. The first three can be analysed from the macroscopic (geometric) view point; to generally emphasise diesel spray and combustion chamber interaction. Droplet distribution defines the microscopic behaviour of spray.

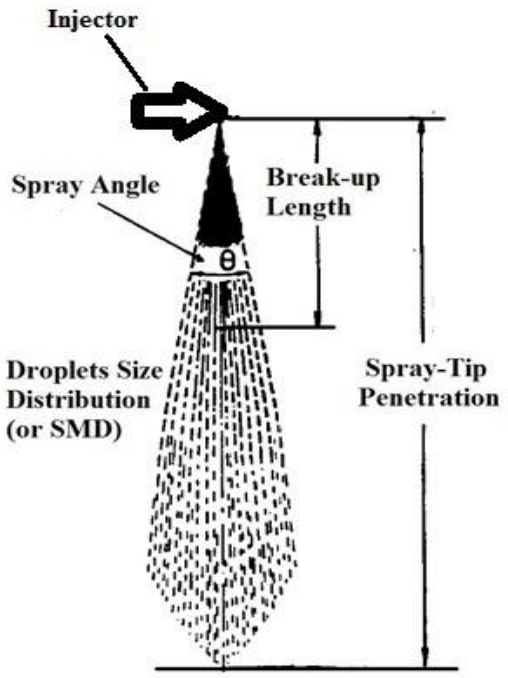

Figure 2-1: Diesel spray parameters (adapted from Hiroyasu et al., (1990))

2.2.1 Microscopic characterisation

The microscopic behaviour of spray depends to a large extent on the atomisation process, which is determined by the injection conditions. Atomisation is the process of converting bulk liquid to droplets. This process is very different at atmospheric

density and at high density (Reitz et al., 1982; Hiroyasu et al., 1989). It is required to achieve atomisation of the liquid fuel into large number of small droplets to create a large surface area for the evaporation of the fuel under operating conditions. However, during injection, the droplet size distribution at any point may not only change with time, but also with injection conditions. The changes may be in terms of the difference in droplet size at the spray core and spray edge, trajectories (scalar field) of individual droplets and the initial velocity due to the atomisation process. For this purpose, the droplets size distribution is often defined by its Sauter mean diameter (SMD), which is very useful in simplifying droplet populations existing in an atomizing process. SMD represents the diameter of droplets which has the same volume/surface relation in the totality of the spray. It is influenced by: the properties of the atomised and atomising fluids, as well as the nozzle design and operating conditions (Chigier, 1976; Lefebvre, 1980). Hiroyasu et al., (1990) reported that SMD decreased with an increase in ambient pressure (or density).

Researchers (Hiroyasu et al., 1989; Hiroyasu et al., 1990) have defined different correlations for calculating SMD. Equation (2-1) shows a general form reported by Heywood, (1988).

$$\text{SMD} = \left(\int D_d^3 d_n\right) \Big/ \left(\int D_d^2 d_n\right) \qquad (2\text{-}1)$$

Where d_n is the number of droplets with (droplet) diameter D_d.

2.2.2 Macroscopic characterisation

The macroscopic properties of diesel spray are characterised by the break-up length, penetration and cone angle. After the liquid spray atomises outside of the nozzle, it breaks up to mix with the ambient gas, while the vapour spray continues downstream,

and evaporates. This situation is caused by the turbulence created by the liquid jet exiting the nozzle. It is the turbulent mixing/transport of the jet that determines the distribution of the jet fluid concentration and its vortex motion (Kawanabe et al., 2008). Moving away from the nozzle, the spray expands further as air-entrainment increases, the spray diverges, its breadth increases and the velocity decreases. The fuel droplets evaporate as expansion continues, while spray tip penetrates further with decreasing injection rate. Spray tip penetration region becomes longer and wider as the ambient air temperature increases, which is due to the lower in-cylinder gas density at higher temperatures (Suh et al., 2008). Longer tip penetration and larger cone angle are desirable for maximum air utilization and better combustion as they increase spray area. In multi-spray DI diesel combustion systems, with little or no air swirling, over-penetration causes impingement of liquid fuel on cool surfaces. This lowers the mixing rates and increases the emissions of the unburned and partially burned species. While in some engine designs where the walls are hot and high air swirling is present, fuel impingement on the walls is beneficial.

In the past, diesel spray atomisation was viewed to be continuous with primary break-up forming droplets by peeling from boundary layers of an intact liquid core which continued far downstream of the nozzle, followed by a secondary break-up of ligaments and large drops (Smallwood et al., 2000). The liquid core was believed to continue downstream, beyond more than 100 nozzle diameters, as shown in Figure 2-2(a). Spray tip penetration measurement shows an initially linear development with time and a sharp transition to square root of time. Hiroyasu et al., (1990) reported this as a transition from an intact liquid core to an atomised spray. A more recent study by Naber et al., (1996) showed that the transition was smooth and that the spray developed from fundamentally liquid to fundamentally gas. The current understanding, shown in Figure 2-2(b), is that the diesel spray structure under normal operating conditions is

completely atomised at or near the orifice exit, without any extended liquid core.

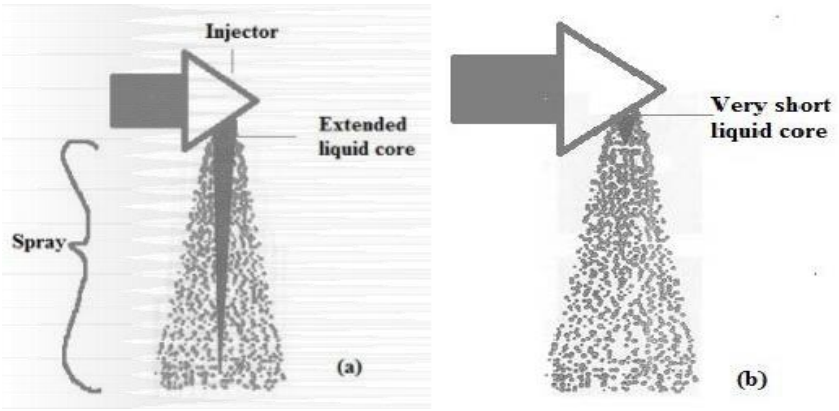

Figure 2-2: Spray with long core (a) and short core (b) (adapted from Smallwood et al., (2000))

After the atomisation and break-up processes, spray evaporation of the jet fuel is crucial before mixing with air. Droplet evaporation is affected by deceleration of the droplet due to aerodynamic drag, heat transfer to the droplet from the air and mass transfer away from the droplet by evaporation. On the other hand, the break-up process depends on the conditions and characteristics of the liquid and the ambient gas. The process is actually divided into two: primary and secondary break-up. During the primary break-up, the remaining intact liquid core (from the fuel jet and sheet) disintegrates into ligaments, large and small drops. These drops are broken down further into droplets during the secondary break-up. Primary break-up mechanisms identified in Stiesch, (2003) were: imploding cavitation bubbles (nozzle-flow phenomenon) since the in-cylinder pressure is naturally higher than the saturated vapour pressure, turbulence-driven instability and aerodynamic forces acting on the liquid surface (Smallwood et al., 2000; Baumgarten., 2006). On the other hand, aerodynamic shear was linked with secondary break-up. Hiroyasu et al., (1990) identified zones of complete and incomplete spray according to the position of spray surface disintegration relative to the injector nozzles (break-up length), and showed that cavitation greatly favoured the atomization process in the complete

spray regime. Complete spray regime occurs when injection velocities are greater than 100 m/s (i.e., an injection pressure difference of more than 8 M Pa). Hiroyasu, (2000) also agrees that cavitation influences break-up: by collapsing and bursting of vapour bubbles, which enhances turbulence and jet instability, and hence jet disintegration. Essentially, the relative contribution of each of the mechanisms on spray break-up varies, depending on the injection parameters such as: the relative velocity between liquid and gas, the liquid and gas densities, the liquid viscosity and surface tension. Hence, several break-up modes can be identified, and characterised by different break-up length and by sizes of the resulting droplets.

The break-up process is also characterised by dimensionless quantities: Reynolds and Weber numbers (Lefebvre, 1989). Weber number (We, ratio of inertial to surface forces) is one of the external flow parameters that control the liquid spray and ambient interaction, while Reynolds number (Re, ratio of inertia to viscous drag) is one of the internal flow parameters that control the liquid and nozzle interaction. Hence, these quantities actually balance the break-up mechanisms. The lower regime of Weber and Reynolds numbers do not apply to diesel injection process, which operates in the atomisation regime of higher Weber and Reynolds numbers. In developing a wide classification of break-up regimes for general applicability, Reitz et al., (1986) considered the injection parameters while defining the dimensionless quantities, as shown below:

$$\mathrm{Re} = \frac{\rho_a V_{inj} d}{\mu} \qquad (2\text{-}2)$$

$$\mathrm{We} = \frac{\rho_a V_{inj}^2 d}{\sigma} \qquad (2\text{-}3)$$

A more convenient classification by Ohnesorge, (1931) was defined as Ohnesorge number (Oh, ratio between viscous drag and surface tension). Since both Re and Oh are formulated in terms of liquid properties only (whereas the density of the ambient gas definitely affects break-up), Reitz and Bracco latter added the density ratio and the following parameters.

$$V_{inj} = C_d \sqrt{\frac{2(P_{inj} - P_{cyl})}{\rho_f}} \qquad (2\text{-}4)$$

$$\rho^* = \frac{\rho_a}{\rho_l} \qquad (2\text{-}5)$$

Where Re =Reynolds Number; We = Weber Number; V_{inj} = Injection velocity, m/s; ρ_a = density of air (or ambient), kg/m^3; $\rho_l = \rho_f$ =density of fuel, kg/m^3 ;σ = surface tension, N/m; d = Nozzle diameter, m; C_d =coefficient of orifice; p_{inj} = injection pressure, bar; p_{cyl} = chamber pressure, bar.

During secondary breakup, fuel droplets further disintegrate. This process is primarily governed by the Weber number, since it results from the trade-off between inertial forces (trying to tear the droplet apart) and surface tension (keeping it together).

Investigations (Hiroyasu et al., 1990; Naber et al., 1996) into diesel spray penetration have been conducted under different conditions: evaporating (produced under hot bomb condition), non-evaporating (produced under cold bomb conditions), vaporising (high-temperature condition: 600K-1400K) and non-vaporising (ambient temperature condition). The spray behaviour under these conditions are different in terms of penetration and dispersion (Wang et al., 1999): even though spray, in general,

penetrates in the liquid phase up to a maximum distance (liquid length) soon after start of injection (SOI), and continue as vapour downstream. Takahashi et al., (1991) reported that penetrations under higher and low injection pressures were almost similar, with respect to insensitivity to the injection pressure, for non-evaporative condition but quite different for evaporative conditions. Under evaporative condition, the spray penetration was sensitive to changes in injection pressure. At low injection pressure, the spray penetration was significantly affected by ambient temperature and evaporation, while spray penetration at higher injection pressure was neither affected by the temperature nor evaporation. The reason for this phenomenon was attributed to the fact that the spray plume was richer for the higher injection pressure spray than that for the lower injection pressure, hence scarcely affected by ambient temperature. Similar trend of environmental effects were observed for the spray angle. Later investigations by Wang et al., (1999) and Alfuso et al., (2005) have also confirmed behavioural differences between diesel sprays under evaporative and non-evaporative conditions. The study by Siebers, (1998) considered the effects of several factors on spray penetration, which included: injection pressure, orifice diameter and aspect ratio, ambient gas density and temperature as well as fuel volatility and temperature. The results, which agreed with some other investigations, showed that: the liquid length decreased with decreased orifice diameter, increased fuel volatility (or fuel temperature) increased ambient density and decreased ambient temperature. Injection pressure had no direct impact on liquid length, whilst the sensitivity to the effects of ambient gas density and temperature declined with increase in injection pressure. The orifice aspect ratio ($hole\ length/hole\ diameter$) had a small and inconsistent effect on liquid length. It was also reported that the liquid length of a multi-component fuel was controlled by the fraction with lower volatility (Myong et al., 2004).

A more current research by Johnson et al., (2012) characterised 3000 bar diesel spray injection under vaporising and non-vaporising conditions. Non-vaporising (inert) condition was achieved by electrically heating the combustion vessel, filled with nitrogen, to 373 K. While a zero per cent oxygen vaporizing environment was achieved through the use of pre- burn procedure, which included electrically heating the combustion vessel to 453 K. The results showed that; with increased injection pressure, the inert spray penetrated more that the vaporizing spray, particularly at high charge densities. There was actually no significant change in liquid length for the vaporizing spray with increased injection pressure. For both conditions, increased charge densities resulted in reduction in the liquid spray penetration. There was a tendency for a reduction in liquid length with increased charge temperature, for the vaporizing spray. Clearly, under the vaporising condition, the spray contracted as a result of cooling of hot entrained gases by droplet evaporation. The high ambient density thus created, inhibited any significant effect of the high injection pressure on the liquid length. Unlike in the non-vaporising condition, where there was dilution of the hot combustion products within the spray. This resulted in the low ambient density that enhanced spray penetration.

Equation (2-6) is a time limit relation proposed by Dent, (1971) for spray penetration under hot bomb conditions;

$$S = 3.07 \cdot \left(\frac{294}{T_g}\right)^{0.25} \cdot \sqrt{\sqrt{\frac{\Delta P}{\rho_g}} \cdot d_n \cdot t} \qquad (2\text{-}6)$$

Where S = penetration length, m; t = time of start of injection, second; d_n = diameter of nozzle, m; ΔP = difference between injection pressure and chamber pressure, bar; ρ_g = density of gas (or ambient air), kg/m^3. For a cold bomb, the expression $\left(\frac{294}{T_g}\right)^{0.25}$ is equal to 1. The expression is a correction factor that accounts for

the temperature of the in-cylinder gas at the nozzle exit.

Liquid length is an important characteristic that defines spray behaviour. It is desired to have optimum (short) liquid spray penetration and longer vapour penetration. Parameters that have the most significant effect on liquid length include: combination of high injection pressure and small hole diameter, and ambient gas density. The injection pressure/nozzle hole combination reduces liquid penetration and improves the mixing of vapour spray (Bruneaux et al., 1999). An increase in ambient density reduces liquid penetration since much of the spray energy is transferred to the ambient. Bruneaux et al., (1999) reported that increase in combustion chamber volume decreased ambient density and temperature, which increased liquid spray penetration. However, the scaling law by Siebers, (1999) derived for the maximum liquid penetration length of a vaporising spray showed no linear relationship between liquid penetration and injection pressure. Investigation by Ahmadi-Befrui et al., (1991) further confirmed this result using spray images acquired with Schlieren for injection pressures of 300 – 1100 bar. It could be observed that only the vapour penetration was significantly affected by the change in injection pressure, unlike the liquid penetration that remained constant regardless. Increase in vapour penetration improves mixing, results in greater premix burning and faster combustion, which can cause an increase in NO_x emission, but with less PM emissions.

Aside from droplet distribution, spray cone angle is another result of the break-up process. It is a common measure of spray dispersion, and shows the fuel macroscopic distribution in the combustion chamber. The cone angle is defined as the angle formed by two straight lines that start from the exit of the nozzle orifice and tangent to the spray outline to a distance of about 60 times the exit diameter of the nozzles. Such delineation is necessary since the cone angle is not constant, but changes with time during injection, mainly due to changes in the shape of spray (Klein-Douwel et al.,

2007). Usually, this angle is between 5 and 30 degrees. Many investigations (Arai et al., 1984; Hiroyasu et al., 1990; Naber et al., 1996) have been conducted to determine cone angle. These works show that the cone angle is mainly affected by the geometric characteristics of the nozzle, the density ratio (ρ*), and the Reynolds number of the liquid (Reitz et al., 1979; Reitz et al., 1982). High injection pressure tends to have wider spray dispersion than low injection pressure. Increasing the injection pressure increases the cone angle up to a maximum value before a gradual decrease. This is desirable because the higher injection pressure causes the spray to leave the nozzle with higher velocity, which increases the spray momentum as well. Such condition induces high level of dispersion, which enhances better atomisation and air/fuel mixing (Wang et al., 1999). Thus spray cone angle (or dispersion) is an indication of the atomization and air entrainment processes that occur downstream of the nozzle.

Several correlations are available for calculating cone angle. One of these correlations, proposed by Dent, (1971) which applies to atomisation regime (of complete sprays), is shown below.

$$\mathrm{Tan}\frac{\theta}{2} = \frac{1}{A}4\pi\sqrt{\rho^*}\frac{\sqrt{3}}{6} \qquad (2\text{-}7)$$

$$A = 3 + 0.28\left(\frac{l_n}{d_n}\right) \qquad (2\text{-}8)$$

Where θ = spray cone angle, (degree); ρ^*= density ratio (see Equation (*2-5*)); l_n and d_n are length and diameter of nozzle, (m); A is the constant for nozzle geometry.

Clearly, for a complete spray regime the dispersion depends mainly on the orifice configuration and density ratio. The reduction in spray penetration with increased

ambient density has been explained in terms of cone angle. Payri et al., (2013) reported that the increase in cone angle at higher ambient densities also increased the volume of hot gas entrained in the spray. The associated increase in kinetic energy, required by the higher density of the volume of gas entrained to complete the momentum transfer, caused the spray to penetrate slower.

Air entrainment (or spray expansion) studies are often conducted by investigating the flow field around a spray. This approach was employed by Sasaki et al., (1998) using a particle imaging velocimetry (PIV) system. Their results showed that a small amount of air was entrained near the nozzle tip, while more air entrainment occurred in the spray mid-section and tip. In addition, increasing the fuel velocity imposed an almost similar increase in the air velocity around the nozzle and less so further on. The study by Ishikawa et al., (1999) employed air density differential as a tracer of air in motion. No change in $\partial m_{air} / \partial m_{fuel}$ was observed, which agrees with Sasaki et al., (1998) and further confirms the jet theory equations of Siebers, (1999). The study by Rajalingam et al., (1999) showed slight difference in air entrainment with injection pressure on the first two-thirds of the spray plume, and a significant difference on the last third. A different study by Rhim et al., (2000) reported that a significant part of the overall gas entrained in a spray plume was entrained from the spray tip. This position is quite different from the widely held view that most of the gas is entrained through the lateral sides of the sprays, and that the gas near the spray tip is just pushed aside by the spray tip. However, the velocity plots agreed with the common view on the gas flow pattern and resulting gas entrainment along the sides of the spray plume.

Another important characteristic of spray is impingement. Impingement can either be spray- on-spray or spray-on-wall. Spray-on-spray impingement (impinging sprays)

investigations are often conducted with impinging nozzles (multi-orifice nozzles). The general characteristics of the impinging spray are a larger cone angle and a shorter penetration than the non-impinging (free) spray. On the other hand, spray-on-wall investigations are usually conducted with more conventional diesel nozzles. Such sprays are characterised by smaller cone angle and a high penetration rate. It is desirable for the injected fuel to be almost completely vaporised before the liquid hits the piston bowl or cylinder liner (Klein-Douwel et al., 2009). This is because of the perceived effects of over-penetration of liquid spray and the consequent wall-wetting, especially under low temperature (Stanton et al., 1998) or low density (Bozic et al., 2010; Genzale et al., 2010) condition. Some of these effects are: dilution of fuel into the cylinder wall oil film, which can increase piston-to-wall friction and component wear (Song et al., 2008); degradation of the quality of bulk engine oil (Morcos et al., 2009); higher emission of unburned hydrocarbons (UHC) and carbon monoxide (CO) and, hence, reduced combustion efficiency (Kashdan et al., 2007; Martin et al., 2008) .The main focus of the broader research of which the present work is a part of, is spray-on-wall interaction and its effect on in-cylinder air utilization.

2.2.3 Effects of injection parameters

The position of the injector, as the most critical component of modern diesel engines, has been highlighted. Its role is set to be more significant as the emission regulations tightens and demand for fuel economy increases. The injector flow dynamics ultimately determines diesel engine performance by influencing spray development (from atomisation to ignition). Interestingly, the flow inside the injector is controlled by dynamic factors (e.g., injection pressure and needle lift) and geometric factors (e.g., orifice conicity and hydro-grinding). The effects of these factors

on spray processes have been studied by researchers (Han et al., 2002; Mulemane et al., 2004; Payri et al., 2008; Payri et al., 2009), though injection pressure and nozzle geometry (orifice diameter and conicity) are commanding more interest. Much has been said about injection pressure earlier in this work, which is a clear pointer that injection pressure drives spray evolution, penetration and interactions. Reduced orifice diameter has also been identified with improved atomisation. Thus rate of penetration increases with injection pressure due to the interaction of increased injection speed and reduced average size of the drops, whilst the highest penetration is almost constant (Zhang et al., 1997).The geometric characteristics of the nozzle is often defined by the variation of its cross-sectional area along its length of its conicity as shown in equation (2-9).

$$K = \frac{(D_{in} - D_{out})}{10} \qquad (2\text{-}9)$$

Where K (K-factor) is the conicity; D_{in} and D_{out} are inlet and outlet orifice diameters in µm, respectively.

On the analysis of the influence of conical and cylindrical nozzle orifices on injection rate, Benajes et al., (2004) observed that conical orifice increased flow efficiency (i.e., discharge co-efficient) and exit velocity, despite the reduction of fuel injection rate due to the smaller exit area. A different comparison of the two nozzle types by Han et al., (2002) confirmed the significant influence of nozzle geometry on primary break-up.Payri et al., (2005) observed choking conditions with cylindrical nozzles, as well as an increase in injection velocity due to the presence of vapour at orifice exit. They also reported that for conical nozzles the mass flow rate was always proportional to the square root of pressure drop, which meant there was no cavitation at the nozzle exit. On spray penetration, researchers (Blessing et al., 2003; Payri et al., 2004) have reported increase in liquid spray penetration and smaller cone angle with increased

conicity for non-evaporative sprays. This was contradicted by Bae et al., (2002), who reported that spray tip penetration and cone angle decreased due to increase in conicity. However, the insight provided by Som et al., (2009) on the subject, showed that conicity suppressed cavitation and turbulence inside the nozzle. From earlier discussion in this work, these are mechanisms that enhance primary break-up. As a result, the break-up process with a conical, was slower, produced larger droplets and increased liquid penetration. Similar investigations have been conducted on spray penetration and liquid length under evaporating conditions for different nozzle geometries (Payri et al., 2008).

As the main driver of in-cylinder spray behaviour, the injection pressure also impacts on the combustion process. The main issue with high injection pressure is NO_x emission, which is as a result of the increased total heat release due to improved atomization and better mixing (Kook et al., 2004). It has been reported (Wade, 1980; Plee et al., 1981) that EGR specifically reduces NO_x by lowering the flame temperature, but at a cost of increased soot (PM) emissions owing to lack of oxidants. Insight provided by Shimazaki et al., (1996), has confirmed that the better mixing associated with high-injection pressure actually caused faster decrease of Oxygen (O_2) concentration, and a more active and earlier air dilution. Consequently, soot oxidation was quicker, which led to smoke emission reduction. It was also confirmed that with EGR, the combustion was poor due to inadequate oxygen concentration. The resulting inactivity of oxidation reaction led to the NO_x emission reduction. Other ways of significantly and simultaneously reducing NOx and PM emissions is by the use of cooled EGR with high injection pressure, or use of optimised injection system and strategy or development of pre-mixed combustion modes, such as the LTCs. Achieving the simultaneous NOx/PM emission with LTC strategy is an active research area. Though the strategy uses high injection pressure and EGR, Pickett et al., (2009)

reported wall wetting as the main LTC challenge. Other significant challenges identified by Lu et al., (2011) included: increased carbon-monoxide (CO) and hydro-carbon (HC) emissions; effect of mixture control at operational range; effective control of fuel properties, injection concepts, bowl geometry and EGR; the effect of EGR and fuel composition on ignition delay, pollutant formation and evolution at high EGR; and means of achieving maximum thermal efficiency.

2.2.4 Summary

Spray characterisation is crucial in order to gain greater understanding of spray behaviour in an engine`s combustion chamber. To reduce pollutant emissions and achieve a high engine performance, it is necessary to know which parameters influence spray development the most. In addition, spray formation and injection process are two important mechanisms of in- cylinder air/fuel mixing, which controls the combustion process and emissions. Thus, the parameters that affect spray characteristics are grouped under: injection system parameters (e.g., nozzle geometry and injection pressure) and combustion chamber parameters (e.g., density, pressure, temperature and turbulence intensity). Other parameters are grouped under fuel property (e.g., density, temperature and volatility) and, in some cases, engine operating conditions (e.g., engine speed and load conditions).

For DI diesel engines, spray atomisation is divided into primary and secondary break-up processes. Primary break-up occur in the region close to the injector nozzle, at high Weber numbers. It is mainly determined by internal nozzle phenomena (e.g., turbulence and cavitation) as well as the interaction between the liquid fuel and ambient gas. Secondary break-up take places further downstream in the spray mainly due to aerodynamic interaction between the spray and the ambient gas. It is largely independent of the nozzle phenomena. However, the atomised liquid spray evolves

into a vaporised fuel jet as it penetrates into the combustion chamber. Spray dispersion and droplet distribution are direct results of the breakdown process. Thus the mixture formation is mainly influenced by the spray expansion (air entrainment), which depends directly on the spray penetration (liquid and vapour) and dispersion (cone angle). Longer tip penetration and larger cone angle are desirable for maximum air utilization and better combustion due to the increased spray area. Spray penetration and cone angle are the most important spray characteristics, and are mainly affected by: orifice diameter, injection pressure, and ambient density and temperature. High injection pressure or low ambient density (i.e., high ambient temperature) permits the spray to penetrate faster than low injection pressure or higher ambient density (i.e., lower ambient temperature). In particular, low injection pressure causes the fuel particles diameter and, hence, the ignition delay (during combustion) to increase. The engine performance will be significantly affected by the poor mixing that will ensue. Spray must be well atomised, with reduced orifice diameter, to achieve proper mixing.

Nevertheless, with high injection pressure, the effects of all other parameters affecting spray development are limited. High injection pressure drives spray (liquid/vapour) penetration, and hence, interactions (spray on spray and spray on wall). It is the high momentum impacted on spray by high injection pressure that makes it travel longer in the combustion chamber. So that penetration is actually controlled by the rate of momentum transfer to the ambient gas, i.e., the growth of the boundary layer between the injected spray and the ambient. The main advantages of high injection pressure are:

- Increased power density of the engine.
- Better air utilization, and hence increase in combustion chamber pressure that will lead to improved combustion and higher efficiency.
- Reduced emissions due to the better air utilisation and improved combustion.

On the other hand, higher injection pressure shortens the ignition delay period and makes homogeneous mixing difficult. This reduces the combustion efficiency and affects engine performance.

2.3 Piston-bowl design

In general, the combustion chamber is made of the upper and lower halves. Upper half consists of the cylinder head and cylinder wall. While the piston head (crown) and piston rings make up the lower half. For the direct injection diesel system, the combustion chamber is basically the volume of space between the flat cylinder head and a cavity on the piston crown. As the entire volume of combustion chamber is located in the main cylinder, fuel is injected into this volume and this type is commonly referred to as open combustion chamber. The common shapes for the open chamber, shown in Figure 2-3, are; shallow depth, hemispherical, cylindrical and toroidal.

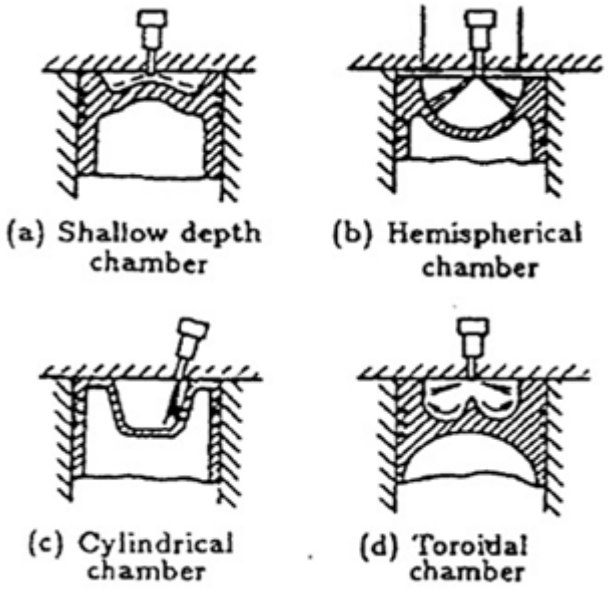

Figure 2-3: Open Combustion Chambers (Curt, 1995)

Shallow depth bowl has a small piston cavity, and normally used for very large engines operating at low speeds. Its low squish is well compensated for by its large

diameter, in terms of air utilization. Unlike the hemispherical and cylindrical chambers with low squish, that makes them very unpopular with modern engine designers due to poor air utilization. The toroidal chamber is designed to generate high squish for improved air utilization. It is well adapted in different configurations for use in modern engines. Generally, piston bowls with large squish area relative to the maximum bowl diameter (e.g. very re-entrant bowl design), are less sensitive to swirl levels than open bowls. This is due to the fact that the high squish velocities generated with such designs improve mixing (Saito et al., 1986).

In the present study, the focus is on the cavity in the piston crown commonly referred to as piston bowl or bowl-in-piston. Conventional designs for piston bowl are the shallow and deep bowl combustion chambers shown in Figure 2-4.

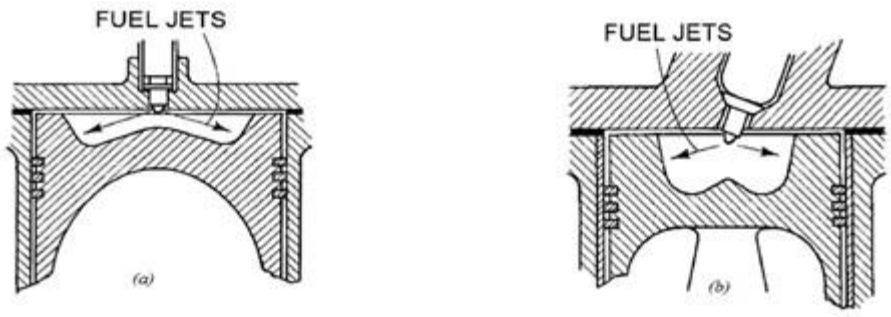

Figure 2-4: (a) Shallow Bowl and (b) Deep Bowl (Heywood, 1988)

Shallow bowls are commonly referred to as quiescent due to their characteristic low swirl, and are utilized in large-bore, heavy duty engine. Deep bowls are applied in medium duty engines, and are characterised by high swirl and squish.

Piston bowl designs are driven by two key facts; the necessary occurrence of the combustion process in the bowl, and the importance of maximizing the air utilization. Applying these concepts has made it possible to achieve different modifications of conventional and non- conventional bowls. The re-entrant bowl is

typical example that is widely used in modern high speed DI diesel engines. Its main geometrical features are shown in schematics (Figure 2-5).

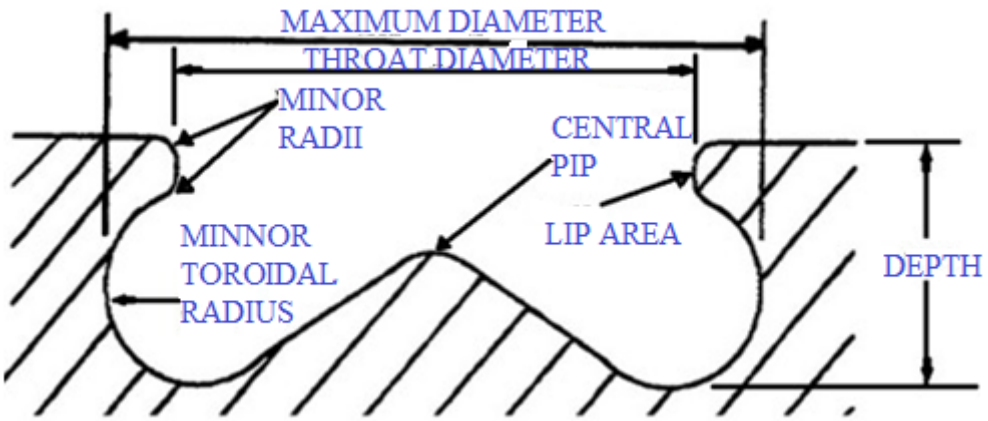

Figure 2-5: Geometrical features of a typical Re-entrant bowl

Maximum diameter is the largest horizontal distance between two points of any face of the piston bowl in section view. The ratio of maximum piston bowl diameter to the piston depth is the aspect ratio. Maximum diameter is a key parameter, and usually specified very early in bowl design. It controls the piston volume, and hence the compression ratio. This diameter affects bulk swirl velocity at the end of compression stroke, because its increase leads to swirl velocity reduction in the bowl (Aorld et al., 1990). Even though this reduces the air/fuel mixing rate, heat transfer and other heat loses are reduced as well. The role of the maximum diameter in wall impingement after injection, as fuel is swept down the bowls into the main toroidal radius, can be influential in smoke production.

Throat diameter is the minimum horizontal distance between the edges of the piston bowl, near the top. The ratio of the throat diameter to the maximum bowl diameter determines the amount of bowl re-entrancy during design. Similarly, the ratio of the throat diameter to the cylinder bore determines the percentage squish area (Hentschel, 1996).

The central pip occupies a particular position in the centre of the bowl, where otherwise the low air velocity exists. It is not desirable for low air velocity to exist in the centre of a swirling flow field, as this will lead to poor rate of air/fuel mixing. With the use of central pip, redistribution is effected in a manner that will cause higher mean airflow velocity and improved air/fuel mixing rate. Although the pip occupies a comparatively small portion of the bowl, it comes in different shapes for different bowl designs. Its shape can be accommodated by slight changes in other key parameters. However, pip design is significantly influenced by injector tip to piston distance, especially under engine operating condition, where thermal expansion and inertial forces must be taken into account. It is also important for the design to prevent wall wetting of the pip by closely approaching fuel sprays.

For a conventional design, the bowl depth is the maximum vertical distance from the piston surface to the bottom of the main toroidal radius. It is an important consideration in smoke reduction, due to wall wetting tendency of the lower bowl surface.

The volume containing the main toroidal radius constitutes a large percentage of the bowl volume, where most of the combustion processes occur. It, therefore, affects airflow, flame propagation and development towards the pip region. The radius also guides the pip design, in order to avoid discontinuous profile in the bowl section (Saito et al., 1986).

Lip area is the side of the bowl where high velocity fuel impinges during injection. It is an impingement area and has a significant effect during the early stages of fuel injection and combustion. By controlling the amount and composition of fuel/air mixture prepared for initial combustion, the ignition delay and initial pressure rise may be affected.

The minor radii blend the face of the piston and the main toroidal radius with the lip area. Even though the radii look quite insignificant in the figure, they can affect airflow resulting from squish during combustion, and change the outflow of hot gases during combustion (Shimoda et al., 1985). Investigations of flow through orifices, nozzles and diffusers suggest that gas flow can be improved by the minor radii, which can also affect turbulence levels (Tindal et al., 1982). The sizes of the radii are constrained by the need to prevent excessive build-up of thermal stresses and hot-spots in the piston bowl.

The introduction of high pressure injection systems has placed the re-entrant bowl design on the front burner of most research investigations, especially on the account of its good combustion characteristics. It has shown good swirl and turbulence characteristics (Payri et al., 2004), and adaptability to modifications that can lead to the improvement of air-fuel mixing. Concerns have also been raised regarding its durability, as piston temperature and thermal transient stress range increase (Winship et al., 1993). However, most of the literatures reviewed for this work featured the re-entrant bowl design or its modified models.

Park et al., (1993), studied the performance of pip through simulation. The introduction of pips in modern engine bowls is to enhance spray break-up and/or direct spray to a desired direction. Wall wetting was reduced as the impaction of spray on pip land, significantly reduced the spray momentum and kinetic energy. Zhang et al., (1995) demonstrated how the re-entrant bowl improved combustion, and hence, emission in comparison with two other different blows. Risi et al., (2003) optimised soot and HC emissions by changing bowl geometry. They were unable to achieve reduction in NOx emission. However, the effect of spray angle was more

significant for NO_x than soot emission; while an increase favoured NO_x reduction, a decrease was best suited for soot reduction. Since both emissions were affected by the throat radius; it was concluded that a narrow and deep bowl design with a shallow re-entrance and a low protuberance on the cylinder axis and spray guidance towards the bowl entrance was good for NO_x reduction. Soot reduction required bowl design with very small re-entrance and reduced bottom inclination. The spray for soot reduction was directed at the bottom of the bowl to promote leaner combustion and faster soot oxidation rate.

Genzale et al., (2006) varied swirl ratio with bowl geometry to achieve more reductions in soot than NOx emissions, under late LTC condition. Similar difficulty was experienced by Gunabalan et al., (2009) in reducing NOx with the re-entrant bowl, as their numerical study showed superior soot oxidation that came with significant combustion temperature rise. The temperature rise must have comtributed to the high NOx emission. Pasupathy et al., (2010) investigated DI turbocharged diesel engine using similar CFD approach. The superior characteristics of the re-entrant bowl in terms of better mixing and faster combustion process for indicated specific fuel consumption (ISFC) and soot emission reductions were established. Increase in NO_x emissions for the bowl was also confirmed. However, in both studies, the soot reduction was larger, which made the re-entrant bowl the best trade-off between performance and emission.

These studies have highlighted the importance of air motion in in-cylinder mixing. It is during the intake stroke that air motion generates flow by interacting with the bowl shape, which is developed during the compression stroke (around TDC) and upon diesel fuel injection (Heywood, 1988; Xueliang et al., 1990). Air motion in the

cylinder is usually characterised by swirl, squish and turbulence (Brandl et al., 1979). The intake port of the engine is designed to create swirl motion upon air induction. It is important to generate a high swirl that will facilitate swirl-squish interaction for the development of turbulent flow field. Intense turbulence leads to efficient combustion, and ultimately less soot and HC emissions at the cost of higher NO_x. Unlike most bowl designs, the re-entrant bowl is capable of high swirl and intense turbulence levels (Arcoumannis et al., 1993). Re-entrant bowls increase squish velocity, turbulence and fuel/air mixing by increasing the area of the piston top which almost touches the cylinder head, whilst keeping the bowl volume, and hence the compression ratio, constant. Therefore, the effect of bowl geometry on air motion basically translates into how well the piston bowl shape enables air utilization for efficient combustion and improved emissions. Actually, it is the bowl geometry that determines the extent of the amplification of the induction-generated swirl during the compression and combustion strokes.

Different investigations (Fitzgeorge et al., 1962-63; Tindal et al., 1982; Morel et al., 1985; Ferguson, 1986; Hiroyasu et al., 1989; Fansler, 1993; Winterbone et al., 1993); Payri et al., (2004); (Song et al., 2008; Prasad et al., 2011; Raj et al., 2012) have been conducted to study in-cylinder flow conditions. These studies established the effects of bowl geometry on flow as well as the superior flow characteristics of the re-entrant geometry. It was also reported that the bowl geometry had no effect on flow during intake and early compression strokes, indicated by insignificant change in swirl numbers and turbulence kinetic energy (TKE). Changes in these parameters were quite significant near TDC, with huge influence on the combustion process. It was at this point that the spatial distribution due to bowl geometry became crucial.

2.3.1 Summary

Piston bowl design has a significant role to play in modern diesel engine

performance. Indeed, piston bowl can drastically reduce emissions with a design that allows the development of appropriate spray shape and structure. Such design will enable sufficient evaporation in a very short time and optimal spray penetration for improved air utilization. However, the inability of any particular design to perfectly satisfy the simultaneous reduction of soot and NO_x emissions has been highlighted. Even with the most popular re-entrant designs, there were still cases of achieving satisfactory level in one and failing in the other, depending on the boundary conditions. It was also observed that the relevance of the piston bowl geometry to emission reduction was relatively unexplored. Bowls used in the investigations review here, either conformed/performed or not. No attempt was made to improve bowl performance by changing the geometry. Targeting spray at specific parts of the bowl with the aim of improving flow near TDC presents opportunity for further investigations. This could lead to drastic reduction in PM emissions. More understanding is therefore needed.

2.4 Spray and piston bowl interaction

The direct result of spray/bowl interaction is wall impingement. For DI diesel engines spray impinging on the walls is inevitable. This is due to the compact nature of the DI engines, where the distance between the nozzle and cylinder walls is short. How fast sprays make this distance before vaporisation depends largely on the injection pressure. Over-penetration of spray may cause impingement on cool surfaces with little air swirl, reducing mixing rate and producing unburned fuel, while under-penetration may result in poor use of air (Stone, 1992).

Earlier discussion in this review has indicated that for DI diesel engines, an atomised liquid spray evolves into a vaporised fuel jet as it penetrates into the combustion chamber. It is therefore convenient to identify the liquid-phase as “spray”, and the

vapour-phase as “jet”. Diesel fuel jet is complex due to the presence of the piston bowl wall in the downstream region. However, it is usually separated into two mixture composition zones (Bruneaux, 2005). They are: the mixing zone on the

upstream sides, where air entrainment due to shear turbulence dominates the jet dynamics, and the stagnation zone at the tip where the jet pushes away the dense ambient gases. This stagnation zone has lower mixing rate, as there are no small scale turbulence.

Spray impingement may be detrimental due to splashing of the liquid-phase on the walls which can increase hydrocarbon emissions. On the other hand, jet impingement produces strong turbulence, enhancing mixing of rich mixture in the core of the spray, and provides an additional mechanism for droplet break-up (Brunello et al., 1991; Borman et al., 1992).When the jet reaches the bowl wall it is diverged into wall-jets. As the wall-jets travel along the bowl wall, they are confined, and when two neighbouring wall-jets eventually collide they form a recirculation zone (Chartier et al., 2012). Held et al., (2013) reported, as shown in Figure 2-6 (a), the existence of small vortex structures which occurred next to the dense jet core due to aerodynamic interaction of the spray and the surrounding gas, before the impact on the wall. They also confirmed the formation of wall jets, but parallel to the wall.

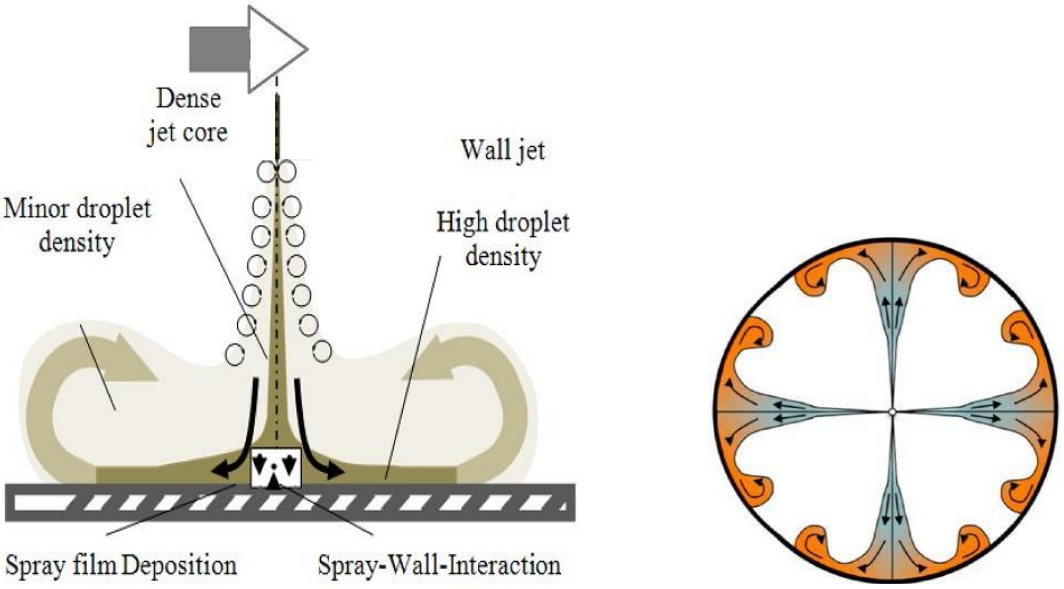

(a) (b)

Figure 2-6: (a) Diesel spray-wall interaction model on a flat wall (adapted from Held et al., (2013). (b) Diesel impingement from a symmetrical multi-hole injector (Chartier et al., 2012)

Investigations by Shimada et al., (1989) presented wall impingement as a means of vaporising spray, to promote mixing with air. The study did not consider wall impingement with respect to the three behavioural patterns identified by researchers (Naber et al., 1993; Arcoumannis et al., 1997). These patterns included: spreading on to the surface without rebound or break-up to form a thin film (wall-wetting); rebounding off the surface; or breaking-up to cause the ejection of secondary droplets, whilst depositing a fraction of their liquid mass on the wall. In addition, exhibition of any of these patterns depends mainly on the wall surface temperature and the droplet thermodynamic properties. For example, under high injection pressure condition the formation of the thin film will occur if the droplet boiling point is higher than the surface temperature of the wall (Naber et al., 1993). This will lead to a very high increase in unburned hydro-carbon (uHC) and soot emissions due to the partial burning that is caused by slow evaporation of wall film (Luckhchoura et al., 2010). Held et al., (2013) also described the behaviour in terms of Weber number, Leidenfrost temperature (T_L) and Nukiyama temperature (T_N) as shown in Figure 2-7.

Nukiyama temperature (T_N) is the temperature at which the heat flow between the wall and the fluid is at maximum. The evaporation time is therefore at a minimum. At Leidenfrost temperature (T_L) there is an isolating vapour film between the droplet and the wall, which confers a local maximum on the evaporation time.

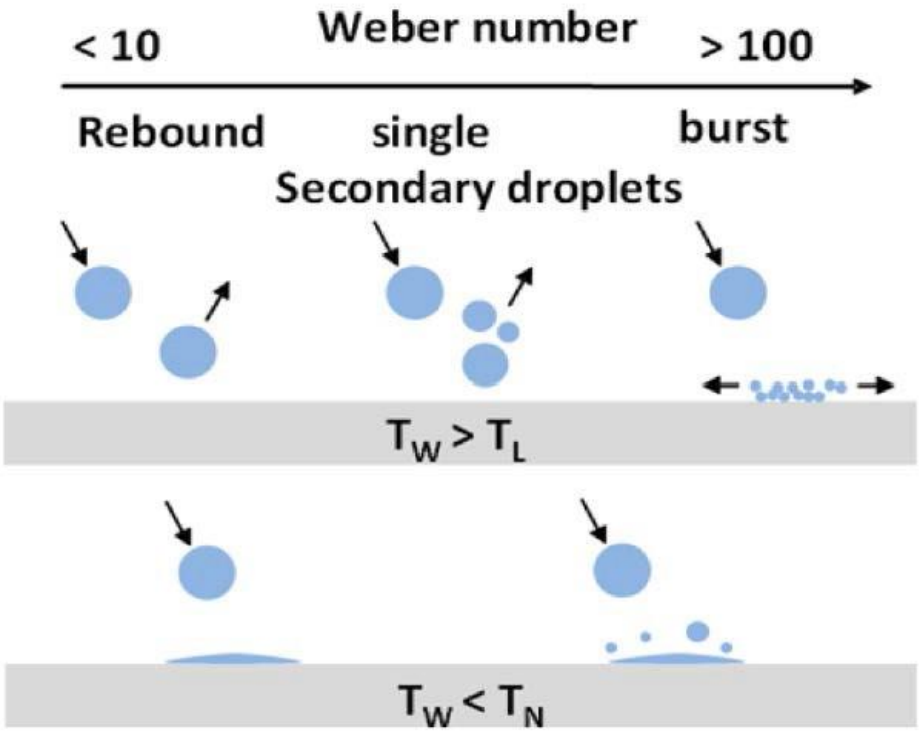

Figure 2-7: Characteristic arrays of droplet impact with a flat wall (Held et al., (2013))

From Figure 2-7, one can see different droplet behaviour, at different Weber numbers, for wall temperatures higher than the Leidenfrost temperature. If the wall temperature is higher than the Leidenfrost temperature ($T_W > T_L$), for Weber numbers smaller than 10an elastic rebound of the droplet can be observed. A development of single secondary droplets occurred between a Weber number of 10 and 100. For Weber numbers higher than 100 the impacting droplet bursts on the surface. If the wall temperature is lower than the Nukiyama temperature ($T_W < T_N$), wall wetting occurs both for low and high Weber numbers. The only difference is that for high Weber numbers small satellite droplets are formed. In general, wall wetting degrades mixing, and hence combustion, and leads to increased emissions. This argument is linked with investigations conducted under relatively low injection pressure; since investigations with injection pressures of 2000 bar and above had generated significant wall jets with increased surface area of the jets, that led to better fuel air mixing (Ryan et al., 1994).

Schünemann et al., (1998) studied the effect of the injection pressure on spray-wall interaction and reported that at higher injection at higher injection pressures the droplet diameter decreased due to higher primary atomization, and the droplets moved with higher velocities. Near the wall there were approximately as many droplets flying towards the wall, as droplets moving the other way, which indicted that there was a reflection of droplets at the wall. At higher injection pressure, the wall jet vortexes moved faster at a higher rotational speed. They also reported that lower wall temperatures cause low gas temperatures above the wall, which increased gas densities and viscosities. The droplet sizes were significantly increased due to slower evaporation, and had higher forces of inertia.

Under high injection pressure, Pickett et al., (2005) found out that the leading edge of jet impinging on a planar cylinder wall would actually decrease soot levels. While jets which were redirected back onto their initial path after impingement produced more soot. Wang et al., (1999) reported that the high injection pressure induced high momentum spray and bowl wall interaction that increased the level of spray rebound, which promoted air entrainment.. The combustion movies by Minami et al., (1990) showed jet-wall interaction and significant combustion process by the wall. While the former was responsible for the improved fuel-air mixing, indications about the latter suggested combustion degradation as a result of the closeness to the wall. Other researchers (Hiroyasu et al., 1989; Kato et al., 1989) are in agreement with the concept that wall impingement becomes more important in the break-up of spray jet and mixing of fuel with air, as injection pressure increases. Kato et al., (1989) further suggested the use of larger combustion chambers for higher injection pressures. On the other hand, some researchers (Hiroyasu et al., 1990; Dodge et al., 1992) argue that the high pressure effect on drop size diminishes at pressures above 1000 bar. Researchers, (Shimada et al., 1989; Shundoh et al., 1991), have also shown that

increasing injection pressure and optimising nozzle hole diameter is an effective combination for better fuel atomization and fuel-air mixing through extended spray penetration, air entrainment and wall impingement. Although, material strengths, increased parasitic losses and fuel system cost impose severe limitations on the maximum practical injection pressure (Pierpont et al., 1995).

Most experimental works seem to indicate that jet wall impingement tends to increase mixing of the fuel with the surrounding air, with increased injection pressure, which is expected to increase turbulence in the wall-jets as an effect of higher impact momentum and higher average flow speeds. However results from numerical analyses (Abraham et al., 2003; Song et al., 2003) are contradictory. Although these disparities seem to originate from the incapacity of numerical simulation in reproducing the complex turbulent structure generated during interaction (the jet wall vortex), the experimental results are often not conclusive enough to be able to validate or contradict the numerical results. For it is often the practice to simplify this complex interaction with the configuration of a plane wall. Where the wall jet is not confined and could expand, with larger area available for mixing which would imply greater air-entrainment. Unlike the wall-jet in engine`s combustion chamber, which is much more confined between the bowl floor and the fire-deck. Such geometry reduces the surface area of the jet so that it cannot increase as much. Furthermore making deductions about spray behaviour from single droplet behaviour (see Figures 2-6 and 2-7) can also produce contradictory results, since the physical background is much more complicated for a spray. Certain parameters will have to be considered. These include: differences in diameters, velocities and Weber numbers, as well as the effects of ambient conditions (e.g. inconsistent turbulent flows, heterogeneous temperatures and pressures).

Further understanding can be gained on the spray-bowl interaction with respect to:

effects on emissions (Docquier, 2002), effects of injection timing (Diwakar et al., 2009; Luckhchoura et al., 2010), effects on cold starting (Osuka et al., 1994), effects on heat transfer (Magnusson et al., 2006), effects on air entrainment (Cossali et al., 1993), location and angle of impingement (Lippert et al., 2001) and effects on distribution and mixing processes (Zhang et al., 2001).

2.4.1 Summary

The interaction between diesel fuel spray and the piston bowl leads to wall impingement with effects that may or may not favour in-cylinder air utilisation, regardless of the injection strategy or combustion concept. The phenomenon is noted to occur at different conditions, such as higher injection pressure, higher ambient temperature, lower combustion chamber densities and engine speeds. Higher injection pressure is the parameter that exerts the most influence on the account of increased spreading angle and penetration velocity, with the favourable possibility of promoting air utilisation. All the studies that bear qualitative agreement have noted improved mixing with impinging jets under increased injection pressure, since the mass of air entrained in a jet is higher in the case of impinging jet compared to free jet. The wall condition has also been mentioned as part of the air entrainment characteristics.

Wall temperature has a significant influence on the heat transfer under evaporating and non- evaporating conditions but no measurable influence on radial penetration. Infact, the presence of a wall affects the entrainment by increasing the entrained mass flow rate in the region close to the wall, depending on the injection strategy and the angle of impingement. Normal impingement produces the maximum effect on air entrainment, while oblique impingement, which produces an asymmetry on the wall spray, lowers the entrained mass flow rate close to the wall. These observations have been found to be correct during the main injection period of a split-injection strategy.

Spray and bowl interaction has also highlighted the significant role played by the piston bowl geometry in the effectiveness of injection strategy in promoting mixing for better combustion and hence, emission reduction.

2.5 Schlieren/shadowgraph techniques

The methods commonly applied to the study of spray employ: mechanical, electrical/electronic or optical techniques. Optical techniques are by far the most frequently used for macroscopic/microscopic spray and combustion characterisation. It is advantageous to use optical techniques because of their sensitivity to changes and non-intrusive nature, as they do not interfere with flow process under observation (Richard et al., 2001). Schlieren is a direct imaging optical technique. It involves qualitative visualisation of spray development, and image capture with high speed camera.

Schlieren imaging derives from Snell`s Law, which states that light slows if it comes into contact with matter (Settles, 2006). When light travels in a homogenous media, such as space or vacuum, it does so uniformly at a constant velocity. In inhomogeneous media, such as fluids in motion, light rays refract and deflect from their continuous path, resulting in Schliere. Schliere is simply the streak-like appearance of the fluid flow visualised through the system. In this work, this technique is applied to exploit the effects of refraction of light rays as it passes through the charged fluids in the combustion chamber. As optical diagnostics for spray studies, the application of Schlieren imaging is due to the presence of high-speed flows involving shocks and large gradients in refractive index.

A simple Schlieren set-up, used for imaging vapour penetration, is shown in Figure 2-8.

It consists of: a light source with variable iris, two concave mirrors, optical engine combustion chamber, adjustable knife edge (Schlieren stop) and a high-speed video camera. The light source produces a parallel beam of light, which passes through the slit created by the variable iris and focused by the first concave mirror. This parallel beam is then deflected by the combustion chamber, which is known as the Schlieren test subject. The image thus created is passed through a second concave mirror, and focused onto the photographic sensor of the high-speed video camera through the knife-edge. The knife edge is a confining aperture that filters light rays for image acquisition in a traditional Schlieren set-up. The test subject actually divides the set-up into two; the upstream part that initiates collimation, and the collection part that enables focusing for image acquisition. For the test subject, two combustion chamber types are commonly used; constant-pressure flow (CPF) vessel and constant-volume pre-burn (CVP) chamber.

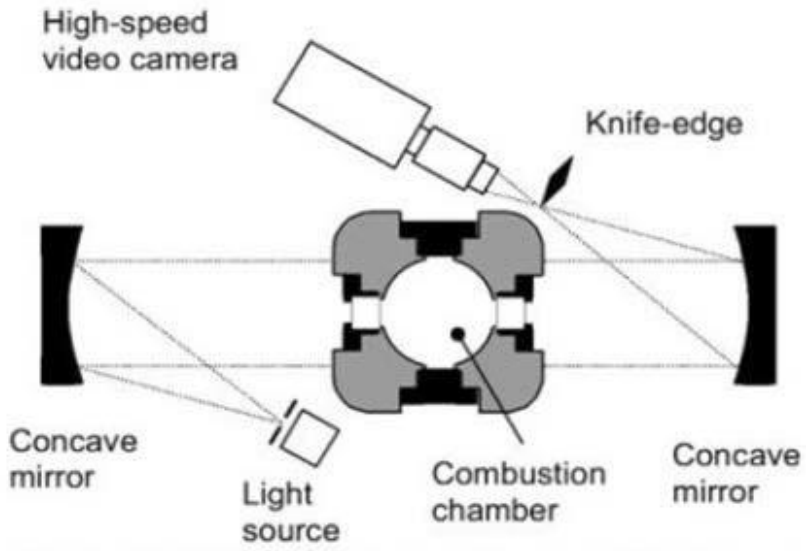

Figure 2-8:Set-up for Schlieren Imaging(Kennard et al., 2002)

Variation in the Schlieren set-up results in two notable visualization techniques; shadowgraphy and interferometry. Schlieren and shadowgraph are more closely related, as they employ the change in refractive index with optical density (and hence, temperature and concentration) to map a thermal or species concentration field. While the Schlieren technique depends on beam refraction towards zones of higher refractive index;

the shadowgraph technique utilizes the change in light intensity due to beam expansion to describe the thermal/concentration field. Thus, for Schlieren technique, small angle of deflection of the light beam as it emerges from the test section is measured. In Shadowgraph, deflection and displacement of the light beam are measured. Due to the rapidly changing complexity of diesel injection and combustion, the high speed diagnostics are often combined, without interference. A typical set-up for simultaneous applications of various high speed imaging techniques, on a fixed-volume combustion vessel, is shown in Figure 2-9. With necessary adjustments, this set-up is capable of the following optical diagnostics; Shadowgraph/Schlieren imaging, Mie-scatter, chemiluminescence imaging, pressure chemiluminescenceand soot luminosity sensing.

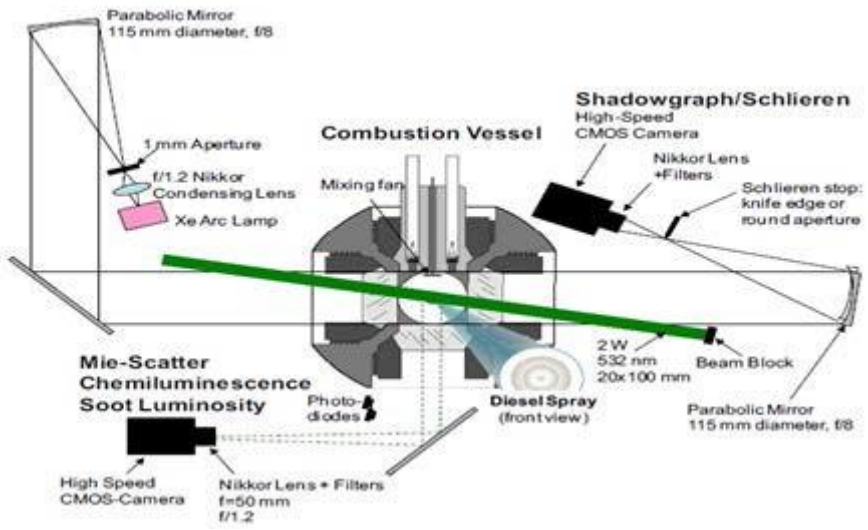

Figure 2-9:High-speed imaging set-up (Lyle et al., 2009b)

The knife edge cut-off, which is commonly used as a Schlieren stop, controls the image contrast, and hence the system sensitivity to refractive index gradients (Settles, 2001). Sensitivity to refractive index gradients increases with cut-off. A round aperture used for same purpose will remove some of the directional sensitivity to refractive index gradients. The use of a round aperture is known as “bright field”, since the Schlieren object is dark whilst the background is bright. A total cut-off of the focal spot

is known as a “dark field” method, since the Schlieren object appears bright above a dark background. System sensitivity is also affected by the distance between the image plane and test section, and the number of filters. In the absence of a knife edge (or 0% cut-off), system sensitivity is weakened, and the system is no longer Schlieren, but a “focused shadowgraph” (Settles, 2001). Optimal camera adjustments, in terms of exposure and frame rate, may be driven by the choice of light source. Thus, the different Schlieren stops that are used include; knife edge, aperture (bright field), cut-off (dark-field) and no stop (shadowgraph). For the schlieren/shadowgraph, three key features are reviewed, and they are: optical alignment, camera setting and system set-up (for improved image acquisition).

2.5.1 Optical alignment

The use of white light as point source for Schlieren imaging is very popular amongst researchers (Lyle et al., 2009b). White light has been considered to be more advantageous than the Laser (Lyle et al., 2009b). Particular type of laser-based techniques is associated with single-image-per-cycle limitation, which makes imaging temporal development difficult, since insufficient information is generated. Speckle effects and diffraction are quite common with laser, unlike white light (Settles, 2001). This is due to the coherence nature of the laser light wave. Speckle effect is characterised by high contrast, high spatial frequency and granular pattern that seem to float in front of the projected image plane. Diffraction is the apparent bending of light wave around edges. It is a serious problem for laser as it passes through confining apertures, e.g. “knife stop” of the Schlieren system. Both phenomena can lead to image degradation. Another disadvantage of the laser is its high energy density, which can cause severe damage to optical components when placed at focal points.

In order to overcome the single-image limitation, high-speed lasers, that are capable of rapid image acquisition, are in use today. The problem of diffraction is solved by setting-up the Schlieren technique with round disc (Pickett et al., 2010) and without any conventional Schlieren stop (Bardi et al., 2012). Lasers also have more advantages, which include; improved image brightness, power efficiency, reduced size of the illumination source and optical system. The high monochromatic brightness of the laser makes it possible to instantly pause a rapidly developing phenomenon for image acquisition, with short camera exposure. Short exposure prevents image blurring by high speed lasers. Laser can also be used with suitable filters (eg chromatic filters), combined with shorter exposure time, to separate combustion luminosity from developing spray (Bardi et al., 2012). In addition, the use of laser is more economical, as only one high speed camera can be used simultaneously for Mie-scatter and Schlieren/shadowgraph techniques.

Focusing a collimated laser beam to a small spot, with a lens, as required for a Schlieren set- up, depends largely on the divergence. The divergence fixes the lower limit of the focused spot size. Satisfactory compromise between the divergence and spot size can only be achieved with a lens of shorter focal length or by expanding the beam. Beam expander was used in the set-up by IFP in Figure 2-10.

Although, the use of lasers present interesting opportunities (Oppenheim et al., 1966), it is difficult to completely eliminate speckle effect. Significant progress has been made with strategies that reduce laser coherence. This is beyond the scope of this work. However researchers have successfully managed to work around the speckle effect (see Figure 2-10), as will be highlighted in section 2.3.

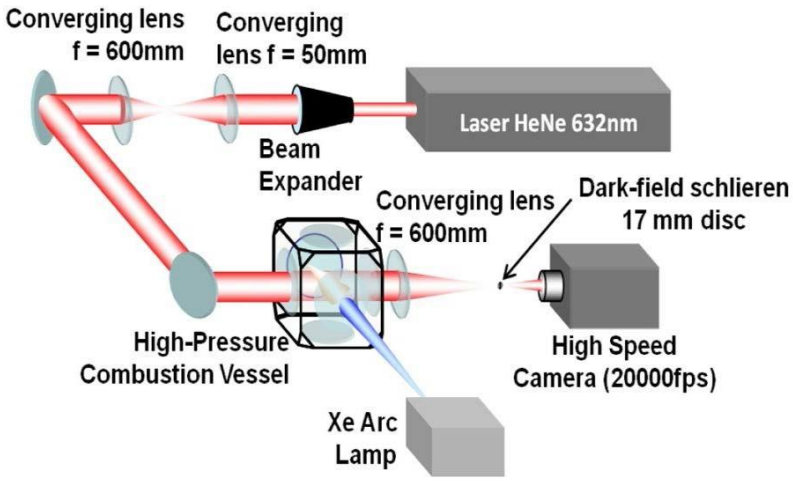

Figure 2-10: Mie-scatter and Schlieren set-up used by IFP (Pickett et al., 2010)

The choice of optics and arrangement vary amongst researchers. In the set-up used by Kennard et al., (2002), the point source produced by sodium light and variable iris was collimated by one concave mirror and passed through the test subject to another concave mirror. The second concave focused the Schlieren image on the camera through the knife edge. This simple set-up is not as involved as the Schlieren part of Figure 2-9, which was used by other researchers (Lyle et al., 2009a; Lyle et al., 2009b; Pickett et al., 2010; Kook et al., 2012). Under the arrangement, the emitted beam from the source passed through the focal length of Nikkor lens and an aperture, before collimation by one parabolic mirror and deflection by the test subject to a second parabolic mirror. The latter focused the beam on the camera through the Schlieren stop, filters and another Nikkor lens. In a set-up similar to that in Figure 2-9, Sandia Laboratories (Pickett et al., 2010) did not use a knife edge, which made the technique a shadowgraph. The choice of a parabolic mirror was more appropriate because of its ability to focus parallel rays of light on its principal focus, and vice versa. Hence, with point source located at its focal point, the resultant beam should be well collimated. The use of the Nikkor lenses, against simple achromatic condensing lenses, on both parts of the set-up was to ensure superior broad wavelength performance. Variations in optical arrangement for Schlieren also include the use of filters and

the configuration of the light source (pulsed/continuous).

2.5.2 Camera setting

A key factor of the Schlieren set-up is that image acquisition depends on the system sensitivity, which in turn depends on optical alignment and camera settings. Researchers have shown the effect of camera settings in capturing optical and quantitative information. In some of the studies (Takeuchi K et al., 1983; Verhoeven D et al., 1998; Arre`gle J et al., 1999; Morgan et al., 2001; Kennard et al., 2002), images were acquired by taking one snapshot of spray per fuel injection. Photographic films or (intensified) charge-coupled device (CCD) were used to register these images. An image sequence for spray development with time was created with a series of injection for each image taken at a different time delay from start of injection. Thus, this strategy necessitated repeating the injection tests, and hence vital information on transient dynamic phenomena could easily be missed.

A different group of works (Rao KK et al., 1992; Naber JD et al., 1996) used high speed cinematography in their investigations. This technique allowed for separate recording of the temporal development of every fuel injection event. It was therefore possible to detect spray dynamics and change in spray behaviour between different injection events. However, conventional high speed film cameras, as used in the identified works, were specialised equipment that required alignment, development and digitising of film material. These made the approach to be time-consuming and labour intensive.

In evaluating the start of injection process, some studies completely assumed that the initial spray development could be determined with sufficient spatial and temporal resolution. This was quite possible for single shot photography or cinematography at

higher frame rate than 15 kHz. However, with the type of camera (Kodak HS Motion Analyser) used by (Dan T et al., 1997; Morgan R et al., 2001), upper limits were set to image acquisition rate (between 4.5 and 9kHz) for complete observation of injection of (multiple) large sprays from a heavy-duty engine with sufficient spatial resolution. Consequently, only few shots could be taken, before the spray travelled up to a distance of 30mm or more. This is a general problem, even for the modern high speed video cameras.

Nevertheless, modern high speed video systems, such as the complementary metal-oxide semiconductor (CMOS), are becoming more popular as they perform better in the study of spray development and spray dynamics. They can be adjusted to suit light source (laser or white) and configuration (pulsed or continuous), as well as the operating conditions.

2.5.3 System set-up

Researchers approach Schlieren set-up differently. Even though the basic components are still deployed, it is however not uncommon to see slight variations that are often unique to the image acquired. In the study by Lyle et al., (2009a), they tracked liquid and vapour penetration simultaneously, using Mie scatter and Shadowgraph/Schlieren (Figure 2-9 set- up), under low temperature conditions. The time-resolved pair, of Schlieren and Mie-scatter images, identifies the instantaneous position of both the vapour and the liquid phases of the fuel spray, respectively. Thus, they used Shadowgraph/Schlieren imaging, with CMOS camera, to measure axial vapour penetration from the variation in refractive index with density. As well as, to identify the boundary between vaporized fuel and background ambient gases. Further analysis of the shadowgragh (vapour boundaries) yielded the jet spreading angle. The results showed injection strategies, such as multiple short injections, that limit

liquid penetration (and hence wall impingement), whilst permitting vapour-phase penetration. Despite these results, multiple injections may not produce optimal performance for low temperature combustion. Besides, low temperature condition creates low density environment where vaporisation is poor and liquid impingement is probable. Fuel injected earlier may ignite and prevent later injections from mixing and achieving less fuel-rich combustion.

Using similar set-up, Lyle et al., (2009b) visualized spray penetration with the Schlieren. High-speed imaging was performed for non-vaporizing, non-reacting and reacting sprays in a high-temperature, high pressure combustion vessel. The work further demonstrated the capacity of high-speed Shadowgraphy/Schlieren to identify transients in auto-ignition and lift-off length well after ignition. Shadowgraph technique was used for the high temperature, high pressure tests. This was because the associated higher ambient density created strong gradients that enabled the detection of vapour boundary, without Schlieren stops. Image correction for background variation in density was effected by considering the image intensity before and at any other time after injection. This method eliminates pre-existing Schlieren effects in order to more easily visualize the actual jet structure. For the non- vaporising condition, the background intensity before injection was simply subtracted from that after injection, as the background features did not change significantly during the injection. Under non-reacting and reacting conditions respectively, changes in background features were observed with injection. Correction was effected by subtracting previously acquired image from current image plus a greyscale offset.

Image correction is very important for image processing, especially at high temperature and pressure conditions, as more interesting spray penetration characteristics are

revealed. In combination with other techniques shown in Figure 2-9, Shadowgraph/Schlieren imaging provided useful information to confirm the usefulness of high-speed imaging in interpreting diesel combustion. However, it is important to note that the application of a no-stop strategy performed very well with image pre-processing in detecting vapour boundary.

Another work by Kook et al., (2012), simultaneously, analysed liquid and vapour penetrations, using Mie-scattering and Schlieren technique respectively. The study was conducted with same Figure 2-9 set-up, under conditions representative of low emission diesel engine operation. Evaporating sprays of six different fuels, including diesel fuel, were investigated. The result showed that liquid-phase penetration increased with fuel density and boiling point. Vapour penetration and spreading angle were not significantly affected by these properties. During the process, a general problem of resolution, which could affect image processing, developed. Given the non-uniformity of the ambient gas in the Schlieren background, it would be difficult to clearly identify vapour region. The non-uniformity was caused by temperature differentials in the ambient gases and boundary layers at combustion chamber`s windows. Optimizing the illumination may have improved vapour region and background contrast. However, the implementation of background correction reduced the effects of the non-uniformity. Interestingly, the result related liquid- phase penetration to fuel density, in agreement with the scaling law (Siebers, 1999). This is important for direct fuel injection. Using a fuel with low boiling point and density eliminates concerns for wall wetting and fuel-in-oil dilution.

As part of the collaboration of the Engine Combustion Network (ECN), Pickett et al., (2010), compared works by two facilities, Sandia National Laboratory and IFP Laboratory, on a diesel fuel sample (ECN-Spray A) penetration using Mie-scatter and

Schlieren set-up. Both facilities used CVP test rigs. To visualise liquid penetration with similar set-up to Figure 2-9, Sandia used a continuous-wave laser source formed into a volume to illuminate the liquid part of the spray. This (side-illuminated) method was preferred to the use of laser sheet in order to ensure that all droplets proceeding from the nozzle were illuminated; and to identify the maximum axial and radial distances of any liquid fuel. The CMOS camera was set to create adequate dynamic range that will identify spray regions where liquid completely evaporates. Another CMOS camera was used to simultaneously capture the vapour phase penetration. Building on the success of Lyle et al., (2009b), Sandia used a no-stop Schlieren (or shadowgraph). Actually, without a Schlieren stop, the focal point of the collection part had adequate sensitivity at the ambient densities of the Spray-A.

In contrast, IFP used the set-up in Figure 2-10 for the simultaneous Mie-scatter and Schlieren imaging. For the former, a xenon arc lamp was used to illuminate the liquid-phase spray region, with the CMOS camera operated at higher resolution, but slower framing period and exposure time than the Sandia set-up. The light source is opposite the spray direction (head- on). A HeNe laser was used for the Schlieren imaging. The sensitivity of the Schlieren system depends on the distance from the spray to the collimating lens and camera (Settles, 2001). This was applied by IFP to achieve the best performance using a dark-field set-up with a 17mm disc placed at the focal point of the collection part, as shown in the Figure. The camera was operated at same resolution and speed as the Mie-scatter, but at a reduced exposure time. In addition, the ECN-Spray A diesel fuel used by IFP was of slightly different composition from that used by Sandia. Notably, one camera was used for the techniques by IFP, but with different settings.

The results, from the two facilities, highlighted the differences in spray appearance and maximum distance of penetration during the early transient stages of spray

development, for the liquid phase. Difference in spray appearance was ascribed to the optical set-up due to the different modes of illumination employed by the facilities. The side-illumination intensity performed better than the head-on, since the latter also employed imaging set-up that caused slower rate of image acquisition. Difference in transients in liquid penetration was believed to be caused by different injector and injector driver configurations. Between the two facilities, the similarities were quite reasonable for vapour penetration and spray dispersion at same times after start of injection (ASI). In general terms, given the complexities of the experiments, the agreement between the liquid, vapour and even reacting flame at the two facilities were remarkable. This was confirmed by the comparison with the model by Naber JD et al., (1996)

Bardi et al., (2012) extended the ECN comparison by including similar measurements from; Caterpillar, GIT, and CMT. Caterpillar used CPF vessel and a (pulsed) Cu laser. The use of a pulsed laser enables adequate control over the camera exposure. In addition to laser, Caterpillar, like IFP, used chromatic filters and reduced the exposure time so as to reject some of the combustion luminosity. The Schlieren technique by Caterpillar (Bardi et al., 2012) did not utilize any stop, but the acquired image still had some darker regions. This was because the camera used was effective in clipping part of the refracted beam. Hence, the technique was classified as Schlieren, and not shadowgraphy. The work has shown the successful application of the laser light to Schlieren imaging by two different institutions with two different test rigs. Different strategies were essentially applied, and the results compared favourably within experimental complexities. It was not particularly stated how Caterpillar and IFP overcome the speckle effect. Perhaps the orientation of the illumination, the type of stop used, the use of lenses (instead of mirrors) and filters may have reduced the effects of laser coherence. This is subject to verification. More importantly, the

progress made with laser, as demonstrated, encourages further application.

2.5.3.1 Image acquisition

The Schlieren set-up, with the camera-lens configuration, for spray visualization ultimately delivers image, which is an overlay of shadowgraph and a focused spray. This suggests that the deflected rays from upstream are missing from the collection system, as they are out of focus. Pastor et al., (2012) presented Schlieren measurements of the ECN-Spray A penetration under inert and reacting conditions, using the set-up in Figure 2-11.

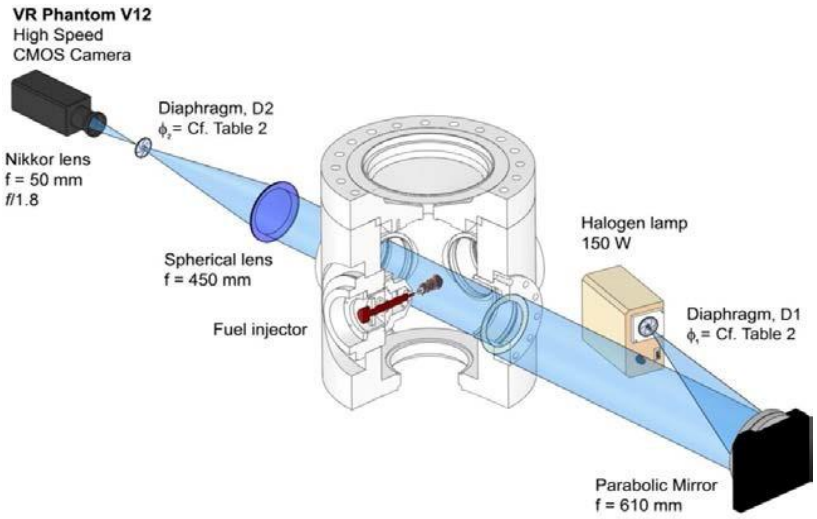

Figure 2-11: Schlieren set-up for Spray A imaging (Pastor et al., 2012)

In the main, they analysed and optimized Schlieren optical set-up in order to improve image processing. The analyses shed more light on focusing (Figure 2-12), and the relationship between ray refraction, filtering at the image plane and resulting image (Figure 2-13). Figure 2-12 shows three different configurations of image focusing of a non-reactive spray. With the de-focused (under-focused and over-focused) images, the camera was believed to have respectively focused onto a plane ahead and behind the spray. An additional demonstration of the scenario is shown by the schematics of Figure

2-14, where M represents the object plane. Clearly, the appearance of the defocused images in Figure 2-10 makes it difficult to conduct the potential computation of the spray boundary. Unlike the focused image, that provided better spray and background contrast. This is also shown in Figure 2-14, as only ray A was focused back to the position of its original path, after deflection. Thus a focused system was recommended, with accurately quantified filtering in the Fourier plane, as the unique solution to create the Schlieren effect. The effect of Fourier filtering is shown in Figure 2-13. In a, b, c and f, bright field is illustrated, with the (low-pass) iris blocking highest diffraction orders and allowing least deflected rays pass through to the camera. Dark field is illustrated by d and e, with the high-pass filter blocking central rays and allowing the higher orders to pass through. Case e is actually an adaptation of d, meant to show black penetrating liquid, white penetrating vapour and grey background. Image f shows the first stages of combustion. These arrangements illustrated the versatility of Fourier filtering in providing numerous possibilities of output for Schlieren images.

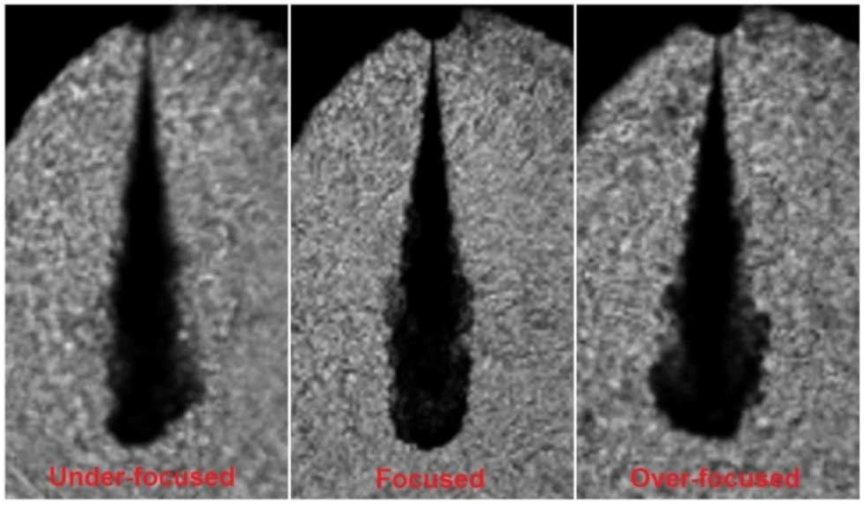

Figure 2-12: Three different configurations of focused shadowgraph (Pastor et al., 2012)

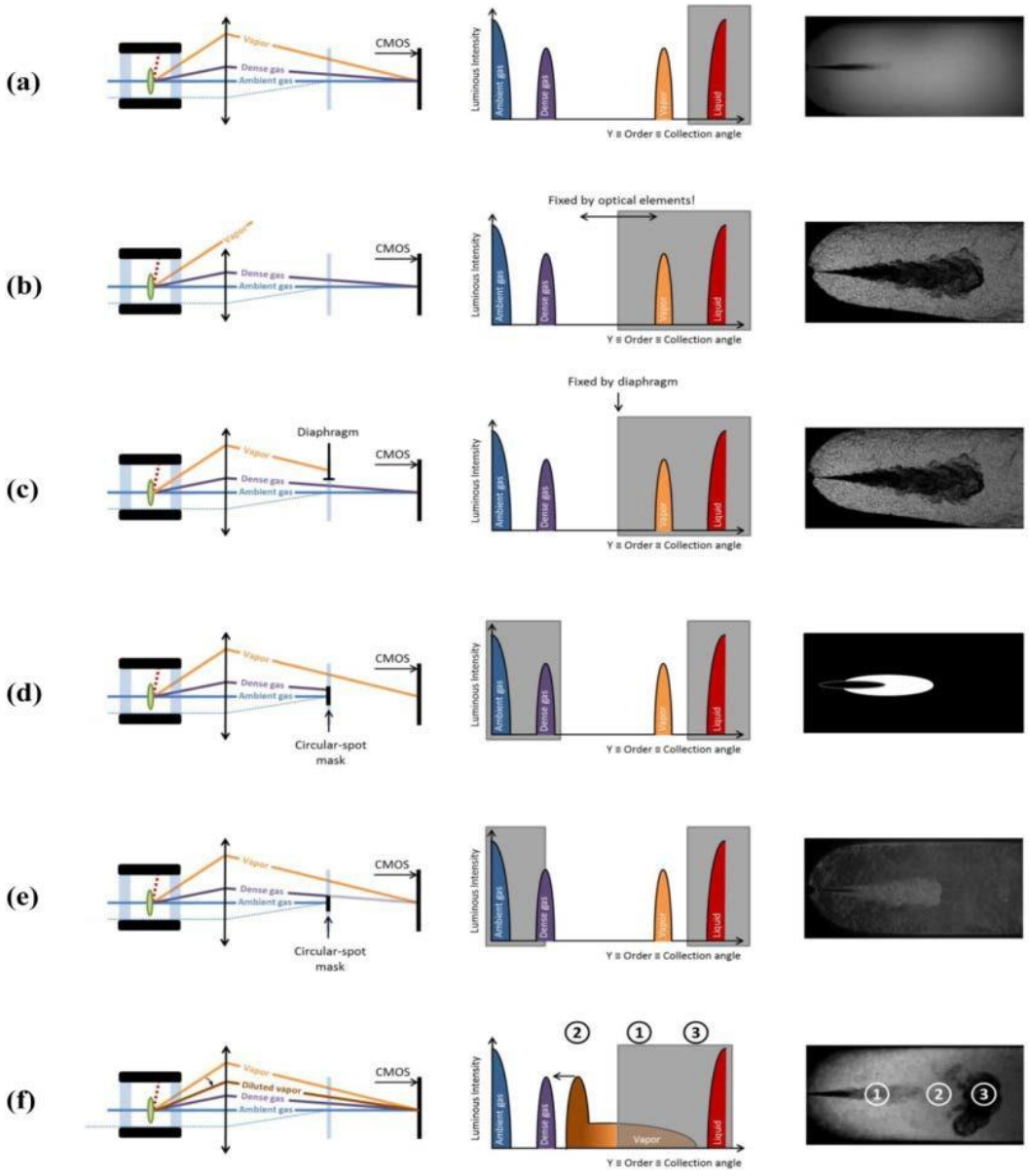

Figure 2-13: Effects of filtering (Pastor et al., 2012)

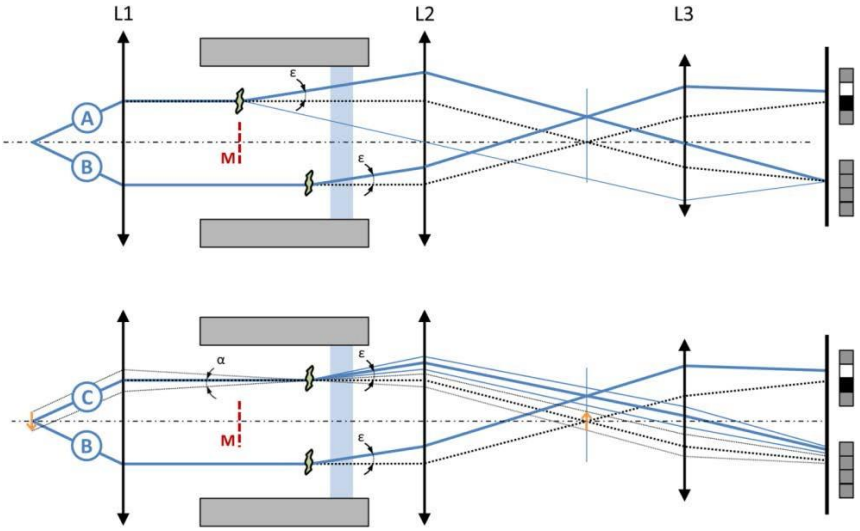

Figure 2-14: Ray refraction by a background structure; (A) in the focused plane; (B) in a defocused plane and (C) in a defocused plane but with an extended light source (Pastor et al., 2012)

Against this backdrop, the optimisation technique by Pastor et al., (2012), used the set-up in Figure 2-9, to focus on the spray and maximise the collection angle in order to optimise filtering in the plane of Fourier. These were implemented by varying the angles of illumination and collection, to force the contrast between the background and spray/flame and obtain images with different levels of intensity. Care was taken to avoid as much as possible the structures caused by in-homogeneity of the ambient gas. To optimise the illumination, the angle of incident between the light source and the mirror was minimised to reduce the beam straightening. For improved collection angle the collection lens was brought closer to the combustion vessel, while the camera lens, and fully opened diaphragm (D2), were placed close to the Fourier plane. Similar strategy was employed by IFP, as explained earlier (Figure 2-10). As the collection lens was brought close to the test subject, the (17mm) disc actually provided the dark field effect by serving as a high-pass filter, which was necessary to improve image acquisition. If a no-stop (shadowgraph) strategy had been

implemented, the performance would have been below optimal. On the other hand, the use of an aperture or knife edge would cause the effect of diffraction to degrade the image.

Finally, even as the advances in technology continue to enable the development of high- fidelity Schlieren diagnostics, studies still show differences in spray measurements. Detailed comparisons have been conducted by Bardi et al., (2012) to identify probable causative factors. These include design-induced variations due to the type of test rig used. Other factors were classified under variations due to experimental set-up, and they covered; illumination source/orientation, boundary conditions and hardware-related issues. Pastor et al., (2012) tried to address variations due to image acquisition, and they developed concept for Schlieren set-up that requires more experiments to be validated. It was also clear from the work that the quality and speed of results of the optical technique employed, and analysis, depended, to a large extent, on the processing algorithm. This understanding was applied by ECN comparisons in Bardi et al., (2012), as all the images acquired by the collaborating institutions were processed with the routine developed by Sandia Laboratories. The algorithm implemented in the routine was relatively insensitive to the optical set-up/ strategy. However, it was ultimately sensitive to the results of the optical technique employed. It is therefore necessary to optimise the technique.

2.5.4 Summary

Schlieren technique provides a dynamic and unambiguous means of conducting qualitative visualisations of diesel fuel spray. This has been facilitated by the advances in computer technology and improved optics production. However more work is required in the design and implementation of Schlieren system. Improving the illumination, optimising image acquisition, limitations of size and portability are on-

going challenges.

From the review, it is clear that the uses of white and laser lights have led to the acquisition of useful images. It was also evident that the traditional Schlieren set-up is gradually giving way to more purpose-driven set-ups. Different types of stops are now possible with the use of laser. Indeed, the dramatic changes in the Schlieren set-up for improved imaging have been facilitated by laser. Laser is offering significant opportunity as a source of illumination, despite the problem of speckle. Its advantages far outweigh its disadvantages. Hence, it is very important to explore this opportunity further, in order to optimise the technique.

2.6 Conclusions of chapter two

The evolution of the diesel engine up to the development HSDI engine, and beyond, has been remarkable. Challenged by ever so strict emission laws, the HSDI design was able to significantly reduce NOx and PM emissions, whilst providing platform for present and future engine optimisation. It has supported increased injection pressure, modified injection equipment/strategy, incorporation of boost systems (supercharger and turbocharger), emission reduction devices and application of EGR, and more recently pre-mixed (LTC) combustion modes. Indeed, modern diesel combustion strategy involves premixed combustion method, which utilizes longer ignition delay to improve fuel-air mixing, and hence, achieve simultaneous reduction of both NO_x and PM emission levels for the purpose of meeting the increasingly stringent emission laws. EGR, which normally has three different effects, is a necessary feature of the LTC mode. These effects are: dilution, thermal and chemical. Dilution, which is the most dominant effect for HSDI engine, reduces inlet charge oxygen concentration. Thermal effect causes an increase in inlet charge heat capacity. While chemical effect leads to modification in combustion process due to dissociation of CO_2 and water

vapour. These LTC challenges can be met by optimising combustion control. It has also been mentioned earlier, that optimising combustion control is a viable alternative to the expensive after-treatment devices. Since it would improve combustion efficiency, and hence engine efficiency.

This research work seeks to develop an understanding of in-cylinder spray behaviour for optimising combustion control. From the literature survey, so many investigations on spray characteristics have been conducted, while very limited understanding of the interaction between spray and bowl for emission reduction is available. Where such knowledge existed, the study types were mainly theoretical and numerical. The effects of wall impingement on mixing have generated contradictory results. Between experiments that used flat walls and real combustion chambers the inability of the former to reflect the effects of real bowl geometry was deemed responsible for the disparity. On the other hand, the contradictory results between experimental and numerical studies was inputted to the simulations in the latter that were unable to reproduce the complex turbulent structure (wall jet vortex) generated during the spray and bowl interaction. Even worse, in terms of combustion characteristics, tested bowls either performed or did not perform. No attempts were made to alter the bowl geometry for a better emission performance. However, a general understanding of spray behaviour has been developed to guide this work. Spray and bowl interaction is characterised by: formation of thin film on wall surface, spray rebound off the wall surface, and spray break-up, with ejection of secondary droplets and deposition of liquid mass on the wall. These characteristics depend mainly on the wall surface temperature and droplet thermodynamics properties (which derives mainly from the injection pressure). Diesel combustion and emission are controlled by spray penetration and mixing, which makes the effects of operating parameters, such as injection pressure and ambient density, on spray characteristics to be

significant. DI diesel engine in-cylinder flow behaviour, around TDC, towards the end of compression stroke, is critical for the combustion process. This depends mainly on the evolution and development of the air inducted at intake. It is also at this point that the complex influence of bowl geometry on flow and combustion is manifest. Piston bowl shapes and structures the flow (spray and air) for combustion. Therefore optimising spray/bowl interaction means improving the mixing of air and spray to reduce incomplete combustion.

3 EXPERIMENTAL METHODS

3.1 Introduction

This chapter describes the measurements of the liquid and vapour penetrations of a diesel fuel spray. For this purpose, different test regimes were conducted. These tests allowed for the determination of the influence that the injection parameters (injection pressure and nozzle geometry) and in-cylinder thermodynamics variable (pressure) had on the penetration of diesel spray under evaporative (non-combusting) conditions. The present investigation was conducted experimentally on the optical engine (Proteus) for visualisation of high pressure (free) spray behaviour. High speed visualisation (HSV) using Mie scattering and shadowgraph techniques (with high speed laser and camera) were used to measure spray penetration. The use of an optical engine, as against the commonly used combustion vessels, was to enable the acquisition of data under real engine operating conditions. It also eliminated those critical background conditions due to strong temperature and pressure differentials commonly experienced with combustion vessel test rigs. The results of this research will provide understanding of free spray behaviour, which when combined with wall-impingement studies will facilitate the development of model for emission reduction. Such model can also lead to savings in the cost of designing piston bowls, as it will be possible to favourably change the performance characteristics by altering the geometry.

In the first part of this chapter, the experimental apparatus and set-up are presented. The second part describes the technique and procedures employed for the visualisation of liquid and vapour spray penetrations respectively. Based on the visualisation, the effects of the: injection pressure, in-cylinder pressure (at the point when the fuel was injected) and nozzle geometry (considering different injector

configurations) on spray (liquid and vapour) penetration were investigated. The third, and final, part is dedicated to the illustration of some spray development visualisations and extraction of measurement data.

3.2 Experimental set-up

The set-ups for the liquid and vapour spray measurement were slightly different, but they were based on the Ricardo Proteus rig, where the tests were conducted under thermodynamic conditions similar to those found in a DI diesel engine. Optical diagnostics using high speed image acquisition equipment were developed and optimised around the Proteus, to visualise in-cylinder spray penetration. The key components and description of the set-up are presented below.

3.2.1 The Proteus

The Proteus is essentially a 2-stroke, liner ported, single cylinder reciprocating rapid compression machine (RCM) installed at University of Brighton. It is capable of high realistic combustion conditions for spray analysis of up to 10 MPa in-cylinder pressure and adjustable intake air temperature of up to 423 K. Figure 3-1 shows the key piece of the Proteus rig, which is a specially designed head (top-hat shape and optical chamber, with window access).

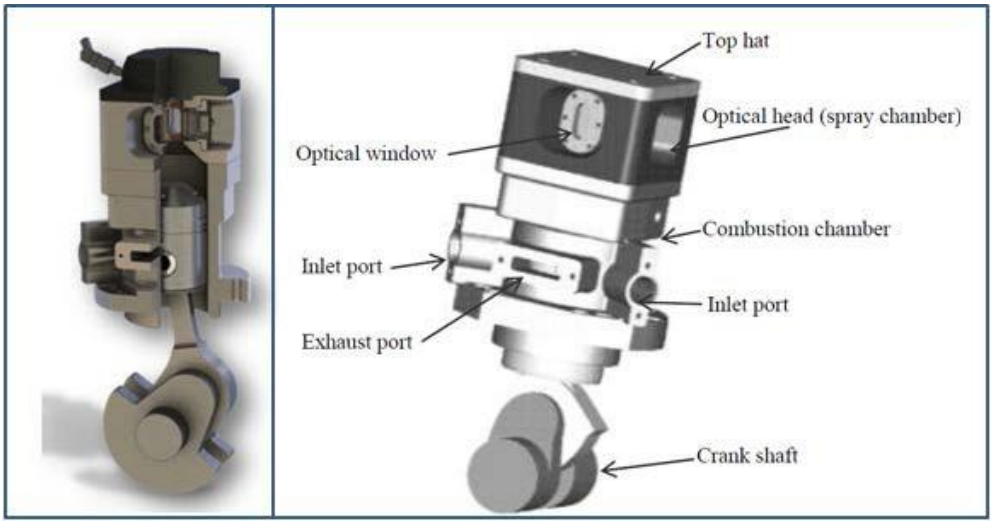

Figure 3-1: CAD drawing of Proteus

The inlet and exhaust ports are located on the cylinder liner, which makes the head free of inlet and exhaust valves. As a result, there is ample room provided by head, with its top-hat design, and the spray chamber, which is complemented by the optical access provided by four removable windows. The head and the spray chamber form a long cylindrical optical chamber, 80mm in length and 50mm in diameter, to enable the visualisation of fully developed fuel spray without impingement. Due to the increased volume of the combustion chamber, as a result of the compromises necessary to implement the optical access, the compression ratio (CR) was reduced. Since the compression ratio is a key element in reproducing similar conditions with production engines, it was therefore necessary to condition the intake air to be representative of production engine. For this purpose, the representative in-cylinder temperatures and pressures were maintained by increasing the boost pressure and temperature up to 0.8 MPa and 373 K respectively. The induced air was then compressed in the engine to achieve the required test conditions (Crua, 2002). In addition, the reduced CR brings some measure of control as early auto-ignition of the fuel/air mixture is avoided. Another consequence of implementing the optical access is less efficient cooling system of the optical combustion chamber compared to a production engine. The Proteus, therefore, operates skip-fire modes to help reduce the thermal load on the

engine. Skip-fire routine is required to avoid unnecessary window fouling, maximise in-cylinder purging and ensure proper laser synchronisation.

Out of the four removable windows, one was used to mount the injector, while the other three were fitted with sapphire glasses to form the optical windows. The size of each window was 25mm in width and 55mm height, and the outer edges of the windows were secured against leakage with an O ring. Window holders secured the sapphire glasses, with a special silicon- based resin (see Figure 3-2). The windows were secured on the Proteus with annealed copper gaskets, which also protected the sapphire windows against the head casting. This design facilitated quick overhaul and cleaning.

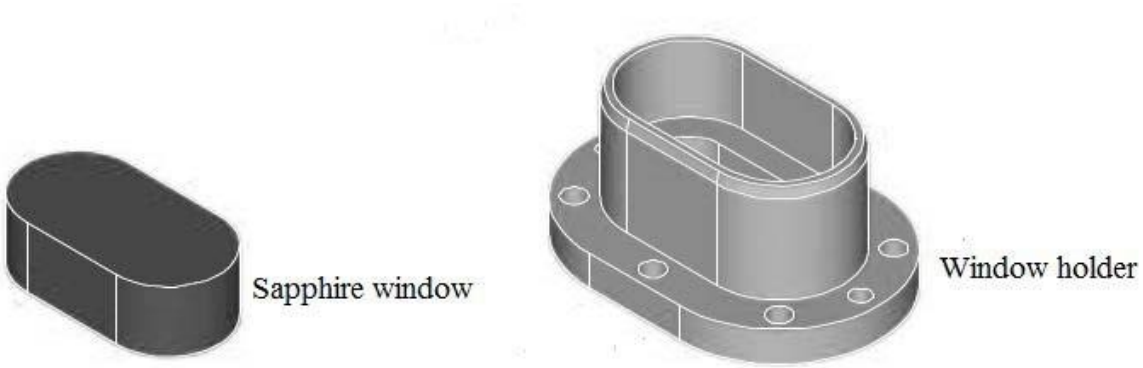

Figure 3-2: CAD drawings of the optical window (Crua, 2002)

Sapphire was considered a suitable material for the window glasses due to its good properties, which included: high mechanical strength, chemical resistance, thermal conductivity and thermal stability. These are vital properties required in a high temperature environment, which is usually encountered during in-cylinder combustion. Under such environment, spectrum absorption (in part or whole) by the window and window fouling are common phenomena that may affect measurements. Sapphire is a synthetic material formed from aluminium oxide (alumina, Al_2O_3), with a single crystal rhombohedra structure and melting point of 2303K. It also has very wide

optical transmission band from ultra violet (UV) to near infra-red (IR) spectrum. As the hardest substance next to diamond, window thickness with sapphire can be made much thinner for the same strength compared to standard optical glass windows.

The design of the Proteus was optimised using Ricardo software (WAVE and VECTIS CFD) for the ports, piston and air motion to achieve efficient scavenging and near quiescent air in the optical chamber. As a result, disturbances due to air motion against spray development, especially at TDC, are reduced with good scavenging efficiency. The Proteus rig was coupled to a DC dynamometer via reduction belts. Under this arrangement, the 3,000 rpm operating speed of the dynamometer, at a reduction gearbox ratio of 6:1, corresponded to an engine operating speed of 500 rpm. In addition, the torque through the dynamo was effectively reduced. Thus for the current study, the Proteus was motored by the dynamometer to 500 rpm, whilst maintaining steady in-cylinder (non-combusting) conditions all through the set of tests.

Usually before initiating motoring operations, the cylinder head was heated by a water jacket (to 85 ^{o}C) and the sump oil (to 35 ^{o}C), which had been heated with immersion heaters, and delivered by the water and oil pumps respectively. This process heated the engine up to realistic operating temperatures before the motoring operation. Losses due to heat transfer from the in-cylinder gas to the surrounding walls were minimised by pumping the heated water and oil before running the engine. The intake air was conditioned to give in-cylinder temperatures and pressures required by the test conditions. Boost air pressure and temperature were PID controlled; engine operating conditions were controlled and monitored by a centrally dedicated control computer using in-house software. The rig was instrumented with sensors for condition monitoring (see Table 3-1 for the sensor specifications). Temperatures were recorded with thermocouples in various key locations, such as: intake, fuel supply,

coolant and oil. Static pressures were measured with strain gauge type pressure transducers at such positions as: intake, oil, fuel supply, and fuel rail. In-cylinder pressure was measured with a Kistler 6125 piezoelectric pressure transducer in conjunction with a Kistler charge amplifier.

Table 3-1: *List of sensors (with the uncertainty of full-scale output, (FSO))*

Sensor	Model	Range [bar]	Uncertainty [%FSO]
Kistler 4045	4045A	0…..500	≤±0.3
Kistler 4067	4067	0…..5000	≤±0.5
Kistler 6125B	6125BU20	0……250	≤±0.5

The specifications of the Proteus rig are: 150 mm stroke, 135 mm bore, 275 mm con-rod length and 2200 cc displacement and 9:1 compression ratio. Its single cylinder design permits spray visualisation under a wide range of operating conditions and easy access of optical diagnostics with minimized amount of test fuel.

3.2.2 Injection system

A high pressure (HP) common-rail system (CRS) fuel injection equipment on the Proteus rig was used for the present study (***Figure 3-3***). It was a relatively flexible system, with less design complications, and capable of achieving injection pressures up to 2000 bar. An electric low-pressure (LP) transfer pump supplied fuel from a reservoir through a fuel filter to the HP pump. The fuel was delivered to the injector according to the test conditions. A heat exchanger was used to return part of fuel to its original temperature prior to entering the reservoir. This was to avoid fuel spill, and a fuel return line was available for the purpose. There was also a unit (electronic control unit, ECU) that directly controlled system`s operation. On a typical engine, the CRS

pump would be driven by crankshaft/camshaft via a belt running at either same or half the engine speed. For the Proteus, an external electric motor was installed to run the pump independently of the engine. Once pumping, the fuel was pressurized to the pre-set rail pressure before the appropriate quantity of fuel was transferred to the rail. This arrangement maintained the required high pressure levels in the fuel rail, and ensured a stable line pressure with minimum fluctuation, which would have been difficult to achieve with crankshaft/camshaft as the driver.

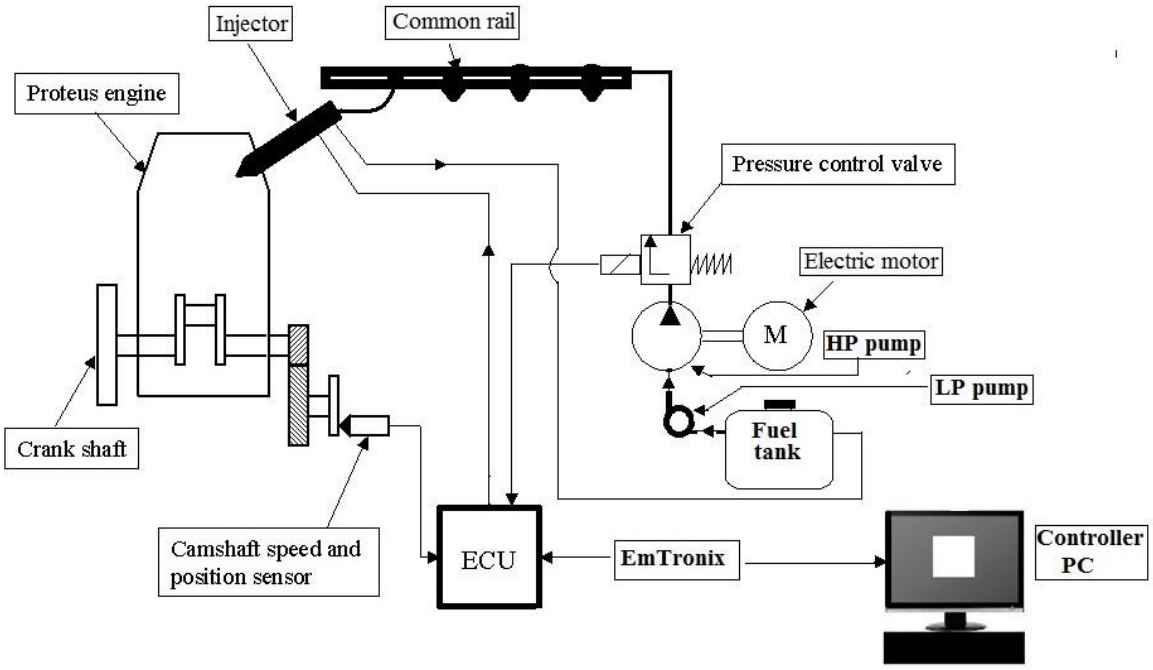

Figure 3-3: Schematic of the Proteus injection system

Different injector configurations by Delphi and Bosch were used for the tests to enable comparison of results (e.g. ***Figure 3-4***(a)). These electrically controlled solenoid injectors had main features in common, which included: solenoid, the control needle, the main needle, the fuel supply and return lines. The common rail and delivery pipe were both instrumented with another Kistler pressure transducer, with the delivery pipe kept short just as in real engines. Only one out of the four common

rail injector outlets was used at any given time, so the other unused three were fitted with plugs. For the rig, a special microprocessor-based controller implemented by the EmTronix system enabled independent control of injection timing, number of injections per cycle, injection duration and rail pressure. The copper- vapour laser (***Figure 3-4***(b)) was operated at 50,000 Hz pulsing frequency to illuminate the in-cylinder spray through the optical window. Phantom cameras (v12.1 and v710), which are CMOS-based high speed camera, were used (***Figure 3-4***(c)) for the tests. They are capable of a very high image acquisition rate at a reduced resolution. For the tests, they were operated in the range 41,000 - 42,000 Hz framing speed for an exposure of 23 - 24 µs.

The rig synchronization logic, which covered triggering of the injector and the secondary devices (laser system and the high speed camera), as well as data acquisition was implemented by the EmTronix programming and the associated hardware, which consisted of: controller computer and the BNC triggering device (see ***Figure 3-5***). Prior to the start of any batch of tests, the injection parameters (e.g. injection angle, injection duration, rail pressure, delay of secondary trigger, etc.) were uploaded to the system via a personal computer. This gave high timing accuracy and good parameter control, even though these settings could be altered during the run.

(a): 2000 bar Delphi DFI 1.5 injector *(b): 50 kHz Laser strobe*

(c): Phantom camera

Figure 3-4: Items for the visualisation tests

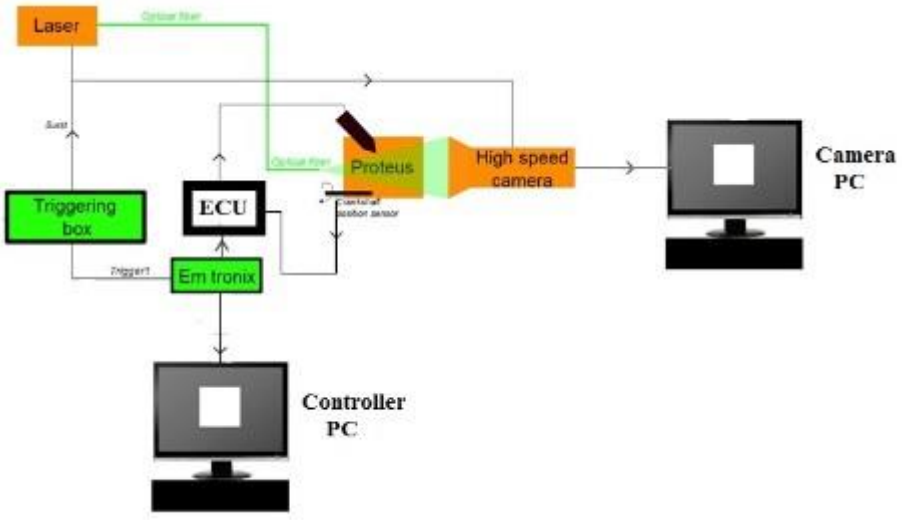

Figure 3-5: Simplified schematics of the Proteus triggering system

3.2.3 Set-up description

Below is a summary of the set-up for the experiments, which was developed around the modern laser diagnostic technique used for the spray measurements.

- Experimental methods
    - High speed visualisation for liquid spray penetration
    - High speed laser shadowgraph for vapour spray penetration
- Optical set-up
    - Copper-vapour laser (CVL):
        - Light source
        - Pulsing frequency, 50 kHz
        - Pulse duration, 10 ns
        - Instantaneous power, 8kW
    - Phantom (v12.1 and v710) high speed cameras:
        - Framing
        - Sample rate, 41,000 – 42, 000 frames per second (fps)
        - Exposure 23 -24 µs
    - EmTronix system and BNC trigger: synchronisation

For all the tests, the key steps included: installation of equipment, engine warm-up, motoring, uploading and adjusting parameters to achieve desired PID, fuel injection, data capture and shut down. A reference fuel with low sulphur content and representative for automotive diesel was used for the experiments. Its properties are attached as appendix A. Engine logs were recorded with AVL Indiset high speed data acquisition system for fast logs (crank angle resolved), and EmTronics data logger for slow logs. For each regime of test, a minimum of fifty (50) videos were recorded with the laser/camera combination. The videos were post- processed with in-house software (Matlab based) and analysed.

3.3 Liquid spray visualisation

Liquid-phase diesel fuel penetration is a paramount consideration in optimising in-cylinder processes, especially for the small-bore DI diesel engines and given the

present trend of engine downsizing. Penetration of the liquid phase fuel is needed to promote fuel-air mixing. Over-penetration can result in fuel impingement on the combustion chamber walls, while under-penetration can lead to an unsatisfactory fuel–air mixture and consequently reduced the combustion efficiency (Park et al., 2009). As a result, visualisation would facilitate a better understanding of the parameters and the processes that control the extent of the liquid-phase fuel in a diesel spray. This is very important to both the engine designer and to those developing multi-dimensional computational models for use as engine design and optimization tools. Present understanding in the area has been developed mainly through: investigating the effective parameters on liquid penetration length, optimizing the combustion conditions to reach the optimum penetration length, and deriving theoretical and impractical governing correlations. More insight is still needed.

The liquid spray visualisation experiments were conducted with four different solenoid- actuated, injectors with sac volume nozzles. Specifications for the injectors are shown in ***Table 3-2***. The diagnostic technique used for this experiment is known as Mie scattering, which is an elastic scattering technique. Mie scattering is used for light scattering of droplets or particles with a diameter size equal to or larger than the wavelength of the used laser beam (Hecht, 2002). The intensity of Mie scattered radiation is given by the summation of an infinite series of terms rather than by a simple mathematical expression. The Mie theory is beyond the scope of this work, and the Mie scatter method that is often used to define particle or droplet sizes is not implemented here. Rather the Mie scatter employed for this work is the applied scattering regime. By this approach, the laser beam was aligned to pass through the vertical plane of the fuel spray and cause elastic scattering of the laser light by the liquid fuel droplets as soon as fuel was injected into the chamber. The high speed camera was positioned perpendicular to the laser illumination to collect the scattered light. This

visualised the liquid fuel distribution and showed the liquid penetration within the spray. For injectors B, C and D experiments, the laser light was collimated, with the intensity reduced by neutral density filters. In this arrangement, the filter was carefully placed between the laser and a collimating lens; so that the laser light was collimated before entering the optical engine. The injector A experiment was not conducted with collimated light. However, the set-ups (***Figure 3-6***) for the liquid penetration tests were essentially similar, and included key items such as: injector, the Proteus, Phantom camera, high speed cupper vapour laser and computers (control and camera PCs).

Table 3-2: Injector specifications

	Model number	**Hole**	**Hole size (mm)**	**Flow (cc/min)**	**Cone angle (⁰)**	**k- factor**
Injector A (Delphi)	DFI 1.5	7	0.131	770	155	2
Injector B (Delphi)	DFI 1.5	8	0.13	860	156	1.5
Injector C (Bosch 3601)	Customised	8	0.137	960	155	1.3
Injector D (Bosch 3603)	Customised	8	0.137	960	155	3.5

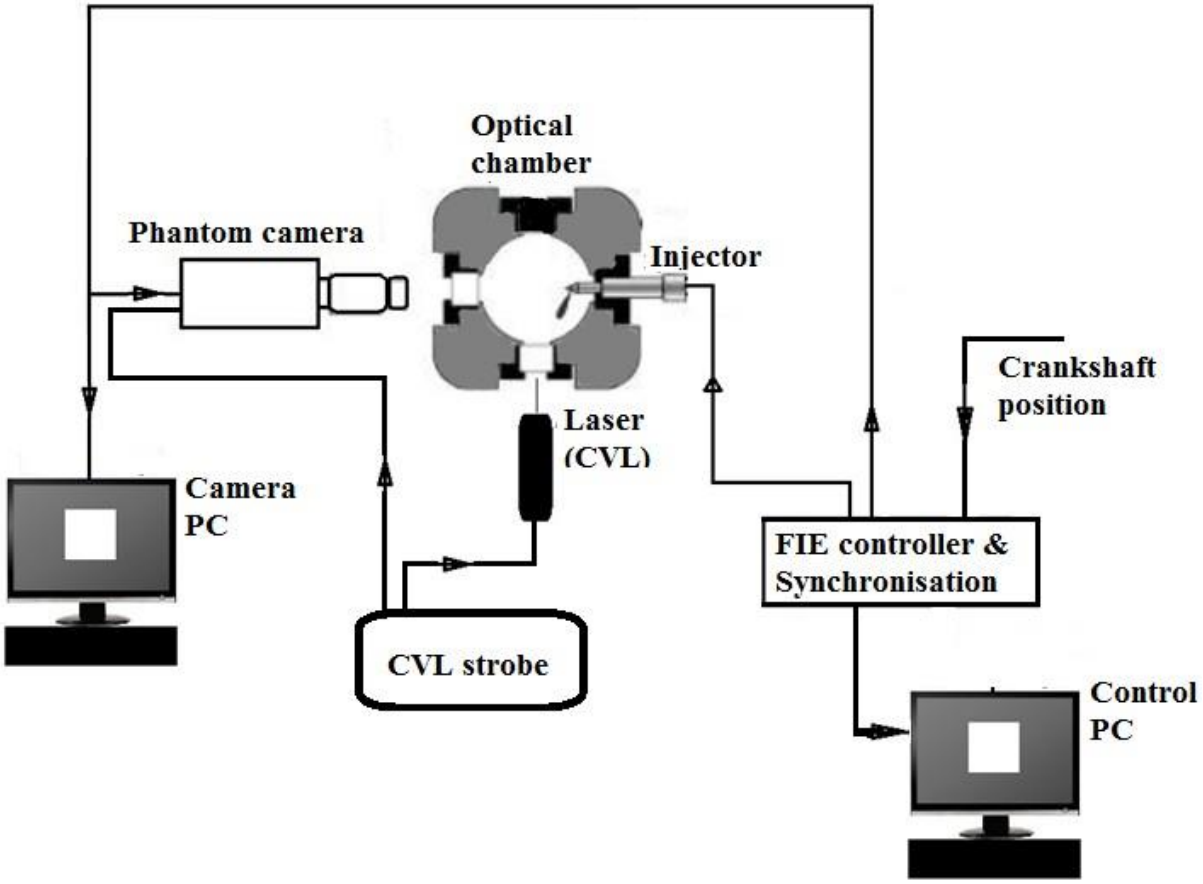

Figure 3-6: Schematic for Liquid spray visualisation

For all the experiments in this work certain key steps were repeated. These included: preparation of the Proteus, camera calibration, determination of spatial factor and spray orientation, setting-up/focussing of the laser, final checks to eliminate all forms of leakages and engine warm-up to the required starting conditions. These steps prepared the engine for the crucial processes of matching the engine with test point condition for actual tests to proceed, and acquisition of video images and logs. In addition, the engine was stopped at intervals, during the tests, to clean the optical windows. For the test conditions, the intake air temperature is determined by the intake manifold temperature (TMAN).

3.3.1 Procedure for Injector A liquid spray experiment

Injector A was used in the set-up (***Figure 3-6***) for target test conditions shown in ***Table 3-3***.

Table 3-3: Target test conditions for Injector A liquid spray tests (generated by the Project partner, Ricardo UK).

Test point **TP**	ntake air temperature **TMAN (^{o}C)**	Peak in-cylinder pressure **ICP (bar)**	Fuel pressure **P (bar)**	Fuelling **(mm^{3})**
1	100	84	2000	65
2	100	84	1600	36.31
3	100	84	1400	36.71
4	100	84	1000	35.31
5	100	84	600	34.86
6	100	50	2000	45
7	100	50	1600	45
8	100	50	1400	45
9	100	50	1000	25
10	100	66	2000	65
11	100	66	1400	45
12	100	66	1000	45
13	100	79	1800	60
14	100	73	1600	50
15	100	40	600	20

The laser provided sufficient illumination for a high speed Phantom v12.1 camera to capture the in-cylinder liquid spray development at a sample rate of 41822 fps from the start of injection. The spray parameters obtained for the injection sample were: liquid phase penetration length, the liquid dispersion angle and spray axis.

- Determination of spatial scale factor – this was calculated before (pre) and after (post) the test using a target (***Figure 3-7***) well positioned in the optical chamber for image acquisition with the high speed camera only. Two points, **A**(x_1, y_1) and **B**(x_2, y_2) at certain picture-elements (pixels) apart, were captured to compare their actual distance apart in millimetres (mm). It was important to calculate the spatial scale factor before and after the test in order to ensure that the settings had not been accidentally modified, which will be indicated by a significant variation in the scale factor value.

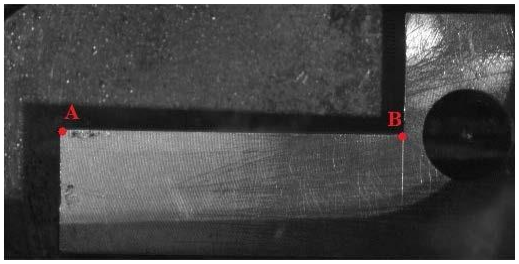

Figure 3-7: Points A and B on target specimen

Pre-test

A = (57 pixels, 125 pixels)
B = (400 pixels, 131 pixels)
Vertical distance between planes **A**/**B** (pixels)

$$=\sqrt{((400-57)^2-(131-125)^2)}$$

= 343.0 pixels

Actual horizontal distance between planes **A**/**B** (mm) = 28.6 mm

Spatial scale factor = $\frac{28.6}{343.0}\,\mathrm{mm}/\mathrm{pixel}$

= **0.0835 mm/pix**

Post-test

A = (56 pixels, 106 pixels)
B = (401 pixels, 130 pixels)
Vertical distance between planes **A**/**B** (pixels)

$$=\sqrt{((401-56)^2-(130-106)^2)}$$

= 344.2 pixels

Actual horizontal distance between planes **A**/**B** (mm) = 28.6 mm

Spatial scale factor = $\frac{28.6}{344.2}\,\mathrm{mm}/\mathrm{pixel}$

= **0.0832 mm/pix**

3.3.2 Procedure for Injector B liquid spray experiment

The test procedures using the set-up in Figure 3-6 were repeated with injector B for target conditions shown in ***Table 3-4***. The laser provided sufficient illumination for the high speed Phantom v12.1 camera to capture the in-cylinder liquid spray development at a sample rate of 42010 fps from the start of injection. Liquid length penetration was the spray parameter obtained for the injection sample.

Table 3-4: Target test conditions for Injector B liquid spray tests

Test Point (TP)	***TMAN*** (°C)	***Peak ICP*** *(bar)*	***Fuel P*** *(bar)*	***Fuelling*** *(mm^3)*
4	100	84	1000	35.31
6	100	50	2000	45
9	100	50	1000	25
14	100	73	1600	50
15	100	40	600	20

- Spatial scale factor – for this and subsequent measurements, the target used earlier was replaced with the target shown in ***Figure 3-8***. This target was calibrated (shown by the grid lines) so that the actual distance between planes in millimetres (mm) could be read off directly.

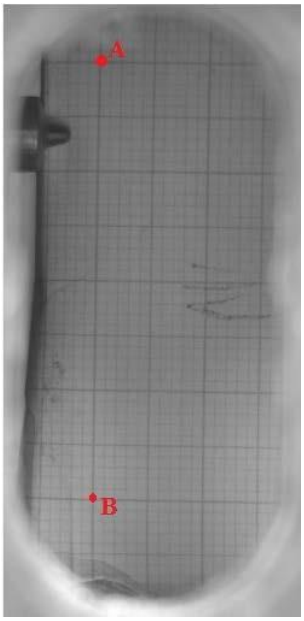

Figure 3-8: Calibrated target

Pre-test

A = (117 pixels, 89 pixels)
B = (111 pixels, 468 pixels)

Vertical distance between planes **A**/**B** (pixels)

$$=\sqrt{((468-89)^2-(117-111)^2)}$$

= 378.9525 pixels

Actual vertical distance between planes **A**/**B** (mm) = 40 mm

Spatial scale factor = $\frac{40}{378.9525}$ mm/pixel

= **0.106 mm/pix.** This value did not change after the tests.

- Spray orientation – whilst setting-up for the tests, it was observed that the spray orientation was different from expected. Hence, a spray orientation check was conducted to find out if the injector was well positioned. The existence of the small angle between the spray plane and the vertical was confirmed when a calibrated target was placed close to the injector plane. Depending on the view (***Figure 3-9***), angles ***x*** and ***y*** were determined. The choices of variables were for illustrative purposes only. This method of determining spray orientation was applied to the remaining tests conducted in this work. The views represented by ***x*** and ***y*** applied to liquid and vapour spray penetrations, respectively. While the values for the variables were taken into account in processing the appropriate video images. Thus, for Injector B liquid spray penetration experiments, only ***y*** (12^o) applied.

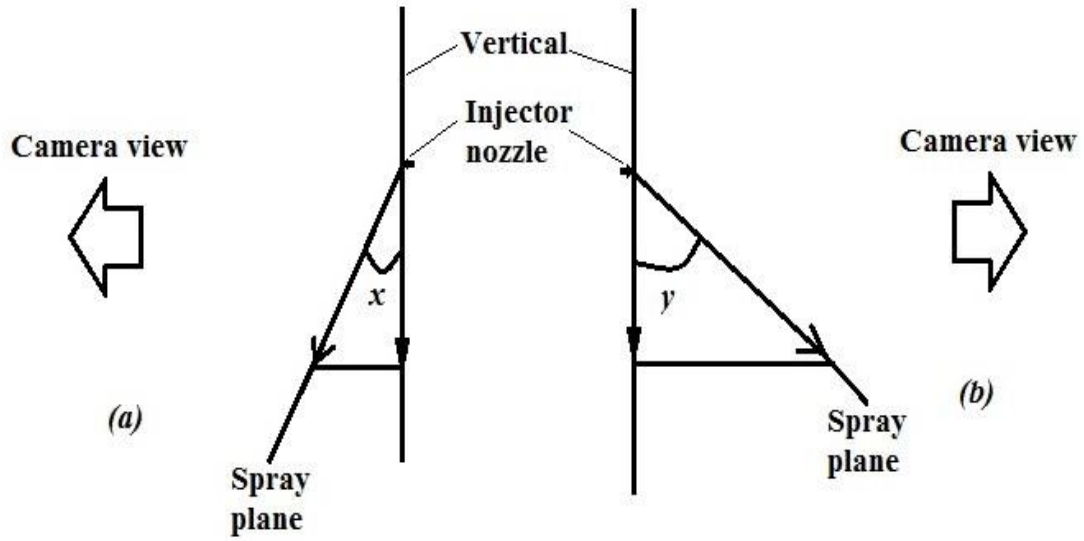

Figure 3-9: Spray orientation

3.3.3 Procedure for Injector C liquid spray experiment

The test procedures using the set-up in *Figure 3-6* were repeated with injector C for

target conditions shown in ***Figure 3-9***, but with a Phantom v710 high-speed camera. This ultra-fast camera and the high speed laser combination enhanced the capture of in-cylinder liquid spray development at every 20µs from the start of injection. Liquid spray penetration, dispersion and axis were the spray parameters obtained for the injection sample.

Table 3-5: Target test conditions for Injector C liquid spray tests

Test Point *(TP)*	***TMAN*** (^{o}C)	***Peak ICP*** *(bar)*	***Fuel P*** *(bar)*	***Fuelling*** *(mm^3)*
2	100	84	1600	36.31
4	100	84	1000	35.31
7	100	50	1600	45
9	100	50	1000	25
14	100	73	1600	50
15	100	40	600	20

- Spatial scale factor –

Pre-test

A = (125 pixels, 49 pixels)
B = (118 pixels, 459 pixels)
Vertical distance between planes **A**/**B** (pixels)

$$=\sqrt{((459-49)^2-(125-118)^2)}$$

= 409.940 pixels

Actual vertical distance between planes **A**/**B** (mm) = 45 mm

Spatial scale factor = $\frac{45}{409.940}\ \mathrm{mm/pixel}$

= **0.1098 mm/pix**

Post-test

A = (90 pixels, 46 pixels)
B = (99 pixels, 454 pixels)
Vertical distance between planes **A**/**B** (pixels)

$$=\sqrt{((454-46)^2-(99-90)^2)}$$

= 407.90 pixels

Actual vertical distance between planes **A**/**B** (mm) = 45 mm

Spatial scale factor = $\frac{45}{407.90}\ \mathrm{mm/pixel}$

= **0.1103 mm/pix**

- Spray orientation – with the method developed in ***Figure 3-9***, the angles ***x*** (8.7^{o}) and ***y*** (13^{o}) were determined. For Injector C liquid spray experiments, only ***y*** (13^{o}) applied.

3.3.4 Procedure for Injector D liquid spray experiment

The test procedures using the set-up in ***Figure 3-6*** were repeated with injector D for target conditions shown in *Table 3-6* with a Phantom v710 high-speed camera. Acquisition at every 20µs from the start of injection was also achieved. Liquid spray penetration, dispersion and axis were the spray parameters obtained for the injection sample.

Table 3-6: Target test conditions for Injector D liquid spray tests

Test Point *(TP)*	***TMAN*** (^{o}C)	***Peak ICP*** *(bar)*	***Fuel P*** *(bar)*	***Fuelling*** *(mm^3)*
2	100	84	1600	36.31
4	100	84	1000	35.31
7	100	50	1600	45
9	100	50	1000	25
14	100	73	1600	50
15	100	40	600	20

- Spatial scale factor –

Pre-test

A = (125 pixels, 49 pixels)

B = (118 pixels, 459 pixels)

Vertical distance between planes **A**/**B** (pixels)

$$=\sqrt{((459-49)^2-(125-118)^2)}$$

= 409.940 pixels

Actual vertical distance between planes **A**/**B** (mm) = 45 mm

Spatial scale factor = $\frac{45}{409.940}$ mm/pixel

= **0.1098 mm/pix**

Post-test

A = (90 pixels, 46 pixels)

B = (99 pixels, 454 pixels)
Vertical distance between planes **A**/**B** (pixels)
= $\sqrt{((454-46)^2 - (99-90)^2)}$

= 407.90 pixels

Actual vertical distance between planes **A**/**B** (mm) = 45 mm
Spatial scale factor = $\frac{45}{407.90}$ mm/pixel

= **0.1103 mm/pix**

- Spray orientation – the angles ***x*** (8.7^o) and ***y*** (13^o) were determined. For Injector D liquid spray experiments, only ***y*** (13^o) applied.

3.4 Vapour spray visualisation

Vapour spray visualisation was conducted with Injectors B, C and D, using the set-up shown in ***Figure 3-10***. The components essentially included a collimating lens and filter, with the high speed camera in a different position from that of liquid visualisation tests. Collimating lens selection depended on the laser diameter and desired collimated beam diameter. The beam divergence has a reciprocal relation with beam radius no matter the type of lens used. Nevertheless, a simple plano-convex lens was selected to provide an optimum trade-off and generate less spherical aberration. Plano-convex lens are simple and cheap: the appropriate diameter and focal length can easily be acquired. The laser beam used for this work was reasonably collimated with very small divergence. Beam divergence of a laser beam is a measure of how fast the beam expands far from the beam waist during propagation. The small beam divergence implemented for this application was therefore necessary to ensure an approximately constant beam radius over the propagation distance. The filters reduced the intensity of the high speed laser to eliminate image saturation.

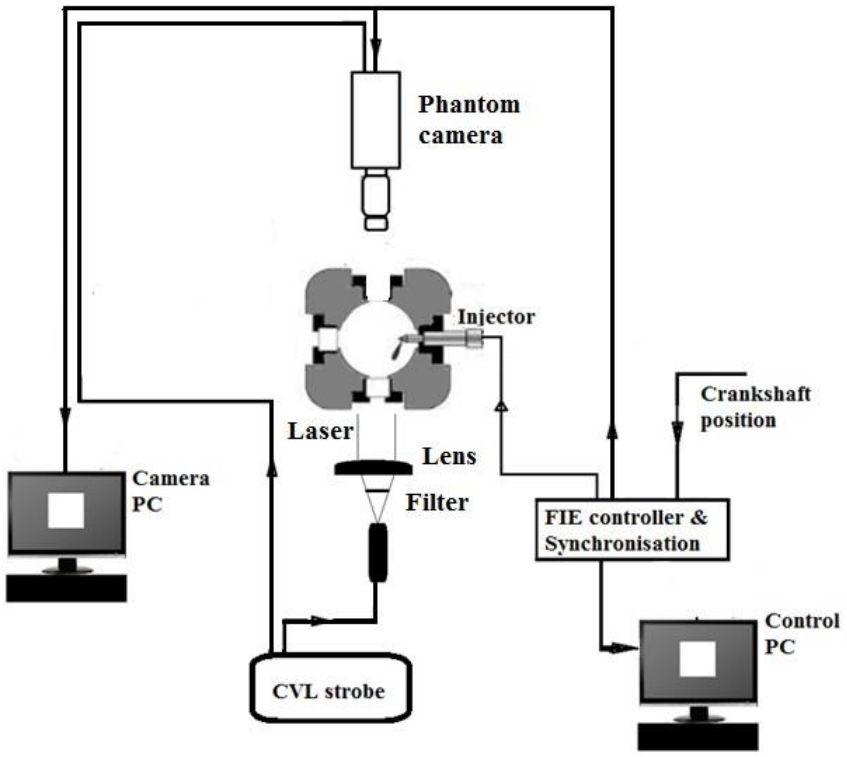

Figure 3-10: Set-up for vapour visualisation

The visualisation of vapour spray penetration is usually conducted with either Schlieren or shadowgraph technique. ***Figure 3-10*** is a shadowgraphy set-up. This was confirmed by testing the sensitivity of the optical instrument to a density change: since a schlieren system is sensitive to the first derivative of density while shadowgraphy is sensitive to the second derivative of density. In the test conducted for the purpose, with the set-up in ***Figure 3-10***, the image in ***Figure 3-11*** (a) was acquired. A typical curve to illustrate the step change in density is constructed in (b), as the parent function (*f(x)*). The first (*f'(x)*) and second (*f''(x)*) derivatives of *f(x)*, shown in (c) and (d) respectively, were determined by identifying the points of inflection: horizontal (maxima and minima points) and vertical. With these points, it was possible to determine the changes in sign of the derivatives (as shown in (b) through (d)). Only (d) significantly matched the AA cross-section on the image in (a). Across AA, shades of white and grey are seen on either side of a continuous black band. The intensity plot at AA would show, the white and grey shades represented as peaks on

either side of a steady darker profile, to confirm the similarity of the section and the profile in (d). It should be noted that only one spray plume was isolated for the exercise, masking of other plumes will be explained later in the text during the actual image processing of the experimental results.

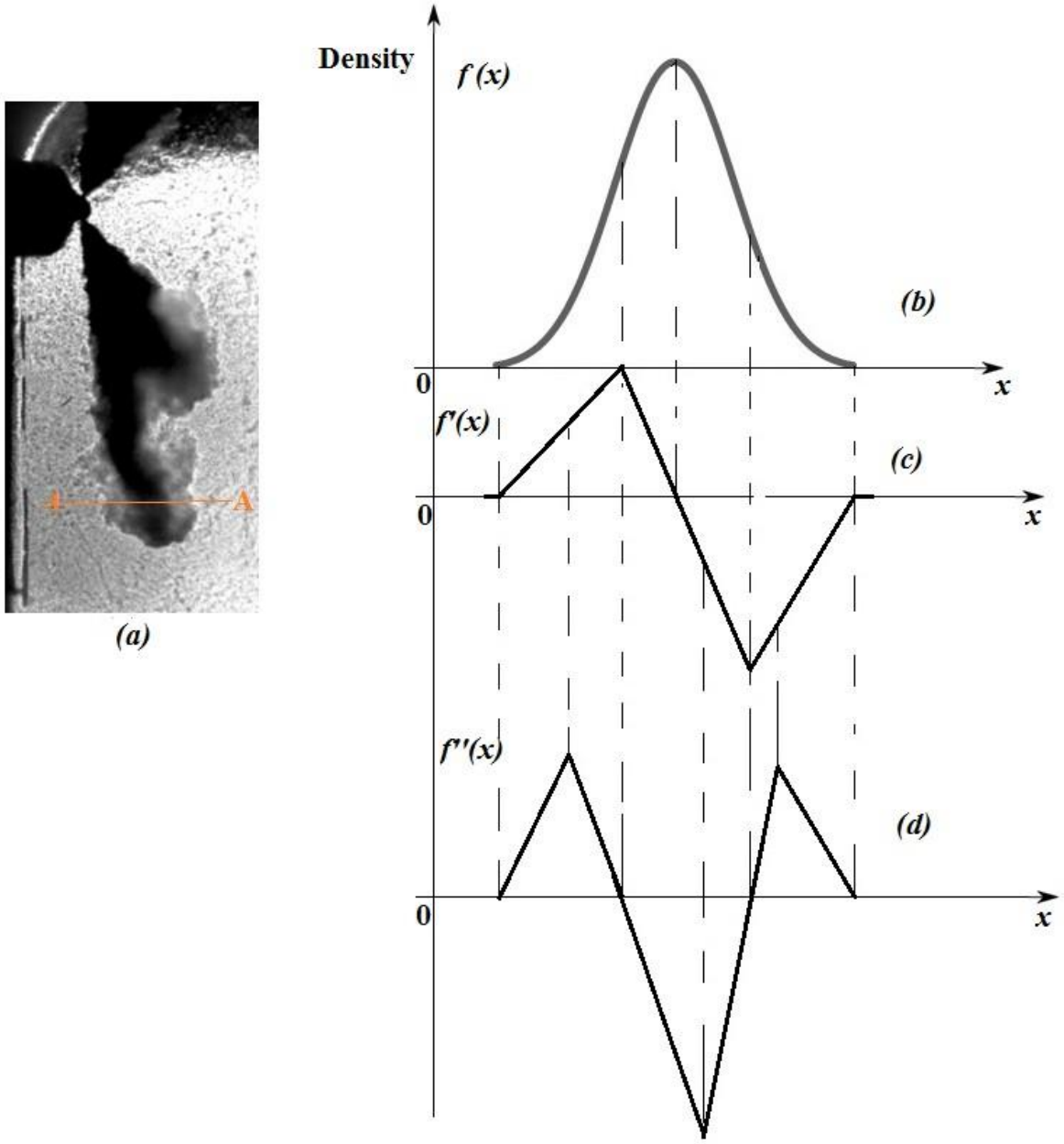

Figure 3-11: Response to density changes

The choice of the shadowgraph technique was informed by the need to get the best out of the high speed laser. Diffraction which is a major problem with the use of laser was reduced with absence of edges (e.g. knife edge and collecting lens). The

shadowgraphy implemented in this work was sensitive enough to capture the edge regions of the spray as shown in *Figure 3-11*(a). Thus the additional sensitivity of a Schlieren set-up, where knife edge and collecting lens are common features, was not desired because it typically enhances the dark or bright regions that should be avoided The pulsing nature of the high speed laser and its monochromatic brightness make it possible to instantly freeze a rapidly developing phenomenon for image acquisition, with short camera exposure. Camera exposure that is shorter than the pulse length prevents image blurring by high speed lasers. For shorter pulse length than the exposure, the freezing is achieved by the short illumination of the laser. Laser can also be used with suitable filters to separate combustion luminosity from developing spray. Other advantages of the laser include: improved image brightness, power efficiency and reduced size of the illumination source

3.4.1 Procedure for Injector B vapour spray experiment

The set-up in ***Figure 3-10*** was used with injector B for target conditions shown in ***Table 3-7***. High speed laser was used together with the Phantom v12.1 camera to capture the in-cylinder vapour spray development at a sample rate of 41822 fps. Vapour penetration was the spray parameter obtained for the injection sample as described later in this chapter.

Table 3-7: Target test conditions for Injector B vapour spray tests

Test Point *(TP)*	***TMAN*** (^{O}C)	***Peak ICP*** *(bar)*	***Fuel P*** *(bar)*	***Fuelling*** *(mm^3)*
4	100	84	1000	35.31
6	100	50	2000	45
9	100	50	1000	25
13	100	79	1800	60
14	100	73	1600	50
15	100	40	600	20

- Spatial scale factor –

  Pre-test

  A = (145 pixels, 22 pixels)
  B = (156 pixels, 342 pixels)
  Vertical distance between planes **A**/**B** (pixels)
  $=\sqrt{((342-22)^2-(156-145)^2)}$

= 319.810 pixels

Actual vertical distance between planes **A**/**B** (mm) = 40 mm

Spatial scale factor = $\frac{45}{319.810}$ mm/pixel

= **0.141 mm/pix.** This value did not change after the tests

- Spray orientation – the angle ***x*** (12) was determined for this experiment.

3.4.2 Procedure for Injector C vapour spray experiment

The test procedures using the set-up in ***Figure 3-10*** were repeated with injector C for target conditions shown in ***Table 3-8***. High speed laser and Phantom v710 high-speed camera were used to capture spray development at a sample rate of 50000. Vapour penetration was the spray parameter obtained for the injection sample.

Table 3-8: Target test conditions for Injector C vapour spray tests

Test Point *(TP)*	***TMAN*** (^oC)	***Peak ICP*** *(bar)*	***Fuel P*** *(bar)*	***Fuelling*** *(mm^3)*
2	100	84	1600	36.31
4	100	84	1000	35.31
7	100	50	1600	45
9	100	50	1000	25
14	100	73	1600	50
15	100	40	600	20

- Spatial scale factor –

Pre-test

A = (125 pixels, 49 pixels)
B = (118 pixels, 459 pixels)
Vertical distance between planes **A**/**B** (pixels)

$$=\sqrt{((459-49)^2-(125-118)^2)}$$

= 409.940 pixels

Actual vertical distance between planes **A**/**B** (mm) = 45 mm

Spatial scale factor = $\frac{45}{409.940}\ \mathrm{mm/pixel}$

= **0.1098 mm/pix**

Post-test

A = (90 pixels, 46 pixels)
B = (99 pixels, 454 pixels)
Vertical distance between planes **A**/**B** (pixels)

$$=\sqrt{((454-46)^2-(99-90)^2)}$$

= 407.90 pixels

Actual vertical distance between planes **A**/**B** (mm) = 45 mm

Spatial scale factor = $\frac{45}{407.90}\ \mathrm{mm/pixel}$

= **0.1103 mm/pix**

- Spray orientation – For Injector C vapour spray penetration experiments ***x*** (8.7^o) was determined and applied.

3.4.3 Procedure for Injector D vapour spray experiment

Testing was also conducted with Injector D using the set-up in ***Figure 3-10*** for the target conditions in ***Table 3-9***. The high speed laser and ultra-fast Phantom v710 provided acquisition frequency of 50000 fps. Vapour spray penetration was the spray parameter obtained for the injection sample.

Table 3-9: Target test conditions for Injector D vapour spray tests

Test Point *(TP)*	***TMAN*** (^{o}C)	***Peak ICP*** *(bar)*	***Fuel P*** *(bar)*	***Fuelling*** *(mm^3)*
2	100	84	1600	36.31
4	100	84	1000	35.31
7	100	50	1600	45
10	100	50	1000	25
14	100	73	1600	50
15	100	40	600	20

- Spatial scale factor –

Pre-test

A = (125 pixels, 49 pixels)
B = (118 pixels, 459 pixels)
Vertical distance between planes **A**/**B** (pixels)

$$=\sqrt{((459-49)^2-(125-118)^2)}$$

= 409.940 pixels

Actual vertical distance between planes **A**/**B** (mm) = 45 mm

Spatial scale factor = $\frac{45}{409.940}\,\mathrm{mm/pixel}$

= **0.1098 mm/pix**

Post- test

A = (90 pixels, 46 pixels)
B = (99 pixels, 454 pixels)
Vertical distance between planes **A**/**B** (pixels)

$$=\sqrt{((454-46)^2-(99-90)^2)}$$

= 407.90 pixels

Actual vertical distance between planes **A**/**B** (mm) = 45 mm

Spatial scale factor = $\frac{45}{407.90}$ mm/pixel

= **0.1103 mm/pix**

- Spray orientation – using the developed method, ***x*** (8.7^{o}) was determined and applied.

3.5 Image processing

This is a critical step in data analysis, where spray parameters are quantified with respect to time after start of injection (ASOI) for every spray plume. After each test regime, the video images (at least 50) generated were saved in the cine format of the phantom camera and stored in an electronic folder. These images were read into Matlab where the post-processing was implemented by opening the images, and subjecting them to enhancement (***Figure 3-12*** and ***Figure 3-13***) and contour analysis. The post-processing is actually based on pixel thresholding and conversion of images to a binary format (Abu-Gharbieh, 2001).

In order to open the images, an in-house adapter code was developed since there was no extension for the native camera format (-cine) in Matlab. The images were corrected for background artefacts and reflections. Since the injectors used in this work were multi-hole, with corresponding number of spray plumes, a mask was applied. Masking tells the software to recognise only a particular spray with inputted pixel coordinates of the orifice. This isolates the spray from other spray plumes. The spray image was then 'binarised' (converted to black and white) using a threshold determined based on the image intensity distribution. The threshold level was subjectively implemented by selecting a complete test run and varying the threshold level to achieve optimum results. This applied to all the images in a particular batch, since it was assumed that the quality of the spray images and the intensity of the laser energy did not change significantly. Masking and thresholding are not only beneficial in eliminating

background spray scatter, they also permit differentiation between interacting spray which reduces interference to measurement.

However, a boundary was traced around the 'binarised' spray. The spray contour thus obtained was analysed with respect to spray penetration and (in some cases) dispersion angle characteristics, taking into account the corresponding spatial resolution and spray angle (where necessary). While the leading edge of the spray boundary defined the maximum liquid penetration, the dispersion angle (cone angle) was calculated as the angle included between the two lines that fitted a fixed portion of the spray contour (***Figure 3-14***). A detached spray slug was observed at the leading edge of the spray of some images. This detached slug was a discontinuous region of the liquid spray, and hence was not considered in defining the penetration length.

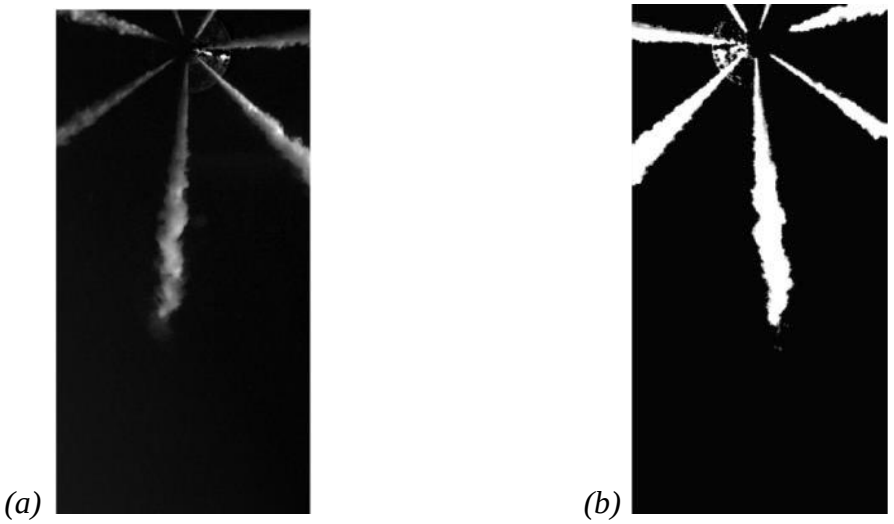

*Figure 3-12**:** Liquid penetration image before (a) and after (b) correction and binarisation. Image captured with injector A in the steady period at TP06 conditions (in-cylinder conditions, 100 ^{o}C, 50 bar and injection pressure, 2000 bar)*

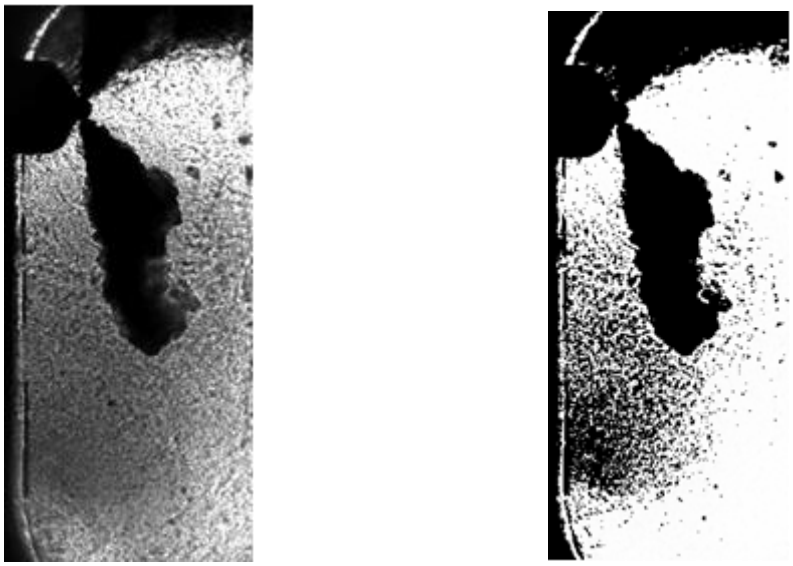

(a) *(b)*

Figure 3-13: Vapour penetration image, before (a) and after (b) correction and binarisation. Image captured with injector B in the steady period at TP15 conditions (in-cylinder conditions, 100 ^{o}C, 40 bar and injection pressure, 600 bar).

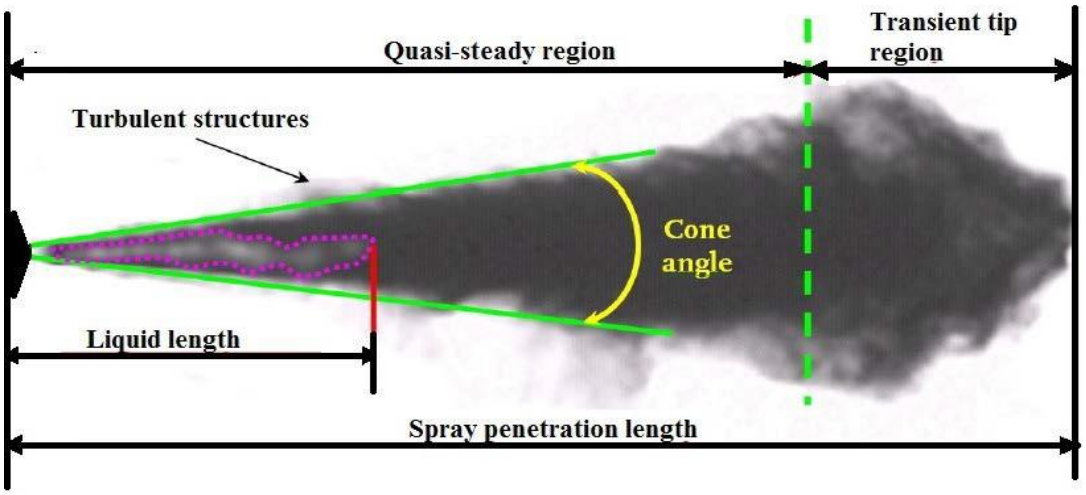

Figure 3-14: Typical spray penetration profile [adapted from the vapour spray image captured with injector B in the steady period at TP15 conditions (in-cylinder conditions, 100 ^{o}C, 40 bar and injection pressure, 600 bar)]

The processing technique described above was executed for each frame of the spray video to determine the temporal variation of spray characteristics. Results were presented for the mean (and median) penetration as a representative value of the spray characteristics. These results were exported to an Excel spreadsheet.

3.6 Engine log analysis

After each test, figures were recorded for various engine parameters. The figures for parameters of interest were processed with an Excel spreadsheet to evaluate the statistics and perform an uncertainty analysis. Through this approach, the actual conditions of the tests were determined.

It is necessary to quantify the errors (which are usually inevitable in any experiment) encountered with the measurements. Standard deviation and the uncertainty analysis are important tools for the purpose. However standard deviation only suggests how measured values deviate from value that the data tends to (average value). As an indication of how precise the values are, standard deviation simply measures error in the data. Analysing the experimental uncertainties is required to take into account all sources of error, both random (error due to human or imprecise equipment) and systematic (error due to equipment or applied technique), that affect the measurement results. Standard deviation and all sources of error are components of uncertainty. Thus uncertainty statement assigns credible limits to the accuracy of a reported value, stating to what extent that value may differ from its reference value (Eisenhart, 1962). In this study, performing an uncertainty analysis is an important aspect of validating the experimental results with any reference (such as the comparison with the Naber JD et al., (1996) model conducted in the next chapter). The analysis will provide coverage with a high level of confidence, and large degree of freedom. In the calculations that will follow, 2 was chosen as the degree of freedom to approximate 95% coverage, which is the probability that the actual value of the quantity estimated is within the interval defined by the confidence limits.

3.6.1 Injector A engine logs for liquid spray test

- Actual test conditions – ***Table 3-20*** shows the actual conditions for the liquid

spray tests conducted with Injector A.

Table 3-10: Actual test conditions for Injector A liquid spray

tests (a): Test summary

Injector:	Injector A (Delphi), 7 holes (155^0, 0.131mm, 2)
Injector condition:	Previously used
Injector crank angle:	TDC
Skipped cycle strategy:	1 fired for every 10 cylces
Camera frame resolution:	512 x 256 pixels, 12bit/pix
Spatial scale factor:	0.0835 mm/pix (pre-test), 0.0832 mm/pix (post-test)
Injection samples:	At least 50 recordings per test point

(b): Actual test conditions as mean values with standard deviation

Test point TP	Fuel tank temperature T (^{O}C)	Intake air temperature TMAN (^{O}C)	In-cylinder pressure @ TDC ICP TDC (bar)	Fuel pressure P (bar)
1	36.7±1.1	99.5 ±0.7	83.3 ±0.9	1946.1 ±
2	30.7±1.3	99.2 ±0.8	83.4 ±1.0	1590.6
3	32.2±0.9	99.9 ±0.5	83.6 ±1.0	1398.7
4	29.8±0.5	99.4 ±0.8	83.7 ±0.8	991.0
5	30.4±0.3	98.3 ±0.5	84.1 ±0.8	590.1 ± 9.0
6	36.6±1.5	99.0 ±0.1	50.4 ±0.1	1991.5
7	16.6±0.3	99.9 ±0.3	49.9 ±0.2	1596.8 ±8.8
8	18.2±0.3	99.4 ±0.2	50.3 ±0.1	1394.8 ±9.8
9	14.8±0.3	101.3 ±0.2	48.8 ±0.2	993.0 ±11.7
10	34.4±1.4	100.5 ±0.3	65.0 ±0.6	1980.9 ±19.5
11	16.9±0.3	99.8 ±0.5	65.5 ±0.6	1395.9 ±12.0
12	16.4±0.3	100.1 ±0.5	65.5 ±0.6	989.6 ±9.6
13	34.5±1.2	98.9 ±0.7	78.0 ±0.8	1789.4 ±17.1
14	31.2±1.1	98.9 ±0.6	72.3 ±0.8	1589.1 ±18.2
15	20.7±0.3	98.9 ±0.1	41.4 ±0.2	592.7 ±10.9

- Engine log statistics – the values of the parameters shown in ***Table 3-20***(b) were determined from the statistics (mean and standard deviation) of the raw engine logs, taking into account the firing conditions (***Table 3-20***(a)), at top dead centre (TDC). TDC was the reference point because it was the point of fuel injection. In addition, since the test points had more unfired than fired cycles, TDC presented a realistic position to study and quantify the actual test

conditions. The calculations are explained below.

- Parameters: intake air temperature (TMAN/^{o}C), in-cylinder pressure at top dead centre (TDC ICP /bar) and fuel pressure (P /bar).

  - Test points: 1, 2, 3, 4, 5, 10, 11, 12, 13 and 14
    № of recorded cycles per test point per parameter = 500
    Skipped cycle strategy = 1 fired for every 10 cycles

    № of fired cycle per test point per parameter = $\frac{500}{10}$ = 50

    № of observations for statistical computations, *n* = 50 fired cycles.

    For each test point, the median, mean and standard deviation of each parameter (T, TDC ICP and P) were computed with 50 as frequency

    Only the mean and standard deviation values were used in ***Table 3-20***(b), as shown in sample calculation with test point 1 in Appendix B

  - Test points: 6, 7 and 8

    № of recorded cycles per test point = 100

    Skipped cycle strategy = 1 fired for every 10 cycles

    № of fired cycle per test point = 2 (TP06), 2 (TP07) and 4

    (TP08) Frequency, n = 2 (TP06), 2 (TP07) and 4 (TP08)

    Same statistics computation as above, for each test point

    See sample calculation with test point 6 in Appendix C

  - Test points: 9 and 15

    № of recorded cycles per test point = 100
    Skipped cycle strategy = 1 fired for every 10 cycles

The fired cycles were difficult to extract

Hence, frequency, *n* = 100 (TP09) and 100 9TP15)

Same statistics computation as above for each test point See sample calculation with test point 15 in Appendix D

- Parameter: fuel tank temperature, (T/^{o}C)
  - Test points: 1 – 15

    № of recorded cycles per test point = 60

    Skipped cycle strategy = 1 fired for every 10 cycles

    The fired cycles were difficult to extract

    Hence, frequency, *n* = 60 (TP 01 – 15)

    Same statistics computation as above for each test point

    See sample calculations with test point 1 in Appendix E

- Uncertainty analysis - In order to calculate the uncertainty, it was determined that the Gaussian probability density function best modelled the data. Thus, from the engine log statistics calculated above, the standard deviation was divided by the square root of the number of observations, for each test point. The quotient (or uncertainty at 68% confidence) was multiplied by 2, to give the uncertainty at 95% confidence level.

Table 3-11: Actual test conditions for Injector A liquid spray tests with uncertainty at 95% confidence level

Test point TP	Fuel tank temperature T (^{o}C)	Intake air temperature TMAN	In-cylinder pressure @ TDC ICP TDC (bar)	Fuel pressure P (bar)
1	36.7±0.3	99.5 ±0.2	83.3 ±0.3	1946.1 ± 7.1
2	30.7±0.3	99.2 ±0.2	83.4 ±0.3	1590.6 ±4.9
3	32.2±0.2	99.9 ±0.1	83.6 ±0.3	1398.7 ±4.8
4	29.8±0.1	99.4 ±0.2	83.7 ±0.2	991.0 ±3.2
5	30.4±0.1	98.3 ±0.1	84.1 ±0.2	590.1 ±2.5
6	36.6±0.4	99.0 ±0.1	50.4 ±0.1	1991.5 ±24.9
7	16.6±0.1	99.9 ±0.4	49.9 ±0.3	1596.8 ±12.4
8	18.2±0.1	99.4 ±0.2	50.3 ±0.1	1394.8 ±9.8
9	14.8±0.1	101.3±0.1	48.8 ±0.1	993.0 ±2.3
10	34.4±0.4	100.5 ±0.1	65.0 ±0.2	1980.9 ±5.5
11	16.9±0.1	99.8 ±0.1	65.5 ±0.2	1395.9 ±3.4
12	16.4±0.1	100.1 ±0.1	65.5 ±0.2	989.6 ±2.7
13	34.4±0.3	98.9 ±0.2	78.0 ±0.2	1789.4 ±4.9
14	31.2±0.3	98.9 ±0.2	72.3 ±0.2	1589.1 ±5.1
15	20.7±0.1	98.9 ±0.1	41.4 ±0.1	592.7 ±2.2

In *Table 3-20*(b) small deviations were recorded across the parameters. It is normal to have values slightly greater than or less than the mean value. The small deviations are therefore an indication of a very precise experiment, which means there are mainly systematic errors. However, the certainty of the results was quantified by narrow error limits in *Table 3-11*. Significant deviation was noticed for TP06 fuel pressure in both tables.

3.6.2 Injector B engine logs for liquid spray tests

- Actual test conditions – *Table 3-12* shows the actual conditions for the liquid spray tests conducted with Injector B.

Table 3-12: Actual test conditions for Injector B liquid spray tests

(a): Test summary

Injector:	Injector B (Delphi), 8 holes (156^0, 0.13mm, 1.5)
Injector condition:	New (unused)
Injector crank angle:	TDC
Skipped cycle strategy:	1 fired for every 5 skipped
Camera frame resolution:	256 x 416 pixels, 12bit/pix
Spatial scale factor:	0.106 mm/pix (unchanged)
Injection samples:	At least 50 recordings per test point

(b): Actual test conditions as mean values with standard deviation

Test point TP	Fuel tank temperature T (^OC)	Intake air temperature TMAN ^{o}	In-cylinder pressure @ TDC ICP TDC (bar)	Fuel pressure P (bar)
4	27.6±0.4	97.4±8.2	80.8 ±7.2	976.2±96.5
6	38.9±2.3	100.4±0.1	50.5 ±0.2	1948.1±19.1
9	25.5±0.3	100.2±0.1	50.2 ±0.2	990.8±9.6
14	28.8±0.6	98.9±0.2	72.7 ±0.4	1595.7±21.4
15	25.1±0.3	99.1±0.2	40.4 ±0.2	595.5±7.4

- Engine log statistics – For each test point, 100 cycles were recorded. Fuel was injected at TDC, and one cycle was fired after every five for each test points. The values of the parameters shown in ***Table 3-12***(b) were determined from the statistics calculations (mean and standard deviation) repeated with the recorded logs. Log data were extracted at TDC, where possible. Otherwise calculations with average cycle values applied.

- Uncertainty analysis - ***Table 3-13*** shows the mean values and standard uncertainties at 95% confidence.

Table 3-13: Actual test conditions for Injector B liquid spray tests with uncertainty at 95% confidence level

Test point TP	Fuel tank temperature T (^{o}C)	Intake air temperature TMAN (^{o}C)	In-cylinder pressure @ TDC ICP TDC (bar)	Fuel pressure P (bar)
4	27.6±0.1	97.4±4.1	80.8 ±3.6	976.2±48.2
6	38.9±0.6	100.4±0.1	50.5 ±0.1	1948.1±10.6
9	25.5±0.1	100.2±0.1	50.2 ±0.1	990.8±5.0
14	28.8±0.2	98.9±0.1	72.7 ±0.2	1595.7±10.7
15	25.1±0.1	99.1±0.1	40.4 ±0.1	595.5±2.1

Table 3-12(b) and *Table 3-13*show precise experiment for all the parameters but fuel pressure. Errors due to human factor/equipment are highlighted by the fuel pressure values. Increasing the number of test points (no of observation) is a probable remedy.

3.6.3 Injector C engine log for liquid spray tests

Actual test conditions - *Table 3-14* shows the actual conditions for the liquid spray tests conducted with Injector C.

Table 3-14: Actual test conditions for Injector C liquid spray tests
(a): Test summary

Injector:	Injector C (Bosch), 8 holes (155^{0}, 0.137mm, 1.3)
Injector condition:	New (unused)
Injector crank angle:	TDC
Skipped cycle strategy:	1 fired for every 5 skipped
Camera frame resolution:	256 x 416 pixels, 12bit/pix
Spatial scale factor:	0.1098 mm/pix (pre-test), 0.1103 mm/pix (post-test)
Injection samples:	At least 50 recordings per test point

(b): Actual test conditions as mean values with standard deviation

Test point TP	Fuel tank temperature T (^{o}C)	Intake air temp temperature TMAN (^{o}C)	In-cylinder pressure @ TDC ICP TDC (bar)	Fuel pressure P (bar)
2	24.4±0.3	100.5±0.1	85.1±0.2	1569.8±16.2
4	24.5±0.3	100.7±0.1	85.0±0.2	994.5±11.6
7	24.1±0.3	100.5±0.1	52.9±0.2	1593.0±15.6
9	24.5±0.3	100.7±0.1	51.3±0.9	995.8±10.3
14	24.6±0.3	98.4±0.1	77.6±0.3	1575.1±14.2
15	25.6±0.3	103.2±0.1	43.7±0.2	597.7±10.8

- Engine log statistics – For each test point, 100 cycles were recorded. Fuel was injected at TDC, and one cycle was fired after every five for each test points. The values of the parameters shown in ***Table 3-14*** were determined from the statistics calculations (mean and standard deviation) repeated with the recorded logs. Log data were extracted at TDC, where possible. Otherwise calculations with average cycle values applied, as shown in the computations for the fuel tank temperature.

- Uncertainty analysis - The table below shows the mean values and standard uncertainties at 95% confidence, for all the Injector B tests.

Table 3-15: Actual test conditions for Injector C liquid spray tests with uncertainty at 95% confidence level

Test point TP	Fuel tank temperature T (^{o}C)	Intake air temperature TMAN (^{o}C)	In-cylinder pressure @ TDC ICP TDC (bar)	Fuel pressure P (bar)
2	24.4±0.1	100.5±0.1	85.1±0.1	1569.8±8.1
4	24.5±0.1	100.7±0.1	85.0±0.1	994.5±5.8
7	24.1±0.1	100.5±0.1	52.9±0.1	1593.0±7.8
9	24.5±0.1	100.7±0.1	51.3±0.2	995.8±2.1
14	24.6±0.1	98.4±0.1	77.6±0.1	1575.1±7.1
15	25.6±0.1	103.2±0.1	43.7±0.1	597.7±5.4

Table 3-14(b) and *Table 3-15* suggest precise and good results of the experiment. Again the errors with the fuel pressure are highlighted.

3.6.4 Injector D engine logs for liquid spray tests

- Actual test conditions – ***Table 3-16*** shows the actual conditions for the liquid spray tests conducted with Injector D.

.

Table 3-16: Actual test conditions for Injector D liquid spray tests
(a): Test summary

Injector:	Injector C (Bosch), 8 holes (155^0, 0.137mm, 3.5)
Injector condition:	New (unused)
Injector crank angle:	TDC
Skipped cycle strategy:	1 fired for every 5 skipped
Camera frame resolution:	256 x 416 pixels, 12bit/pix
Spatial scale factor:	0.1098 mm/pix (pre-test), 0.1103 mm/pix (post-test)
Injection samples:	At least 50 recordings per test point

(b): Actual test conditions as mean values with standard deviation

Test point TP	Fuel tank temperature T (^oC)	Intake air temperature TMAN (^oC)	In-cylinder pressure @ TDC ICP TDC (bar)	Fuel pressure P (bar)
2	24.5±0.3	100.8±0.1	85.5±0.2	1595.1±11.2
4	24.6±0.3	100.5±0.2	84.8±0.2	999.6±10.7
7	23.4±0.3	98.7±0.1	50.7±0.2	1602.4±10.6
9	23.5±0.3	97.2±0.1	50.1±0.6	994.6±12.8
14	24.0±0.3	100.7±0.1	79.0±0.2	1597.3±14.7
15	23.8±0.2	96.8±0.1	42.9±0.2	598.7±6.4

- Engine log statistics – For each test point, 100 cycles were recorded. Fuel was injected at TDC, and one cycle was fired after every five for each test points. The values of the parameters shown in Table 3-16were determined from the statistics calculations (mean and standard deviation) repeated with the recorded logs. Log data were extracted at TDC, where possible. Otherwise calculations with average cycle values applied, as shown in the computations

for the fuel tank temperature.

- Uncertainty analysis - *Table 3-17*shows the mean values and standard uncertainties at 95% confidence.

Table 3-17: Actual test conditions for Injector D liquid spray tests with uncertainty at 95% confidence level

Test point TP	Fuel tank temperature T (^{o}C)	Intake air temperature TMAN (^{o}C)	In-cylinder pressure @ TDC ICP TDC (bar)	Fuel pressure P (bar)
2	24.5±0.1	100.8±0.1	85.5±0.1	1595.1±5.6
4	24.6±0.1	100.5±0.1	84.8±0.1	999.6±5.4
7	23.4±0.1	98.7±0.1	50.7±0.1	1602.4±5.3
9	23.5±0.1	97.2±0.1	50.1±0.1	994.6±2.6
14	24.0±0.1	100.7±0.1	79.0±0.1	1597.3±7.3
15	23.8±0.1	96.8±0.1	42.9±0.1	598.7±3.2

Table 3-16(b) and *Table 3-17* are further confirmation for the presicion implemented for all parameters except the fuel pressure, with all the injectors. As suggested an increase in the number of observations could improve the effects of human factor and imprecise equipment errors for the fuel pressure parameter.

3.6.5 Injector B engine logs for vapour spray tests

- Actual test conditions –Table 3-18 shows the test conditions reached with Injector B during the vapour spray tests.

Table 3-18: Actual test conditions for Injector B vapour spray tests (a): Test summary

Injector:	Injector B (Delphi), 8 holes (156^0, 0.13mm, 1.5)
Injector condition:	New (unused)
Injector crank angle:	TDC
Skipped cycle strategy:	1 fired for every 5 skipped
Camera frame resolution:	256 x 512 pixels, 12bit/pix
Spatial scale factor:	0.141 mm/pix (unchanged)
Injection samples:	At least 50 recordings per test point

(b): Actual test conditions as mean values with standard deviation

Test point TP	Fuel tank temperature T (^oC)	Intake air temperature TMAN	In-cylinder pressure @ TDC ICP TDC (bar)	Fuel pressure P (bar)
4	27.4±0.3	99.3±0.2	82.3 ±0.6	996.3 ±8.3
6	31.2±1.7	100.1 ±0.1	48.2 ±0.2	1863.5 ±20.4
9	21.8±0.3	98.4 ±0.4	49.8 ±0.3	998.2 ±7.7
13	30.4±2.3	99.3±0.2	79.9±0.5	1802.9±27.0
14	43.8±1.0	100.3 ±0.1	72.3 ±0.4	1595.7 ±21.4
15	20.8±0.3	99.1 ±0.2	40.4 ±0.2	595.5 ±7.4

- Engine log statistics – For each test point, 100 cycles were recorded. Fuel was injected at TDC, and one cycle was fired after every five for each test points. The values of the parameters shown in ***Table 3-18*** (b) were determined from the statistics calculations (mean and standard deviation) repeated with the recorded logs. Log data were extracted at TDC, where possible. Otherwise calculations with average cycle values applied, as shown in the computations for the fuel tank temperature.

- Uncertainty analysis - ***Table 3-19*** shows the mean values and standard uncertainties at 95% confidence.

Table 3-19: Actual test conditions for Injector B vapour spray tests with uncertainty at 95% confidence level

Test point TP	Fuel tank temperature T (^{o}C)	Intake air temperature TMAN (^{o}C)	In-cylinder pressure @ TDC ICP TDC (bar)	Fuel pressure P (bar)
4	27.4±0.1	99.3±0.1	82.3 ±0.3	996.3 ±5.1
6	31.2±0.4	100.1 ±0.1	48.2 ±0.1	1863.5 ±4.9
9	21.8±0.1	98.4 ±0.3	49.8 ±0.2	998.2 ±4.9
13	30.4±0.6	99.3±0.1	79.9±0.3	1802.9±17.1
14	43.8±0.3	100.3 ±0.1	72.3 ±0.4	1595.7 ±12.0
15	20.8±0.1	99.1 ±0.1	40.4 ±0.1	595.5 ±1.4

3.6.6 Injector C engine logs for vapour spray tests

- Actual test conditions – ***Table 3-20*** shows the test conditions reached with Injector C during the vapour spray tests.

Table 3-20: Actual test conditions for Injector C vapour spray tests (a): Test summary

Injector:	Injector C (Bosch), 8 holes (155^{0}, 0.137mm, 1.3)
Injector condition:	New (unused)
Injector crank angle:	TDC
Skipped cycle strategy:	1 fired for every 5 skipped
Camera frame resolution:	256 x 512 pixels, 12bit/pix
Spatial scale factor:	0.1098 mm/pix (pre-test), 0.1103 mm/pix (post-test)
Injection samples:	At least 50 recordings per test point

(b): Actual test conditions as mean values with standard deviation

Test point TP	Fuel tank temperature T (^{o}C)	Intake air temperature TMAN (^{o}C)	In-cylinder pressure @ TDC ICP TDC	Fuel pressure P (bar)
2	23.4±0.3	99.4±0.2	86.7±0.2	1591.9±18.5
4	24.2±0.4	99.7±0.2	86.5±0.2	997.3±9.7
7	23.5±0.3	98.9±0.1	52.1±0.2	1598.0±18.5
9	23.7±0.3	100.5±0.1	50.8±0.7	995.4±13.5
14	23.8±0.3	100.2±0.1	75.9±0.2	1591.3±13.2
15	21.7±0.3	99.8±0.1	42.8±0.2	595.6±12.8

- Engine log statistics – For each test point, 100 cycles were recorded. Fuel was injected at TDC, and one cycle was fired after every five for each test points. The values of the parameters shown in ***Table 3-20***(b) were determined from the statistic calculations (mean and standard deviation) repeated with the recorded logs. Log data were extracted at TDC, where possible. Otherwise calculations with average cycle values applied, as shown in the computations for the fuel tank temperature.

- Uncertainty analysis - ***Table 3-21*** shows the mean values and standard uncertainties at 95% confidence.

Table 3-21: Actual test conditions for Injector C vapour spray tests with *uncertainty at 95% confidence level*

Test point TP	Fuel tank temperature T (^{o}C)	Intake air temperature TMAN (^{o}C)	In-cylinder pressure @ TDC ICP TDC (bar)	Fuel pressure P (bar)
2	23.4±0.1	99.4±0.1	86.7±0.1	1591.9±9.3
4	24.2±0.1	99.7±0.1	86.5±0.1	997.3±4.9
7	23.5±0.1	98.9±0.1	52.1±0.1	1598.0±9.3
9	23.7±0.1	100.5±0.1	50.8±0.2	995.4±2.7
14	23.8±0.1	100.2±0.1	75.9±0.1	1591.3±6.6
15	21.7±0.1	99.8±0.1	42.8±0.1	595.6±6.4

3.6.7 Injector D engine logs for vapour spray tests

- Actual test conditions – *Table 3-22* shows the test conditions reached with Injector D during the vapour spray tests.

Table 3-22: Actual test condition for Injector D vapour spray tests (a): Test summary

Injector:	Injector C (Bosch), 8 holes (155^0, 0.137mm, 3.5)
Injector condition:	New (unused)
Injector crank angle:	TDC
Skipped cycle strategy:	1 fired for every 5 skipped
Camera frame resolution:	256 x 512 pixels, 12bit/pix
Spatial scale factor:	0.1098 mm/pix (pre-test), 0.1103 mm/pix (post-test)
Injection samples:	At least 50 recordings per test point

(b): Actual test conditions as mean values with standard deviation

Test point TP	Fuel tank temperature T (^oC)	Intake air temperature TMAN (^oC)	In-cylinder pressure @ TDC ICP TDC (bar)	Fuel pressure P (bar)
2	23.8±0.3	95.4±0.1	86.6±0.2	1598.2±21.4
4	23.1±0.3	97.5±0.2	86.2±0.1	1008.8±17.3
7	22.7±0.3	98.8±0.1	52.5±0.1	1597.0±8.5
9	22.3±0.3	97.0±0.1	52.9±0.5	995.6±10.7
14	22.7±0.3	101.3±0.1	77.3±0.2	1601.0±8.9
15	20.2±0.3	100.9±0.2	43.5±0.2	595.4±9.1

- Engine log statistics – For each test point, 100 cycles were recorded. Fuel was injected at TDC, and one cycle was fired after every five for each test points. The values of the parameters shown in *Table 3-22* were determined from the statistic calculations (mean and standard deviation) repeated with the recorded logs. Log data were extracted at TDC, where possible. Otherwise calculations with average cycle values applied, as shown in the computations for the fuel tank temperature.

- Uncertainty analysis - The table below shows the mean values and standard uncertainties at 95% confidence, for all the Injector B tests.

Table 3-23: Actual test conditions for Injector D vapour spray tests with uncertainty at 95% confidence level

Test point TP	Fuel tank temperature T (^{o}C)	Intake air temperature TMAN (^{o}C)	In-cylinder pressure @ TDC ICP TDC (bar)	Fuel pressure P (bar)
2	24.5±0.1	100.8±0.1	85.5±0.1	1595.1±10.7
4	24.6±0.1	100.5±0.1	84.8±0.1	999.6±8.7
7	23.4±0.1	98.7±0.1	50.7±0.1	1602.4±4.2
9	23.5±0.1	97.2±0.1	50.1±0.1	994.6±2.1
14	24.0±0.1	100.7±0.1	79.0±0.1	1597.3±4.5
15	23.8±0.1	96.8±0.1	42.9±0.1	598.7±4.5

3.7 Conclusions of chapter three

In this chapter, experimental measurements of in-cylinder spray development, using optical diagnostics, have been reported. The optical techniques employed were not intrusive, and have high temporal and spatial resolution that enabled transient fuel injection process to be recorded. The effects of the characteristic parameters are presented in the next chapter.

Clearly, the results obtained from the optical engine were influenced by compromises in the design of the combustion chamber geometry that satisfies the requirements for optical access. This fundamental difference between the optical engine and real (metal/production) engine, may lead to the introduction of errors. These errors should be quantified to ensure the results are useful and not misleading.

Firstly, the single-cylinder mode and separated air management system for inlet air allows a significant flexibility in terms of inlet pressure, temperature and gas composition. Such flexibility could be unrealistic with real engines that have fixed turbocharger, air-cooler and EGR system. Secondly, the available load-speed range for the optical engine was limited due to concerns for the mechanical characteristics of certain parts. For example, the optical window material cannot sustain the high

pressures and pressure derivatives that go with the upper load range. Thirdly, due to the window material, which is a poorer conductor of heat than aluminium and steel, heat losses are lesser in the optical engine than the real metal engine. This can lead to higher combustion chamber wall temperatures. One of the reasons behind the skipped fire operation was to maintain moderate temperatures. As a result, it will not be possible to use the exhaust for EGR operation because it will be diluted by the motored cycle. Finally, diesel fuel used with real engines contains a large number of components such as poly-aromatic hydrocarbons that can disturb laser diagnostics, or other species that can cause unwanted laser-induced fluorescence. Consequently, this cannot be used on an optical engine. Instead a special type of diesel fuel is used (see Appendix A). This type is usually imparted with special properties, such as enhanced air-entrainment, for optimal performance.

Errors due to measurement were quantified by the prediction limits of the standard deviation and confidence limits of the uncertainty statement. Small deviations indicated very precise experiments, whilst highlighting the effect of systematic errors. Experimental uncertainties generally arise from unavoidable difficulties in making a measurement, limitations of the equipment, or even ambiguities in the specification of what is to be measured. The uncertainty analyses provided acceptable credible limits in quantifying the relative effects of these factors at an expanded confidence level of 95%.

However, optical diagnostics has led to the development of significant understanding of in- cylinder spray development. The rather simple and inexpensive traditional diagnostics techniques often use physical probes. This is inherently intrusive, and may lead to severe problems by causing chemical, temperature and flow disturbances. It must be mentioned that faithfully replicating real engine characteristics is difficult. The differences between optical and metal engines are inherently unavoidable.

Attempts were made in this work to provide optimal conditions for the optical diagnostics to be implemented.

4 SPRAY CHARACTERISATION

The experiments of the previous chapter derived from the understanding that the efficiency of the combustion process of the HSDI diesel engine, from the point of view of either the engine efficiency itself or pollutant emissions, depends mainly on the injection process characteristics. Indeed, the injection process, together with air motion, is primarily responsible for the in-cylinder air/fuel mixture formation (Kato et al., 1989; Shenghua et al., 2000). The parameters that influence spray behaviour are grouped under: parameters of diesel fuel injection and parameters of the environment in which the spray is injected. Experimental data, such as that generated in previous chapter, are needed to understand the processes better, to identify the controlling parameters and to provide initial data and comparative values for computer models of actual sprays.

Over the years, diesel spray characteristics have been studied with different techniques for different injection conditions. Quite often the results have not reflected real engine conditions, either due to simplified injection conditions (e.g. single shot or continuous steady process) or injection ambience that is far from engine-like. In addition, the atomisation process is known to be very different at atmospheric density and at high density (Reitz et al., 1982; Hiroyasu et al., 1989). In this chapter, an attempt is made to quantify and predict the spray behaviour as a function of the parameters governing the injection process. The experimental data was processed (see Appendix F) for analyses. Parameters studied were the injection pressure as influential system parameter, in-cylinder pressure as a representative parameter external to the system, and nozzle geometry.

4.1 Effect of injection pressure

Figure 4-1, Figure 4-2 and Figure 4-3 show the effect of injection pressure on measured spray characteristics (penetration and dispersion) for injector A spray conditions. Only test points 1 through 5 were considered due to the wide injection pressure range (600-2000 bar) and common in-cylinder pressure of 84 bar.

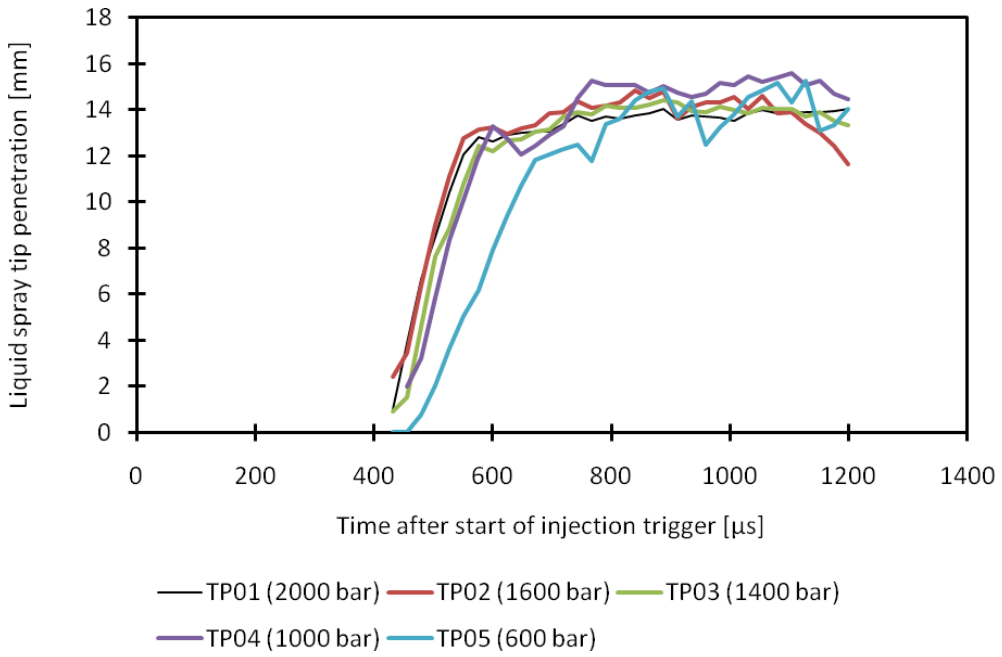

Figure 4-1: Effect of injection pressure (84bar gas pressure)

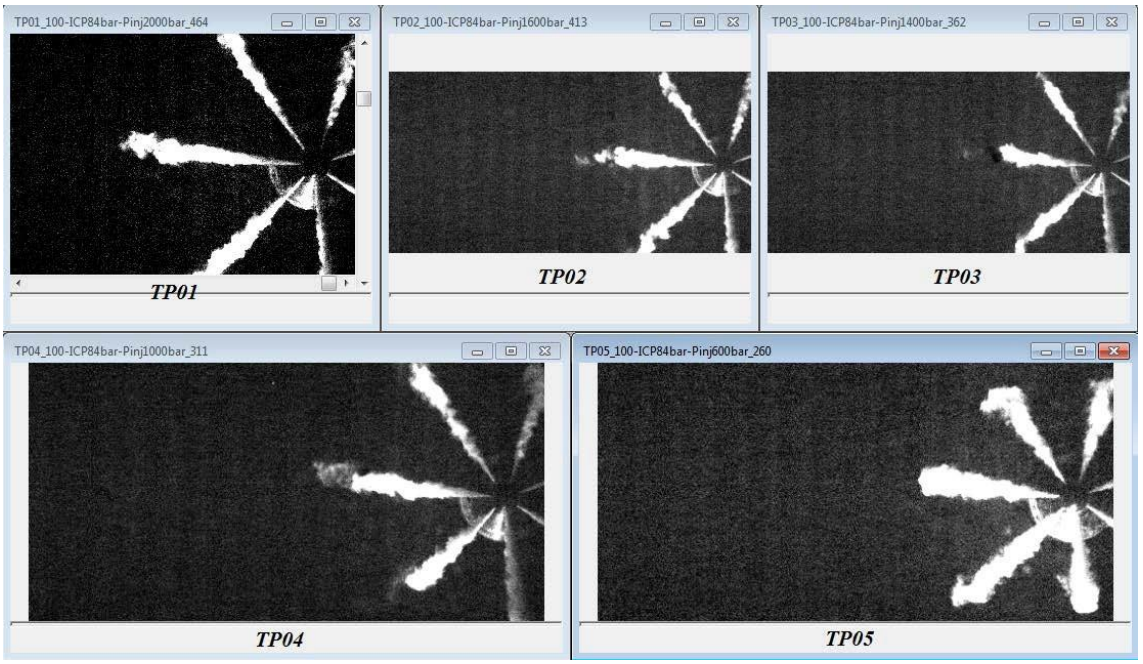

Figure 4-2: Image data showing liquid spray penetration at TP01 through TP05

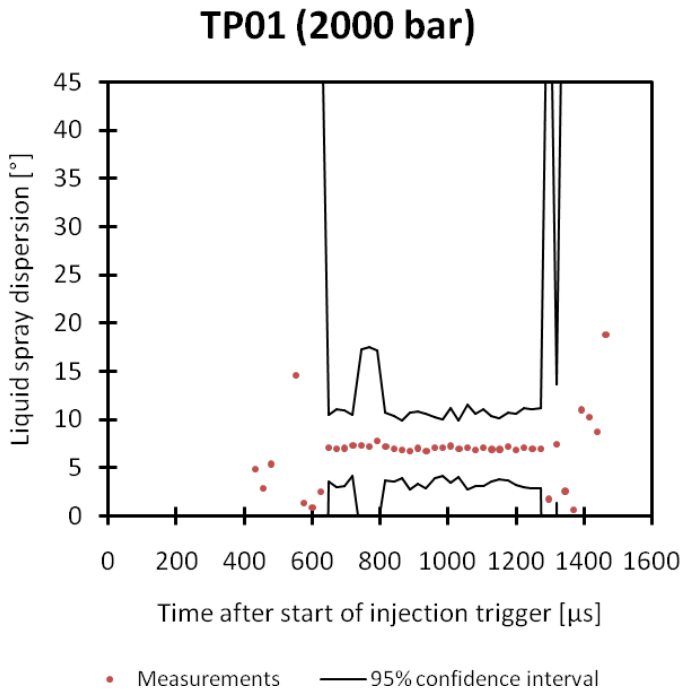

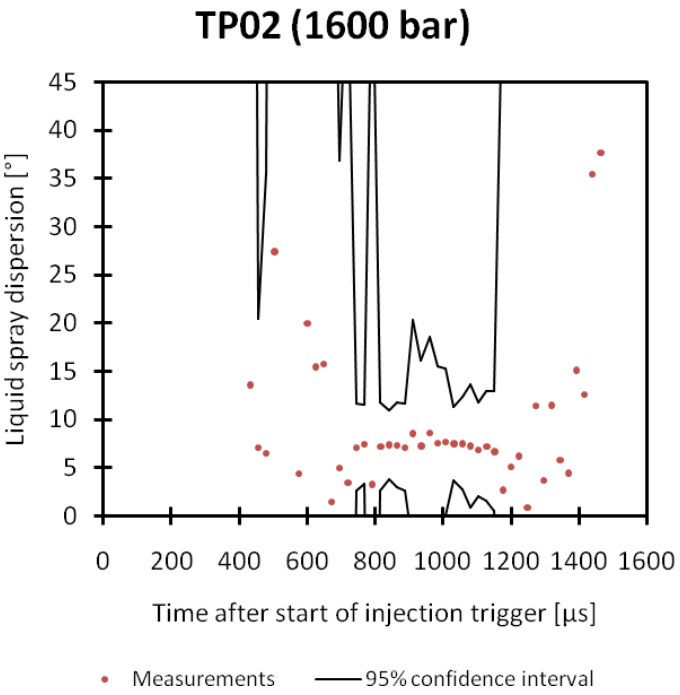
TP02 (1600 bar)
Liquid spray dispersion [°]
45
40
35
30
25
20
15
10
5
0
0
200
400
600
800
1000
1200
1400
1600
Time after start of injection trigger [µs]
Measurements
95% confidence interval

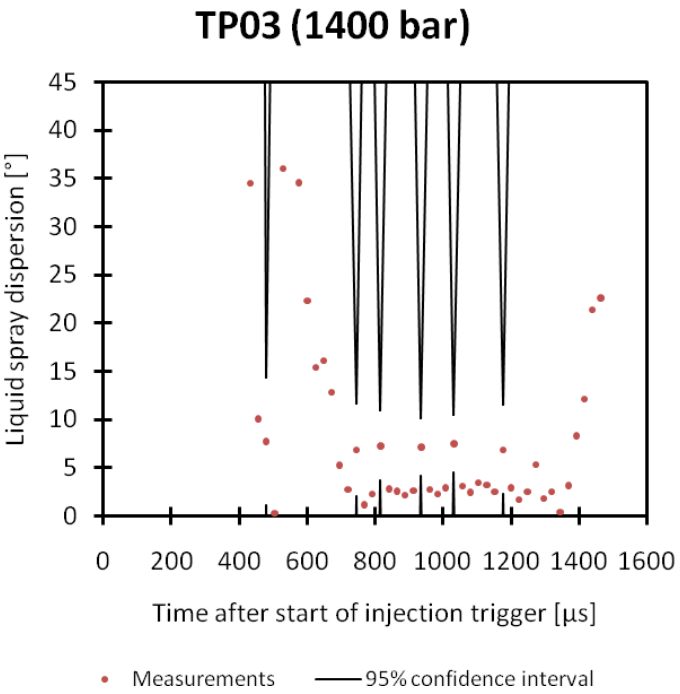
TP03 (1400 bar)
Liquid spray dispersion [°]
45
40
35
30
25
20
15
10
5
0
0
200
400
600
800
1000
1200
1400
1600
Time after start of injection trigger [µs]
Measurements
95% confidence interval

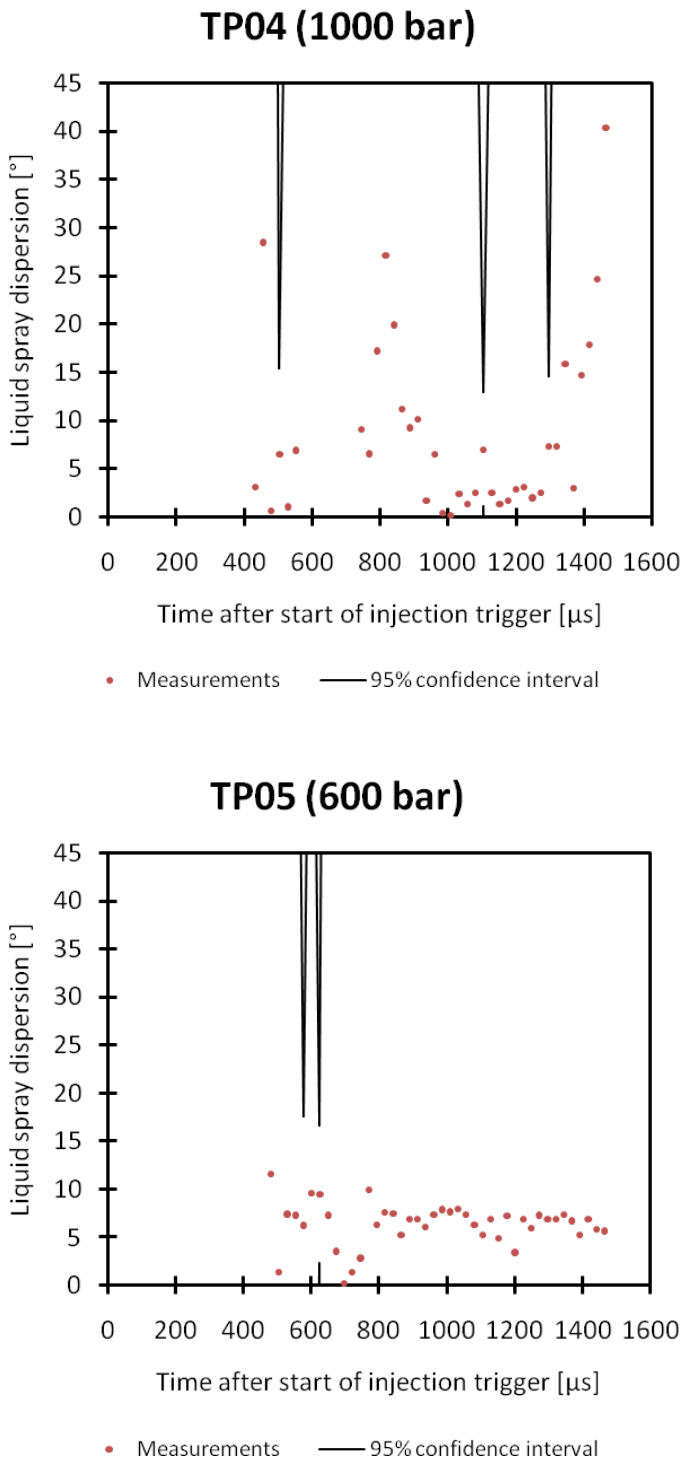

Figure 4-3: Liquid spray dispersion with injector A measurements

Changes in the fuel injection pressure do not show a clear trend in Figure 4-1. There is an indication that the time for the liquid tip to attain maximum liquid length increases as the injection pressure decreases from TP01 through TP05. In Figure 4-2, the following key observations can be made:

- Liquid ligaments are seen in the spray periphery under both low and high injection pressure conditions, but tend to disappear quicker under the former than the latter due to improved aerodynamic interaction.
- The spray under low injection pressure had larger jet diameter than under high injection pressure (see TP05).
- Existence of vortices along the side surface of the spray, which is an indication of increasing air entrainment.
- Reduction of liquid spray penetration as the injection pressure reduced from TP01 through TP05 (see Figure 4-2). The reduction in spray penetration is more marked for TP04 and TP05, which is due to increase in spray dispersion, especially for the two test points as shown in Figure 4-3.

A clearer trend for the effect of injection pressure is shown in Figure 4-4, for liquid (L) and vapour (V) penetration measurements conducted with injector B at in-cylinder pressure of 50 bar. Only test points 6 and 9 are chosen for comparison due to the wide difference in injection pressure for the same in-cylinder pressure. The difference in time delay between the two test points, and the apparent reduction in liquid spray penetration constitute artefacts of the analysis.

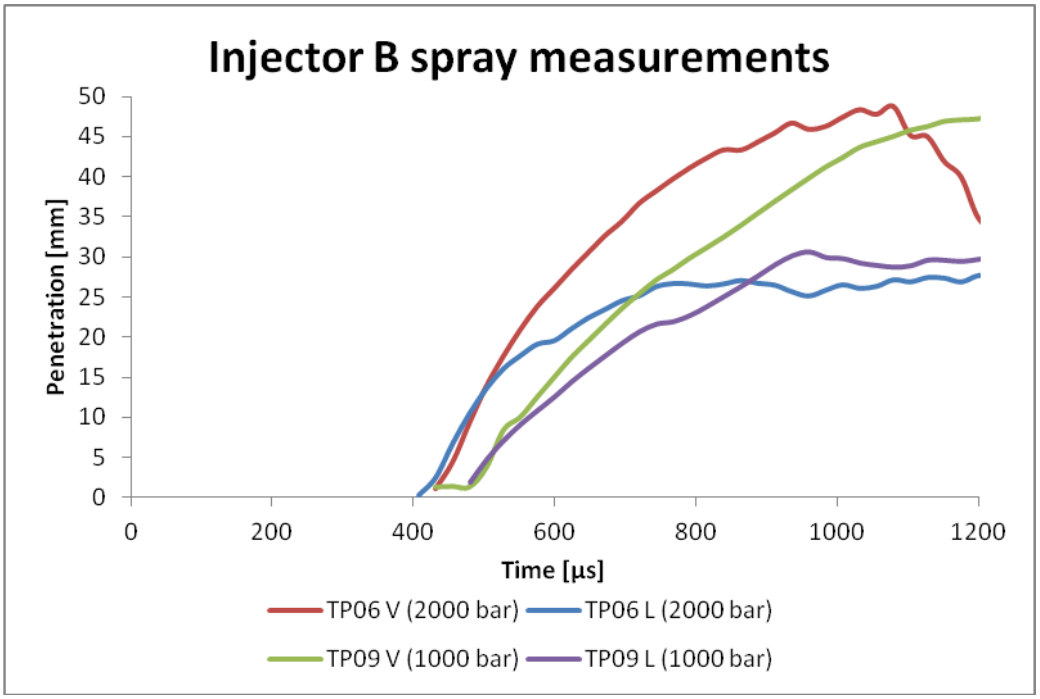

Figure 4-4: Effect of injection pressure (50bar ICP)

Naber JD et al., (1996) developed spray penetration correlation by introducing length and time scales that took into account the parameter that are generally considered to have significant effect on spray penetration. This model was implemented in this work to enable comparison with the injector A measurements, which was conducted across a broad range of test points. Thus, in Figure 4-5, the results from injector A liquid spray penetration measurement, at different injection pressures and 95% confidence level, are compared with this model (shown in grey band).

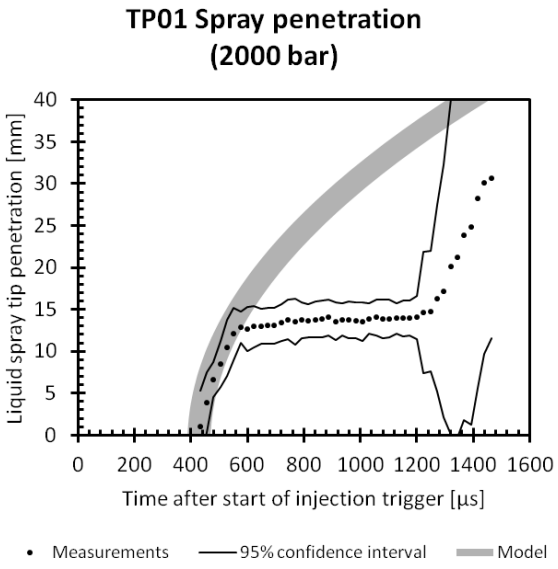
TP01 Spray penetration
(2000 bar)
Liquid spray tip penetration [mm]
Time after start of injection trigger [µs]
Measurements
95% confidence interval
Model

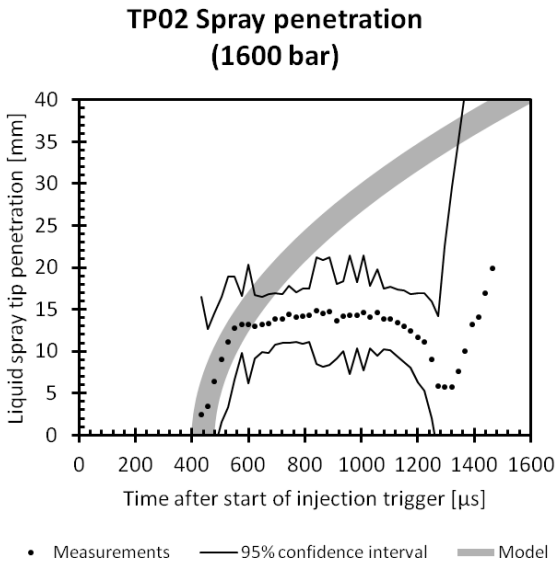
TP02 Spray penetration
(1600 bar)
Liquid spray tip penetration [mm]
Time after start of injection trigger [µs]
Measurements
95% confidence interval
Model

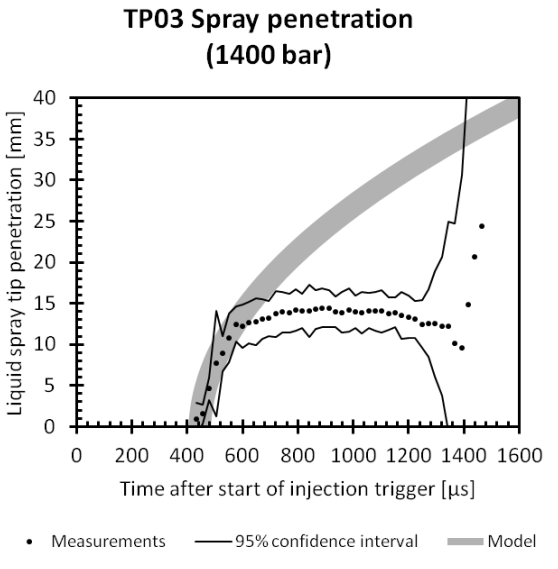
TP03 Spray penetration
(1400 bar)
Liquid spray tip penetration [mm]
Time after start of injection trigger [µs]
Measurements
95% confidence interval
Model

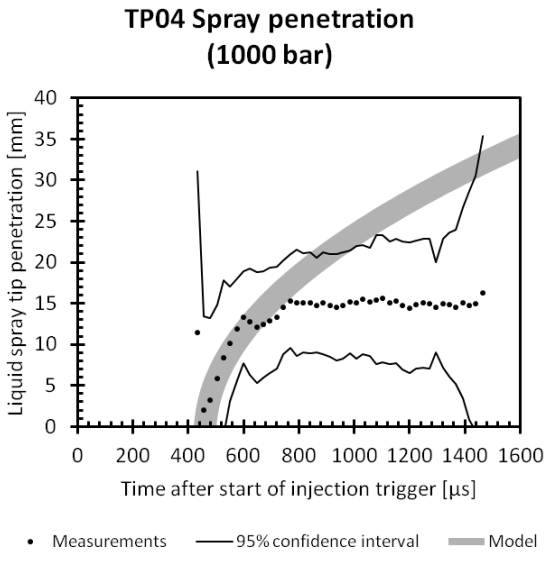
TP04 Spray penetration
(1000 bar)
Liquid spray tip penetration [mm]
Time after start of injection trigger [µs]
Measurements
95% confidence interval
Model

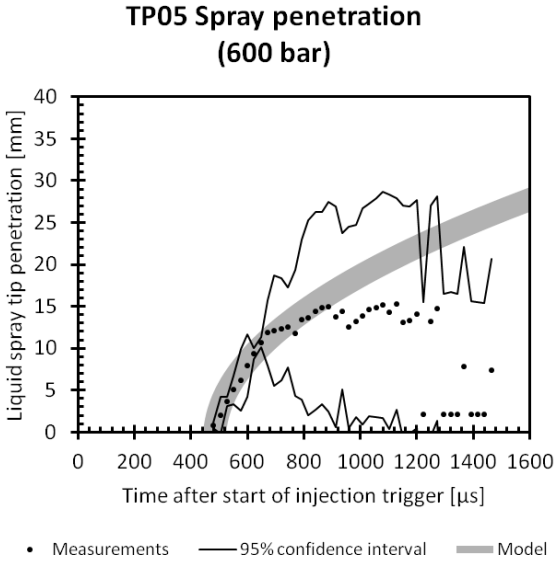
TP05 Spray penetration
(600 bar)
Liquid spray tip penetration [mm]
Time after start of injection trigger [µs]
Measurements
95% confidence interval
Model

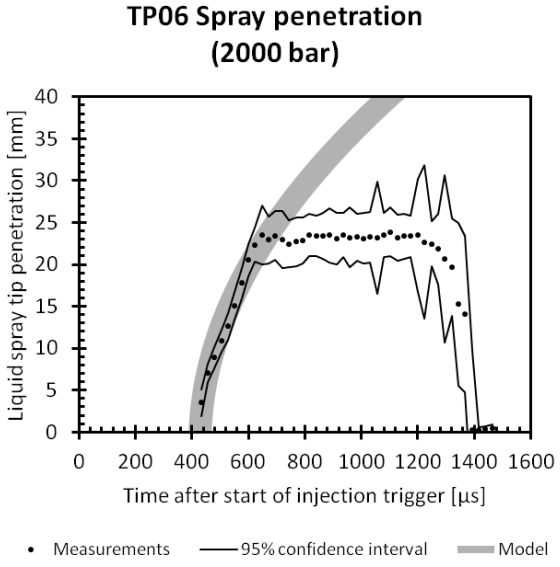
TP06 Spray penetration
(2000 bar)
Liquid spray tip penetration [mm]
Time after start of injection trigger [µs]
Measurements
95% confidence interval
Model

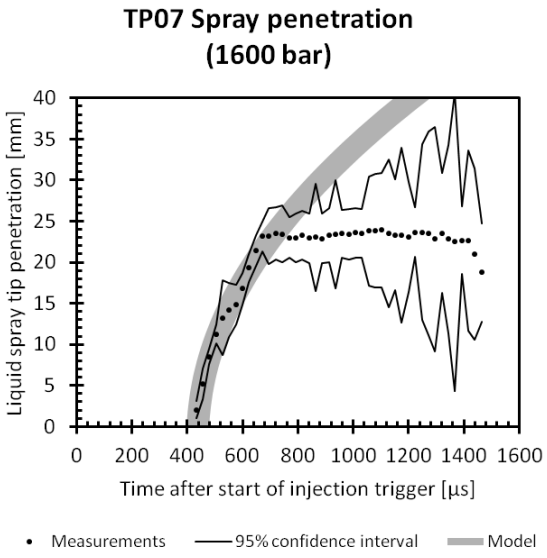
TP07 Spray penetration
(1600 bar)
Liquid spray tip penetration [mm]
Time after start of injection trigger [µs]
Measurements
95% confidence interval
Model

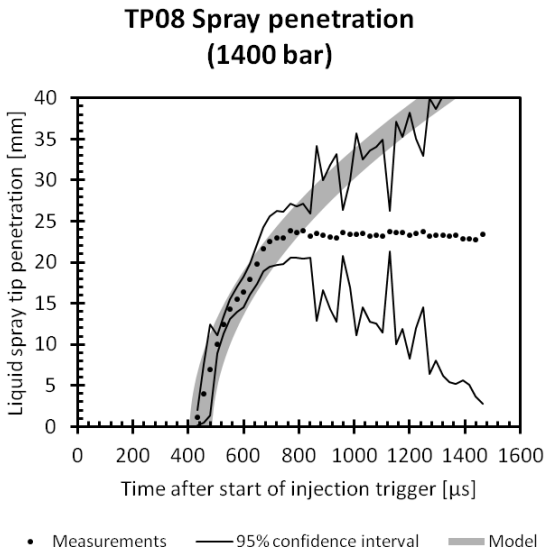
TP08 Spray penetration
(1400 bar)
Liquid spray tip penetration [mm]
Time after start of injection trigger [µs]
Measurements
95% confidence interval
Model

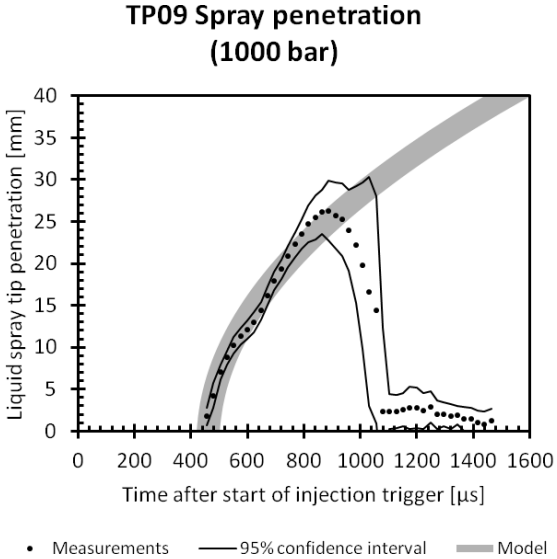
TP09 Spray penetration
(1000 bar)
Liquid spray tip penetration [mm]
Time after start of injection trigger [µs]
Measurements
95% confidence interval
Model

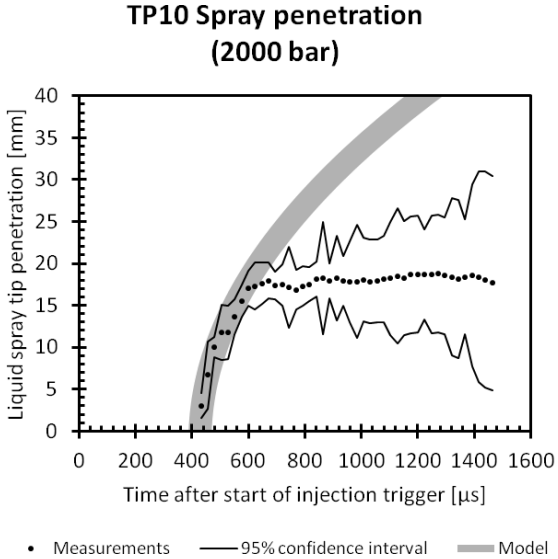
TP10 Spray penetration
(2000 bar)
Liquid spray tip penetration [mm]
Time after start of injection trigger [µs]
Measurements
95% confidence interval
Model

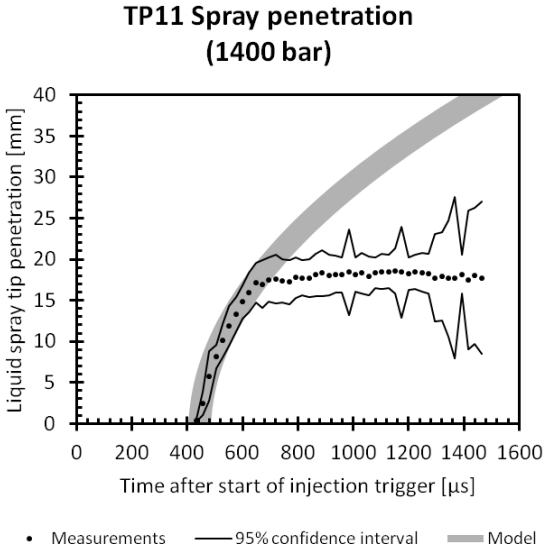
TP11 Spray penetration
(1400 bar)
Liquid spray tip penetration [mm]
Time after start of injection trigger [µs]
Measurements
95% confidence interval
Model

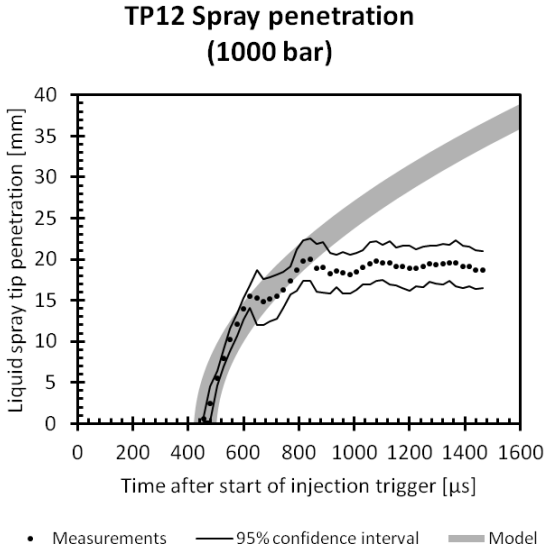
TP12 Spray penetration
(1000 bar)
Liquid spray tip penetration [mm]
Time after start of injection trigger [µs]
Measurements
95% confidence interval
Model

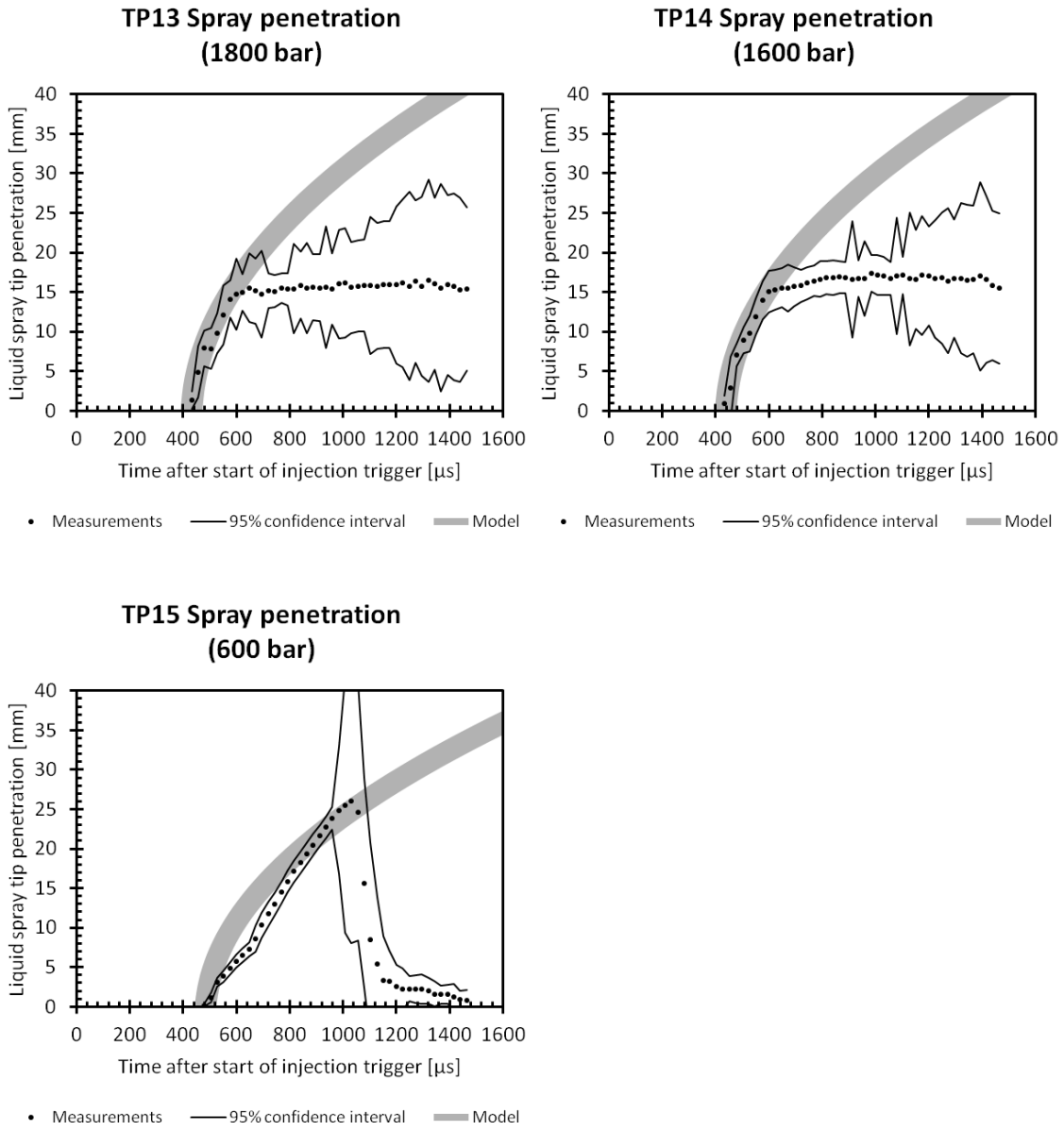

Figure 4-5: Comparison of Injector A liquid spray penetration measurements with Naber model at different injection pressures.

Under the conditions of the experiments, increase in injection pressure has no direct/visible effect on liquid spray penetration. It has been reported that the higher the injection pressure, the higher the velocity/momentum, which causes the jet to penetrate further into the combustion chamber (Naber JD et al., 1996). This effect is quite noticeable in the transient part of the liquid phase penetration as shown in Figure 4-1and Figure 4-4. Clearly from the same figures, the (quasi) steady part of the liquid spray penetration is not affected by change in injection pressure. The oscillations

observed at the steady part of the liquid spray penetration in Figure 4-1was due to processing algorithm, which was designed to pick up the undisrupted core liquid length attached to the injector tip. Moreover, a slight positive slope is observed at the steady period (Figure 4-1). Researchers (Pickett et al., 2010; Payri et al., 2012) have attributed the effect to two factors. Firstly, the temperature of the fuel at the beginning of the injection is higher because the injector sac is always in direct contact with the high temperature gas of the combustion chamber; during the injection the fuel flowing from upstream of the sac cools down the injector tip. This causes the temperature of the fuel at the orifice outlet to decrease during the injection, which impacts on liquid length (Payri et al., 2012). Secondly, for long injections, low temperature fuel–air mix is re-entrained in the spray causing a decrease in the effective ambient temperature and an increment in liquid length. Taking the large size of the chamber into account as well as the tendency of the slope to decrease at the end of the injection, the first fact was generally considered to be responsible for the observed phenomenon observed.

Other significant trend can be found in Figure 4-4, which shows that the vapour spray travels further than the liquid part of the spray. The figure also shows that increase in injection pressure increases vapour spray penetration (Naber JD et al., 1996). In fact, vapour penetration profiles have been shown to depend on both injection pressure and in-cylinder density (Crua, 2002). It was further suggested that the mechanism for the vapour transport was the gas motion induced by the liquid phase momentum exchange, from the droplets to the gas phase. To support these facts, increased penetration of the vapour was observed at higher injection pressures and lower gas densities, which was when the liquid phase had a higher momentum. As regards the comparison in Figure 4-5, the liquid spray penetration measurements with injector A are in good agreement with the model, especially from TP01 through

TP14. The penetration results of TP15 did not conform to the grey band of the model. It should be noted that the injector has been used in the past for several tests. Consequently, the fidelity of some of its key parts, e.g. valve and nozzle, may not be as expected, which may be responsible for such variation. In addition, the apparent reduction in liquid penetration shown in some of the measurements in Figure 4-5 are artefacts of the analysis.

On the effects of injection pressure, the application of the high-pressure injection system increases the amount of fuel injected per crankshaft angle, causing the liquid spray velocity to increase. With the high liquid spray velocity, the momentum interaction between the fuel droplets and the ambient gas is enhanced, causing the total entrained gas mass flow rate to increase significantly. The higher velocity induces higher level of dispersion (as seen in *Figure 4-2*), and consequently better atomization and air/fuel mixing. It has also been reported that the enhancement of the fuel droplet and ambient gas interaction depended on the ambient gas density: there is a tendency for the spray dispersion (or spreading angle) to increase with increase in ambient gas density, thus increasing the volume of hot gas entrained in the spray (Borthwick et al., 2002). However, the increased liquid spray momentum that is associated with an increased injection pressure is consumed in atomizing the fuel. Under lower injection condition, the turbulent energy that initiates spray interaction with the ambient air is reduced. This leads to the reduced liquid spray penetration observed for TP05 in *Figure 4-2*. Interestingly, the apparent increase in liquid spray diameter in TP05 (Figure 4- 2), which agrees with the increased spray dispersion in Figure 4-3, suggests significant air entrainment. Thus increased dispersion leads to shorter liquid spray penetration.

Another key observation from Figure 4-4, mentioned earlier, suggests that the liquid

phase of the spray reaches a maximum penetration distance (liquid length) soon after the start of injection, while the vapour phase of the spray continues to penetrate downstream. This agrees with understanding from literature (Naber JD et al., 1996; Johnson et al., 2013). Liquid length depends on the ambient and fuel injection conditions (Browne et al., 1986; Kim et al., 2003), and has been shown to be limited by mixing (Siebers, 1999). This means that significant thermal energy and mass are mixed into the spray to produce local thermodynamic conditions where the fuel is vapour phase. An explanation of why vapour spray penetrated more than the liquid phase can be given using the spray transport medium. For the liquid phase of the spray, penetration is possible so long as droplet`s average size remains the same. By increasing the injection pressure, the Sauter Mean Diameter (SMD) of the spray decreases. This is because the higher injection pressure not only causes higher momentum; it also provides more energy due to higher injection velocity which results in smaller droplet sizes. Consequently, droplets evaporate faster, and hence suppress the penetration of the liquid tip. Thus vapour penetration is related to the total air entrainment rate and fuel-air mixing.

In diesel engines, it is crucial for the diesel fuel to be completely vaporised before hitting the piston bowl wall or cylinder liner. This is because over-penetration of liquid fuel sprays and cylinder-wall wetting can be a serious concern, especially at low-temperature environments (Stanton et al., 1998) or at low-density in-cylinder conditions (Genzale et al., 2010). Actually, the dilution of liquid fuel spray into the cylinder wall oil film can increase piston-to-wall friction and component wear (Oinuma et al., 2005) and degrade the quality of bulk engine oil (Morcos et al., 2009). Cylinder wall-wetting also contributes to higher emission of unburned hydrocarbons (UHC) and

carbon monoxide (CO), which reduces combustion efficiency (Drake et al., 2003; Kashdan et al., 2007; Martin et al., 2008).

4.2 Effect of in-cylinder pressure

The Figures below, from experiments with injectors A and B, show the effect of in-cylinder pressure (ICP) on spray penetration..

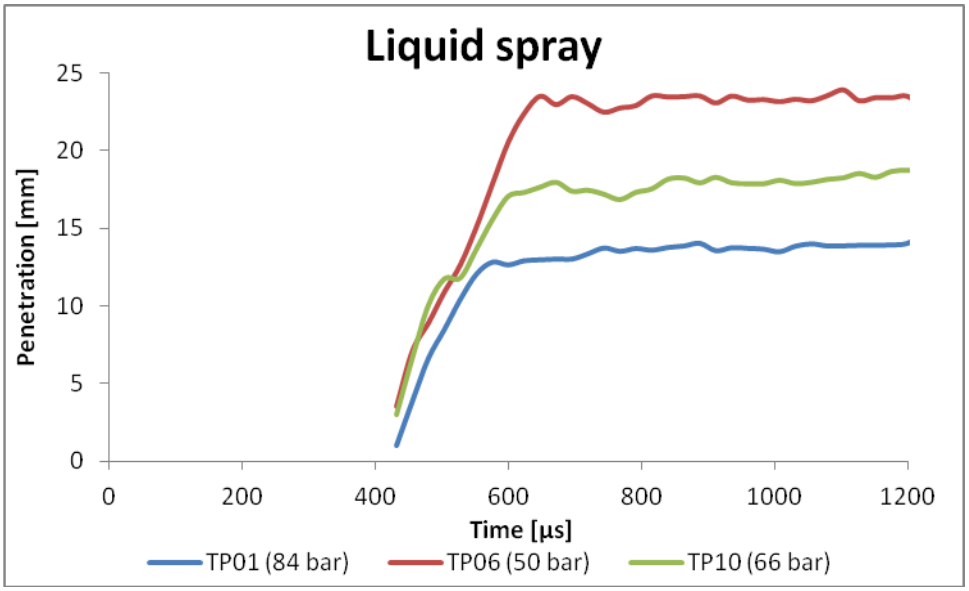

Figure 4-6: Spray measurement with injector A at different ICP (insert) and common injection pressure of 2000 bar.

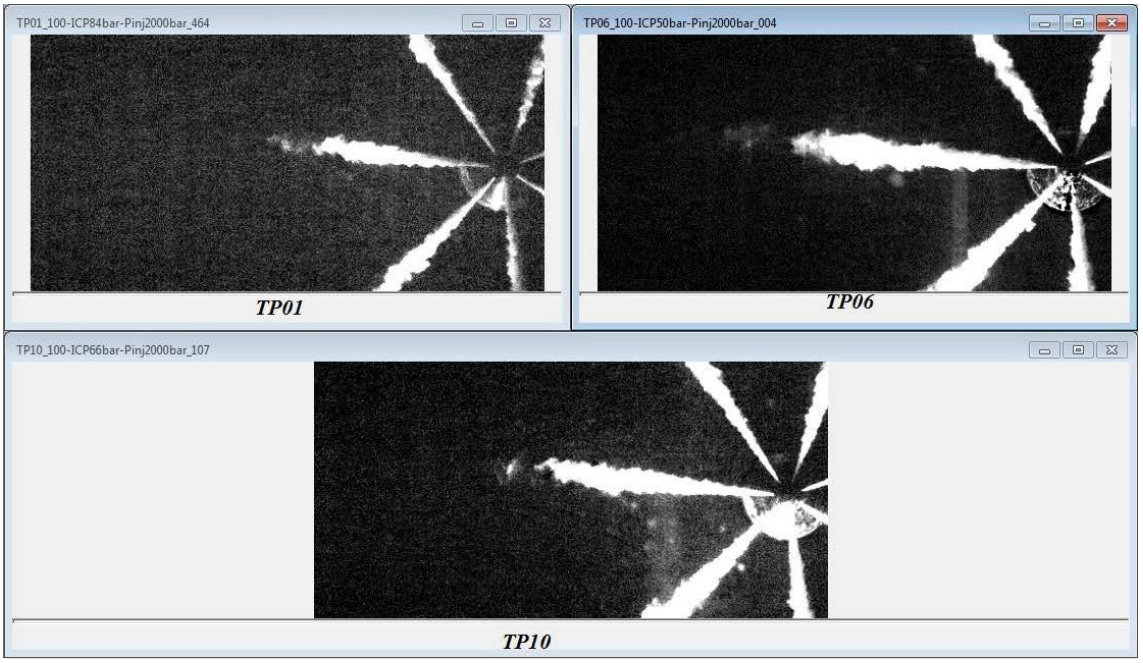

Figure 4-7: Image data from injector A measurements for the selected test points

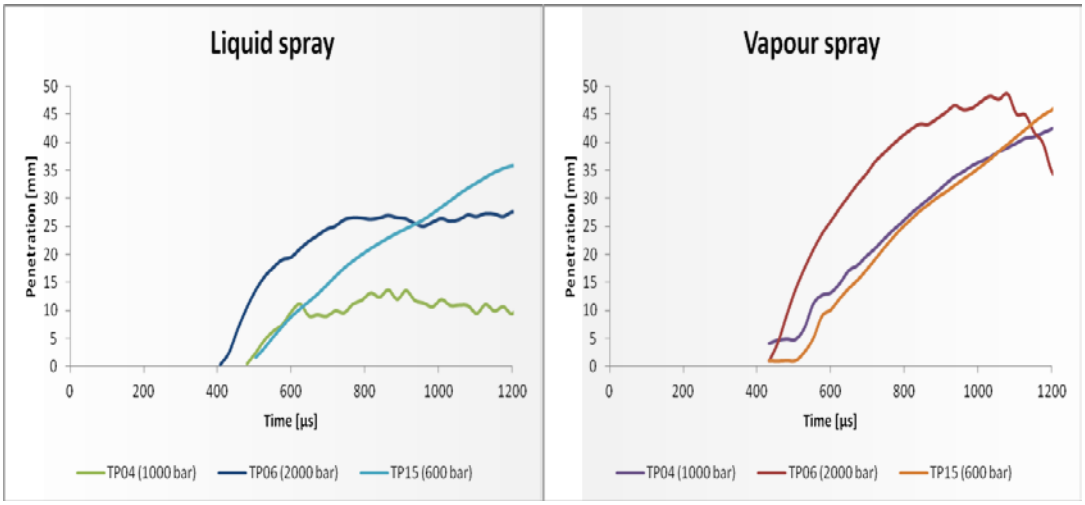

Figure 4-8: Spray measurement with injector B at different injection pressure (insert) and different ICP of 84, 50 and 40 bar for TP 04, TP06 and TP15 respectively.

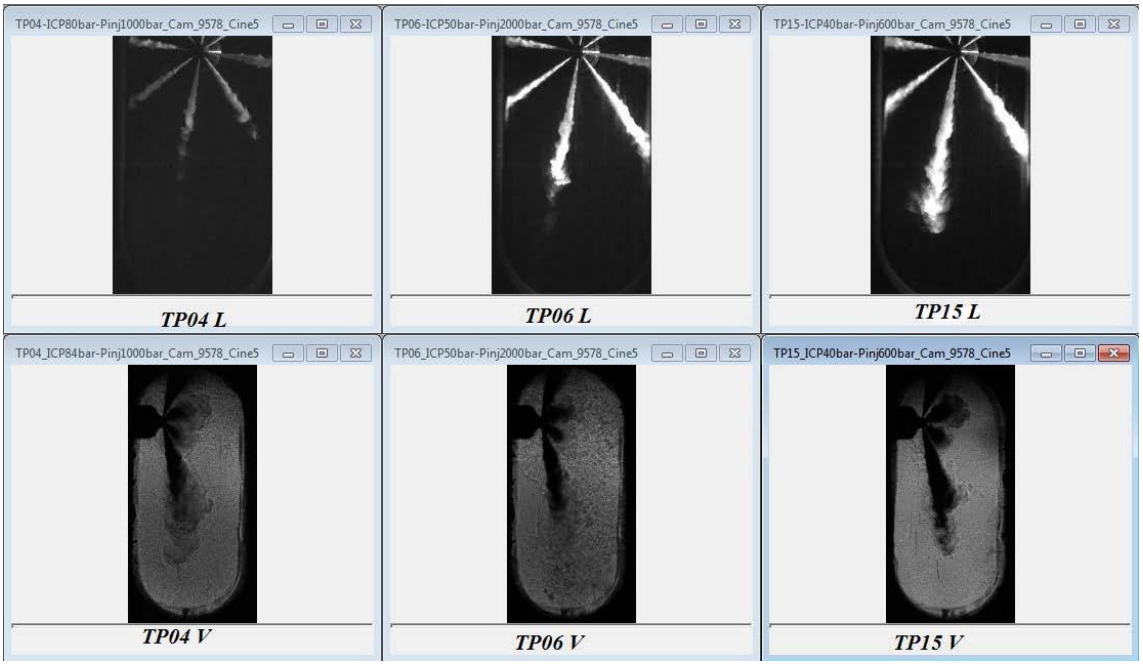

Figure 4-9: Liquid (L) and vapour (V) image data from injector B spray measurement acquired for TP04 (84 bar in-cylinder pressure and 1000 bar injection pressure), TP06 (50 bar in-cylinder pressure and 2000 bar injection pressure) and TP15(40 bar in-cylinder pressure and 600 bar injection pressure).

The trend of decrease in spray penetration with increase in in-cylinder pressure is clearer in Figure 4-6 than in Figure 4-8. It is also evident that the time to reach the maximum penetration decreases with increasing in-cylinder pressure. These trends are due mainly to the effects of air (cylinder) temperature on the fuel droplet evaporation process.

In the dilute spray region, increased in-cylinder pressure and temperature cause spray evaporation in the combustion chamber (Soljo et al, 2011). Researchers (Siebers, 1999; Siebers, 2009) reported that vaporisation was mixing limited. This proposed that the liquid fuel spray would be completely vaporised at an axial distance where the total hot entrained air contained adequate energy to vaporise the spray. From the point of view of fluid mechanics, the evaporation of droplets involves simultaneous heat and mass transfer processes. The heat of evaporation is transferred from surrounding hot gases to the drop surface by conduction and convection, while vapour is transferred to the surrounding by convection and diffusion. The evaporation rate is dependent on the thermo-physical properties of the fuel and the surrounding air. For very high in-cylinder pressure and temperature, evaporation is quick since the latent heat drastically decreases for high temperatures (Soljo et al, 2011). As the hot entrained air initiates evaporation of the spray, the fuel cools and contracts. These processes significantly reduce droplet dispersion and hence liquid spray penetration as shown in Figure 4-6, Figure 4-8 and Figure 4-9 (Bougie et al., 2005; Arcoumanis et al., 2008).

The role of the ambient density in the context of the evaporation is identified. For the contraction initiated by the fuel cooling, the combustion chamber volume is reduced thus increasing the ambient density (Naber JD et al., 1996; Johnson et al., 2012). Studies have also shown that a combination of high injection pressure and low ambient density (or low injection pressure and high ambient density) enhances spray penetration (Bruneaux et al., 1999). This is because high injection pressure leads to larger momentum transfer from spray to surrounding gas, while high ambient density is associated with increase in spray dispersion. From earlier discussions, the former has the tendency to increase (liquid) spray penetration, while the latter has the tendency to reduce (liquid) spray penetration due to increased aerodynamic

interaction. Actually with high ambient density, the higher density of the volume of gas entrained, due to increased dispersion, requires more kinetic energy to complete the momentum transfer, and this reduces the liquid spray penetration. The contraction on cooling and effect of ambient density is possible for a vaporising condition. Under non-vaporising condition, the hot entrained gas would be diluted within the spray. This would result to low ambient density that would enhance (liquid) spray penetration (Johnson et al., 2012).

4.3 Effect of nozzle geometry

The effect of injector nozzle geometry was investigated by comparing the spray characteristics of the conicity of all the nozzles used in this work. In Figure 4-10, injector A is compared with injector B, Figure 4-11compares injector C with injector D, while an excerpt from the image sequence of liquid spray penetration from the injectors is shown in Figure 4-12.

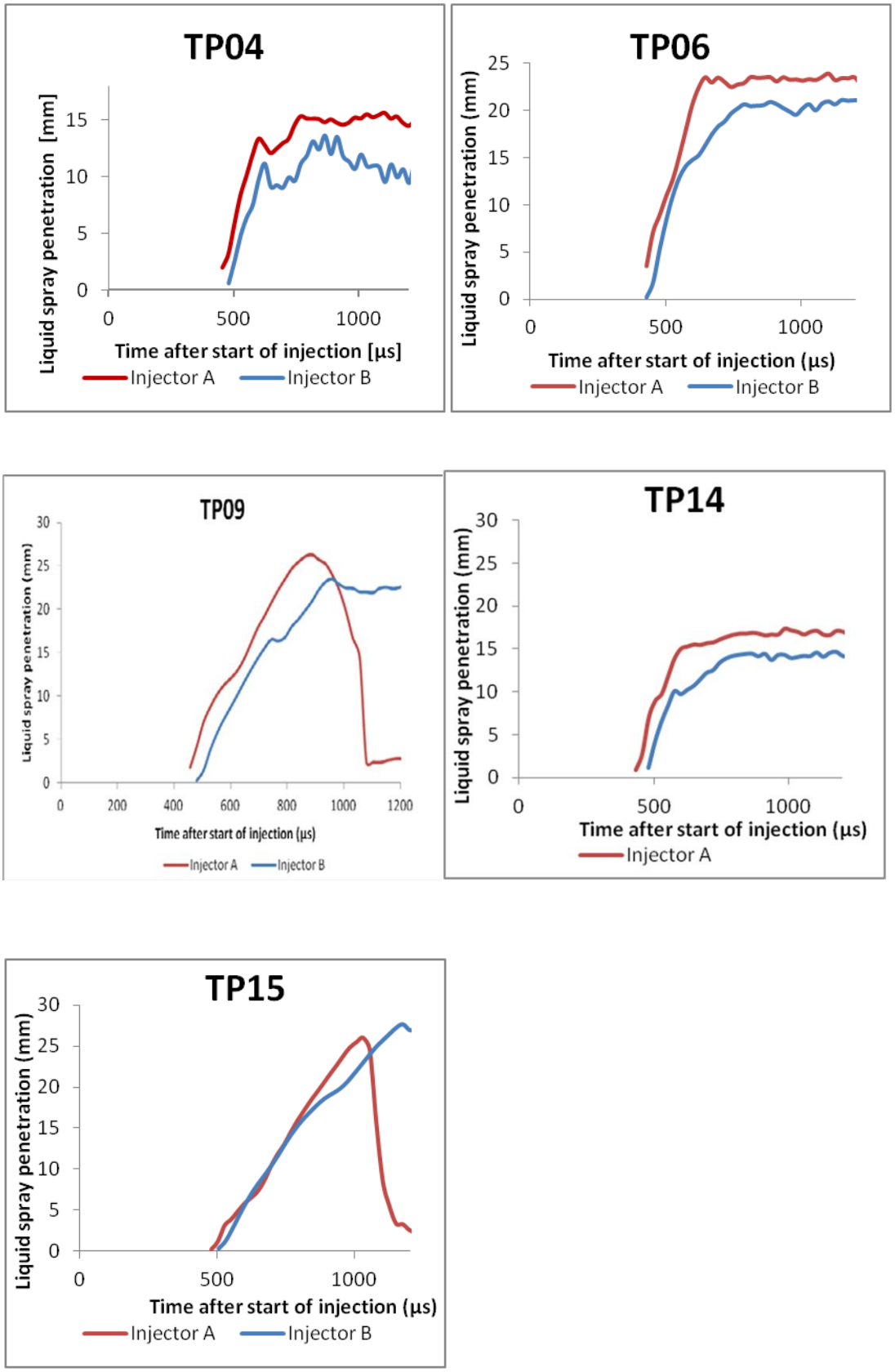

Figure 4-10: Comparison between injectors A and B liquid spray tip penetration measurements

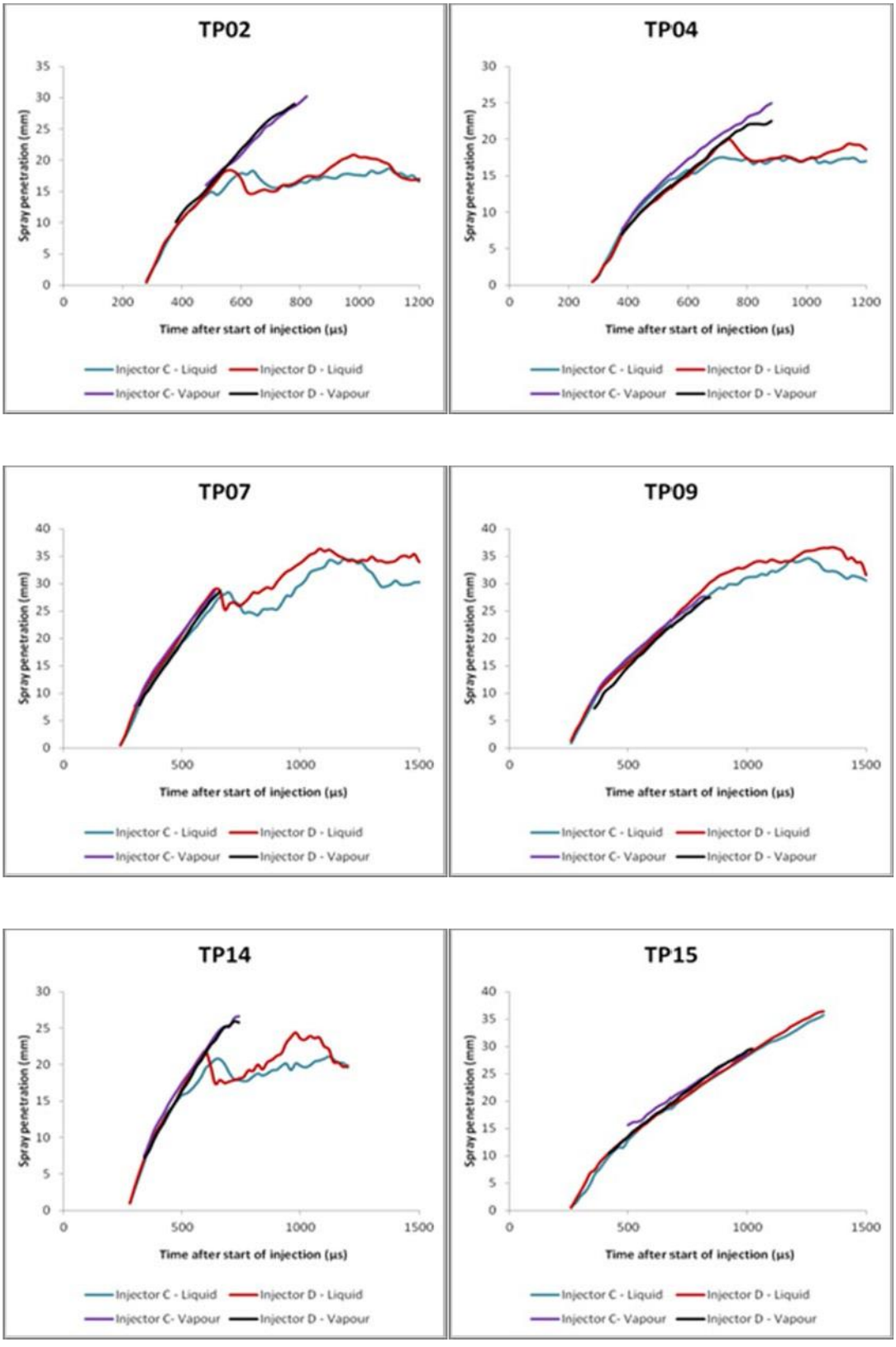

Figure 4-11: Comparison between injectors C and D spray (liquid and vapour) penetration measurements

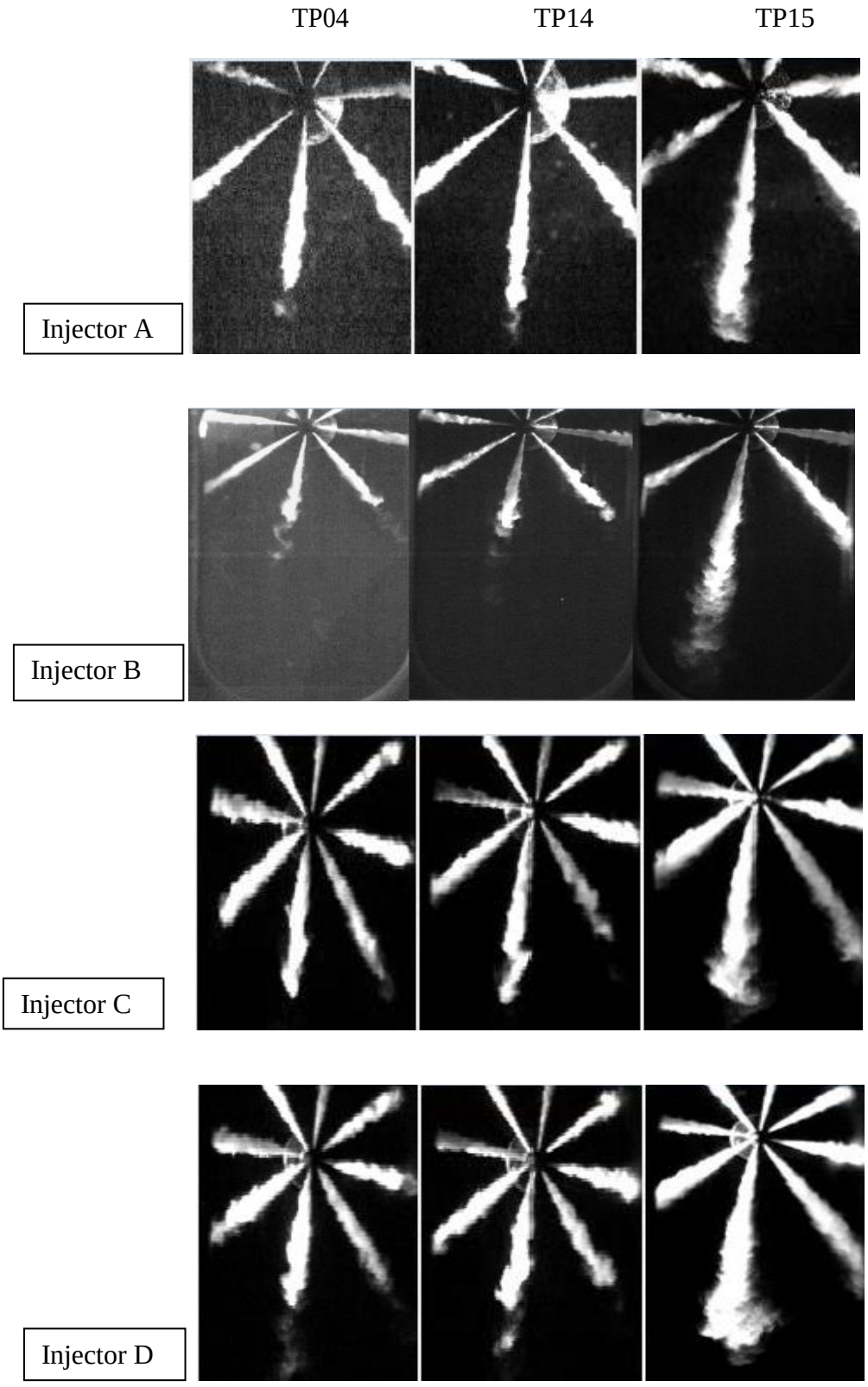

Figure 4-12: Image sequence for selected liquid spray penetration from all the injectors

Earlier in *Table 3-2*, the k-factor for all the injectors A to D were specified as: 2, 1.5, 1.3 and 3.5 respectively. These values define the conicity of the injectors since, the

higher the k- factor the greater the injector conicity. Results from the plots and observations of the image sequence indicate that nozzles with higher k-factor cause higher spray (liquid and vapour) penetration as well as increased nozzle exit velocity and density with increase in conicity (Petkar et al., 2004; Montanaro et al., 2013).

By the definition in Equation 2-9, k-factor can have a negative, zero or positive value. Spray hole (or orifice) with a negative conical shape factor exhibit an orifice with increasing diameter towards the nozzle exit. With a positive value of the conical shape factor, the orifice diameter decreases towards the exit (Figure 4-13). These two configurations implement a conical (or tapering) profile. A zero value for k (i.e. no conicity) indicates a cylindrical orifice since the diameters are equal. This and the negative k-factor nozzle profiles give rise to cavitation since the fuel flow pressure is very much likely to fall below the vapour pressure of the liquid and lead to the formation of vapour bubbles. Excessively strong cavitation can cause damage to the nozzle by inducing erosion. A controlled amount of cavitation would not damage the nozzle, but would provide some advantages such as increased turbulence and fuel atomisation, as well as keep the nozzle free of coke deposit that may otherwise interfere with the fuel flow.

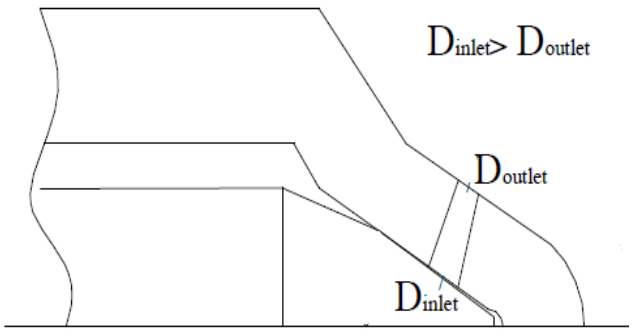

Figure 4-13: k-factor nozzle configuration

The nozzles used for this work are conical nozzles with positive k-factor. The observed trend of increased spray penetration for high k-factor, was because conicity reduces

cavitation and turbulence levels inside the nozzle orifice, which slows down primary breakup, leading to larger droplets, increased spray penetration, and smaller dispersion. Consequently, the vaporization rate and fuel air mixing are reduced, and in the event of combustion, ignition will occur further downstream. However under conditions of high injection pressure, the improved spray velocity which leads to high spray (liquid and vapour) penetration will result in better mixture formation and hence better combustion. Studies have shown that compared to cylindrical nozzles, conical nozzles have higher exit density, velocity and discharge coefficient, even though the fuel injection rate is lower due to smaller exit diameter (Ohishi et al., 2001; Petkar et al., 2004; Montanaro et al., 2013). These characteristics can be attributed to the suppression of cavitation by conical nozzles. Due to the tapered cross section of a conical nozzle, the maximum cross sectional area of the spray hole is utilized. This means same hydraulic (fuel) flow quantity with smaller geometric hole diameter (i.e. higher discharge coefficient), hence the tendency of bubble formation is minimized.

Since the pressure gradient in a diesel nozzle orifice can be over 2000 bar/mm of orifice length the occurrence of cavitation is unavoidable. High injection pressure results in different degree of turbulence and cavitation in internal flow, as well as changing aerodynamic interactions. The intensity of cavitation depends on the degree of conicity. Thus between injectors A and B (with k = 2 and 1.5 respectively) the liquid spray penetration with the latter is higher because of the reduced effects of cavitation and turbulence, and hence improved spray velocity. The same explanation applies to injectors C and D (with k =1.3 and 3.5 respectively). From the image data, no cavitating spray is observed: since there is no spray with the diameter at the nozzle exit bigger than the nozzle diameter. Spray with larger diameter than the exit nozzle contains high vapour content and suggests cavitation in the flow. However, liquid sprays are observed to penetrate further with increased jet diameters at

low in-cylinder pressure (e.g. TP15), as the k-factor increases. An explanation for this observation is that since the nozzle hole converges towards the exit as the k-factor increases, the fuel injection rate continues to reduce. In the absence of cavitation and turbulence that facilitate break-up and atomisation, the liquid density increases. Under this condition, low ambient density will favour liquid spray penetration. This observation should be investigated further.

Vapour penetration also improved, even ever so slightly, for higher k-factor nozzles as shown in TP02, TP04 and TP14 in Figure 4-11. There is not much vaporisation for the other test points. Low in-cylinder pressure was responsible for the poor vaporisation in TP15. However, the TP04 plot, in particular, shows significant deviation from the expected. It was observed that during the transient injection, the liquid spray from the lower k-factor nozzle (Injector C) penetrates more than liquid spray from the high k-factor nozzle (Injector D) at some point. This observation should also be investigated further.

4.4 Uncertainty analysis for the penetration length

The degree of measurement uncertainty of the spray penetration was greater for the earlier part of the spray development, as shown with the sample calculation in Appendix G. In any image the measurement of the penetration may be inaccurate by ±1 pixel. This translates into a larger percentage of the total spray length when the spray length is shorter, which would be during the early part of the spray. For most of the penetration measurements, excluding the first image of the spray tip from the orifice, the degree of uncertainty ranged from 0.25-3.5%. The maximum uncertainty in the measurement of the penetration was determined as 7.12% for Injector A. This was for the first spray image. Similar analysis applies to other injectors with uncertainty measurements calculated as follows: 9.06% (Injector B), 9.41% (Injector C) and 9.41%

(Injector D).

4.5 Conclusions of chapter four

The spray characterisation of high pressure injectors has been analysed by investigating the effects of change in injection pressure, in-cylinder pressure and nozzle geometry. It was observed that increasing the injection pressure did not significantly increase the liquid spray penetration. High injection pressures create fast atomization due to high turbulence inside the nozzle and bigger aerodynamic interaction outside the nozzle. Consequently, the increased fuel spray momentum induced by the increased injection pressure was consumed in the fuel atomizing process. Vapour spray penetration was observed to increase with increase in injection pressure. In-cylinder pressure affects liquid spray penetration depending on droplet evaporation caused by increase in air temperature and ambient gas density and its effect on spray dispersion. High in-cylinder pressure induces increase in air temperature that enhances spray evaporation and hence suppresses liquid spray penetration. On the other hand, the ratio of ambient density to the injected liquid density depends on the in-cylinder pressure. Even though cavitation in diesel injector nozzle occurs mainly due to pressure variations, observations in this work have shown that k-factor nozzles can reduce cavitation tendencies and improve spray velocity by slowing down primary break-up to enhance liquid spray penetration (reducing dispersion) for better mixture formation, and hence better combustion. Furthermore the comparison of the injector A measurements with the Naber model, which was in good agreement is important. The positive result gives a quantitative guidance for a future use of the injector and data. It also confirms the reliability of the experimental methodology employed

From this spray characterisation, the significant influence of injector design and

characteristics (nozzle geometry and injection pressure) and ambient condition (in-cylinder pressure) on HSDI diesel engines spray development was established. This concerns the propagation and dispersion of a high-speed liquid fuel jet into a highly charge in-cylinder environment: its break-up into droplets, vaporization, and in the event of combustion, its ignition. These are processes that directly affect subsequent combustion, soot formation and exhaust gas emission. As a result research studies continue to investigate in-cylinder parameters and optimize characteristics. For example, vapour penetration is an important in- cylinder parameter. The cessation of the penetration of the liquid phase of the spray after liquid length is achieved, and the further penetration by the vapour phase have important implications for direct-injection diesel engines. Increase in vapour penetration improves mixing, results in greater premix burning and faster combustion, which will cause an increase in NOx emission, but with less PM emissions. Under favourable conditions, optimisation in this area will aim to achieve adequate liquid spray penetration and further penetration by only the vapour spray until it impinges on the chamber walls. This is because both under- penetration and over-penetration of liquid spray have been mentioned to have adverse effects. In contrast the impingement of vapour spray on the chamber walls is desirable, and will lead to the formation of a wall jet. Eventually the jet would wrap around to form vortex and influence air entrainment of the free jet. More vortexes enhance air entrainment rate. One way of improving the chances of vortex formation is to guide the vapour spray upon impingement. Based on this, and under favourable in-cylinder conditions (e.g. high injection pressure), it is intuitive to suggest that a well-designed combustion chamber with optimised internal contours would facilitate the development of these vortexes for efficient air/fuel mixing. Thus in this context, the effectiveness of the injector system to a large extent depends on the combustion chamber geometry.

5 CONCLUSIONS

In this study, experiments were carried out to characterise the spray from selected injectors by applying optical techniques on an optical research engine, the Ricardo Proteus. Spray propagation offers significant opportunity to optimise diesel engine combustion for pollutant emission reduction, and hence ensure compliance with emission laws. It is difficult to study all the factors affecting spray development, however an effort was made here to investigate three key parameters (injection pressure, in-cylinder pressure and nozzle geometry) that could provide the necessary insight on in-cylinder spray behaviour. The results of the spatially and temporally resolved optical diagnostic measurements of spray propagation were processed and analysed to discuss the effects of these key parameters.

5.1 Optical technique

Optical diagnostics using high speed image acquisition equipment were developed and optimised around the Ricardo Proteus, to visualise in-cylinder spray penetration. Shadowgraph and Mie scatter techniques were successfully implemented to generate useful data from the spray characterisation. This study has proven that a spray can be characterised in situ rather than inferring spray behaviour from fixed volume combustion chamber investigations. As a result, this study can validate the data obtained from fixed volume chambers to predict spray behaviour. The key differences between the optical and the production engine were identified. An improved understanding of the differences between optical and production engines facilitates the development of appropriate strategies to compensate for these differences on the optical engine. Some of these differences are however unavoidable as they are necessary compromises for the implementation of optical accessibility. Most importantly, the ability to ensure fully representative in-cylinder spray behaviour at

different conditions and the flexibility of applying different optical techniques ultimately increase the value of optical engine data, highlighting the importance of using such engine as a veritable research tool.

5.2 Spray characterisation

The results of the measurements conducted in this study have provided answers for the two research questions presented in chapter one. It has been possible to identify three key parameters that drive in-cylinder spray behaviour: injection pressure, in-cylinder pressure and nozzle geometry. The effects of these parameters have been quantified by interpreting observed trends with support from the understanding gained from literature.

The results suggest that increase in injection pressure induces increase in momentum which controls the transient injection stage of liquid spray penetration up to the liquid length. During the steady state injection, which starts from the liquid length, the increase in injection pressure has no effect on liquid tip penetration. For liquid spray, the high energy provided by the increased injection pressure is compensated by an equivalent increase in air entrainment, and therefore evaporation. An expected trend is observed for vapour penetration, which increases with increase in injection pressure. The effect of nozzle geometry is based on the k- factor. The higher the k-factor: the greater the conicity, the lesser the cavitation and the longer the spray penetration.

Spray penetration is crucial for diesel combustion. It has been shown to be a process of momentum transfer between spray droplets and the ambient gas. This will continue to make high injection pressure an appealing parameter. High injection pressure provides the capability that enables characterisation of high pressure diesel fuel sprays and combustion for emission (PM and NOx) reduction to satisfy legislative requirements. Higher injection pressures improve atomisation and fuel-air mixing,

enabling increased EGR application, for simultaneous reduction of PM and NOx.. A well optimised injector nozzle, with highly conical characteristics will facilitate the realization of these important benefits of high pressure injection, especially if complemented with optimised piston bowl geometry. This is why the measurements conducted in this study, with the sophisticated equipment and techniques employed, are crucial. The characterisation of in-cylinder spray is very useful in determining the geometric design of high speed direct injection diesel engine combustion chamber. For example, under low speed and light load conditions, the unburned hydrocarbon emissions will be reduced greatly if contact between the fuel spray (liquid length) and the combustion chamber wall is avoided. Under a high speed regime and heavy load, the requirement is different.

The liquid spray measurements that was compared with Naber`s model showed a close match. Such comparison is very important for this work as it provides a quantitative guidance for a future use of the data generated, and at the same time, it confirms the reliability of the experimental methodology employed. Based on this understanding, one can conclude that the data generated in this work could be used in place of real engine data, if the latter is not available.

5.3 Recommendations for further work

This work did not only provide an insight into in-cylinder spray behaviour, it has also provided data for validating spray model. It would be more beneficial to repeat the characterisation with a piston bowl for impingement studies. The understanding provided from the present work will provide the necessary guidance and basis for comparison. The next logical step is to select some of the experimental conditions and replicate them on a conventional research engine. This will provide the opportunity to assess the effect of the piston bowl, especially in terms of

understanding the percentage reduction in pollutant emissions that could be achieved.

It has also been observed that the Matlab code used to process the image data would need to be developed further, to make it a standardised in-house processing algorithm. During the processing of image, some data were lost due to incomplete code.

Image processing with Matlab was quite challenging during the present study. Other challenges were encountered in trying to create engine-like ambient condition in the Proteus, and running at very high injection pressure (especially 2000 bar) without damaging the cylinder gasket. There was also the incessant cleaning of the optical windows due to fouling, during which valuable time was wasted, since the engine was stopped and re-started on each occasion. Nevertheless, the research skill acquired far outweighed these challenges. Through my training on experimental research methods covered, I was able to review past literature to gauge current understanding, learnt about the key parameters and techniques I would be working with and narrow down my research area. With the knowledge gained from literature review, I was able learn how to set-up for experiment, control the key quantities (air, water and oil) for engine start-up, reflect the operating conditions on the engine, conducting the actual experiment with the chosen technique, generating and processing data. Setting-up for the spray characterisation was also instructive, as the final result depended so much on getting every detail right. Besides, the collimated laser shadowgraphy technique employed for this work, until now, had not been implemented in the laboratory, here in Brighton, unlike the Mie-scattering technique. As a result time was spent conducting series of mock trials and researching relevant literature to develop the necessary understanding. The critical task for the technique is to optimise the system sensitivity (based on the high speed laser and camera employed) for quality

image acquisition. My training also taught me how to handle and process large amount of data in the form of images and engine logs. Excel and Matlab were the sofwares deployed for the tasks. It is indeed gratifying to know that all the efforts culminated in the generation of data that are relevant and useful.

References

Abraham, J., A. Khan and V. Magi (2003). "Jet-Jet and Jet-Wall Interactions of Transient Jets from Multi-Holes Injectors." SAE 1999-01-0513.

Abu-Gharbieh, R. (2001). Laser sheet imaging analysis for combustion research. Chalmers University of Technology, Goteborg, Sweden.

Ahmadi-Befrui, B., B. Wiesler and E. Winklhofer (1991). "The propagation of fuel sprays in a research diesel engine - a joint numerical and experimental analysis." SAE Technical Paper 910181.

Alfuso, S., L. Allocca, M. Auriemma, G. Caputo, F. E. Corcione, A. Montanaro and G. Valentino (2005). "Analysis of a high pressure diesel spray at high pressure and temperature environment conditions." SAE Technical Paper 2005-01-1239.

Aorld, M. L., C. Espey, T. Litzinger, D. A. Santavicca and R. J. Santoro (1990). "A study of non-swirling and swirling, and their effects on spray flow fields and combustion in an optically-accessible, D. I. Diesel Engine." SAE Paper 900396.

Arai, M., M. Tabata, M. Shimizu and H. Hiroyasu (1984). "Disintegrating process and spray characterization of fuel jet injected by a diesel nozzle." SAE Technical Paper 840275.

Arcoumanis, C., C. Bae, R. Crookes and E. Kinoshita (2008). "The potential of di-methyl ether (DME) as an alternative fuel for compression-ignition engines: a review." Fuel 87: 1014–1030.

Arcoumanis, C., A. Hadjiapostolou and J. Whitelaw (1991). "Flow and Combustion in a Hydra Direct-Injection Diesel Engine." SAE Technical Paper 910177.

Arcoumannis, C., A. F. Bicen and J. H. Whitelaw (1993). "Squish and swirl-squish interaction in motored model engines." ASME J Fluid Mech: 105-112.

Arcoumannis, C., M. Gavaises and B. French (1997). "Effect of fuel injection processes on the structure of diesel sprays." SAE Paper 970799.

Arre`gle J, Pastor JV and R. S (1999). "The influence of injection parameters on diesel spray characteristics." SAE Technical Paper 1999-01-0200.

Bae, C., J. Yu, J. Kang, J. Kong and K. O. Lee (2002). "Effect of nozzle geometry on the common-rail diesel spray. SAE Paper No. 2002-01-1625; 2002." SAE Paper No. 2002-01-1625.

Bardi, M., R. Payri, L. M. Malbec, G. Bruneaux, L. M. Pickett, J. Manin, T. Bazyn and C. Genzale (2012). "Engine combustion network: comparison of spray development, vaporization, and combustion in different combustion vessels." Atomization and sprays 22(10): 807-842.

Baumgarten., C. (2006). Mixture formation in internal combustion engines. Berlin Heidelberg, Springer.

Benajes, J., J. V. Pastor, R. Payri and A. H. Plazas (2004). "Analysis of the influence of diesel nozzle geometry in the injection rate characteristics." Fluids Engineering 126: 63-71.

Bergstrand, P. and I. Denbratt (2002). "The Effects of Leaner Charge and Swirl on Diesel Combustion." SAE Technical Paper 2002-01-1633

Blessing, M., G. Konig, C. Kruger, U. Michels and V. Schwarz (2003). "Analysis of flow and cavitation phenomena in diesel injection nozzle and its effects on spray and mixture formation." SAE Paper 2003-01-1358.

Block, M. C. (2007). A Report on Engine Technologies for Non-road Tier 3 and Tier 4. USA, EMISSTAR LLC.

Borman, G. L. and W. L. Brown (1992). Pathways to Emission Reduction in Diesel Engines. 2nd Int. Conference on Fluid mechanics, Combustion, Emission and Reliability in Reciprocating Engines. Capri, Italy.

Borthwick, R. P. and P. V. Farrell (2002). "Fuel Injection Spray and Combustion Chamber Wall Impingement in Large Bore Diesel Engines." SAE Technical Paper 2002-01- 0496.

Bougie, B., M. Tulej, T. Dreier, N. Dam, J. T. Meulen and T. Gerber (2005). "Optical diagnostics of diesel spray injections and combustion in a high-pressure high- temperature cell." Appl Phys B 80: 1039–1045.

Bozic, G., S. Kook, I. W. Ekoto, B. R. Petersen and P. C. Miles (2010). Optical investigation into wall wetting from late-cycle post-injections used for diesel particulate filter regeneration (ICEF2010-35075). ASME Int Comb Engine Div Fall Tech, San Antonio, USA.

Brandl, F., C. W. Revenrencic and J. C. Dent (1979). "Turbulent air flow in the combustion bowl of a D. I. diesel engine and its effect on engine performance." SAE Paper 790040.

Browne, K., I. Partridge and G. Greeves (1986). "Fuel property effect on fuel/air mixing in an experimental diesel engine " SAE Paper 860223.

Bruneaux, G. (2005). "Mixing Process in High Pressure Diesel Jets by Normalized Laser Induced Exciplex Fluorescence Part I: Free Jet." SAE 2005-01-2100.

Bruneaux, G. (2005). "Mixing process in high pressure diesel jets by normalized laser induced exciplex fluorescence Part II: Wall impinging versus free jet." SAE 2005-01- 2097.

Bruneaux, G., M. Causse and A. Omrane (2011). "Air entrainment in diesel-like gas jet by simultaneous flow velocity and fuel concentration measurements, comparison of free and wall impinging jet configurations." SAE 2011-01-1828.

Bruneaux, G., D. Verhoeven and T. Baritaud (1999). "High Pressure Diesel Spray and Combustion Visualization in a Transparent Model Diesel Engine." SAE technical Paper 1999-01-3648.

Brunello, G., S. Callera, A. Coghe, G. E. Cossali and F. Gamma (1991). LDV and PDA Characterization of Spray-Wall Interaction. ICLASS-'91. Gaithersburg, USA.

Chartier, C., J. Sjoholm, E. Kristensson, O. Andersson, M. Richter, Bengt Johansson and M. Alden (2012). "Air-Entrainment in Wall-Jets Using SLIPI in a Heavy-Duty Diesel Engine." SAE Paper 2012-01-1718.

Chigier, N. A. (1976). "The Atomization and Burning of Liquid Fuel Sprays." Progress in Energy and Combustion Science 2: 97-114.

Cossali, G. E., A. Coghe and G. Brunello (1993). "Effect of Spray-Wall Interaction on Air Entrainment in a Transient Diesel Spray." SAE Technical Paper 930920.

Crua, C. (2002). Combustion processes in a diesel engine. SCEM/CAE. University of Brighton, Brighton. Ph.D.: 271.

Curt, P. R. (1995). "Combustion Chamber Design." Journal of Automobile Engineering 3(14).

Dan T, Takagishi S, Senda J and F. H (1997). "Effect of ambient gas properties for characteristics of non-reacting diesel fuel spray." SAE Paper 970352.

Dec, J. E. (2009). "Advanced compression-ignition engines: understanding the in-cylinder processes." Proceedings of the Combustion Institute 32: 2727-2742.

Dent, J. C. (1971). "A Basis for the Comparison of Various Experimental Methods for Studying Penetration." SAE Paper 710571.

Diwakar, R. and S. Singh (2009). "Importance of Spray-Bowl Interaction in a DI Diesel Engine Operating under PCCI Combustion mode." SAE Technical Paper 2009-01- 0711.

Docquier, N. (2002). "Optical Investigation of the Effect of fuel Jet Wall Impact Position on Soot Emissions in a Single Cylinder Common Rail Direct Injection Diesel Engine." SAE Technical Paper 2002-01-0495.

Dodge, L. G., T. J. Callahan, T. W. Ryan , J. A. Schwalb, C. E. Benson and R. P. Wilson (1992). "Injection Characteristics of Coal-Water Slurries in Medium Speed Diesel Equipment." ASME Paper ICE No. G00646 vol 16.

Drake, M., T. Fansler, S. AS and G. Szekely (2003). "Piston films as a source of smoke and hydrocarbon emissions from a wall-controlled spark-ignited direct-injection engine." SAE Paper 2003-01-0547.

Eisenhart, C. (1962). "Realistic Evaluation of the Precision and Accuracy of Instrument Calibration Systems." Research National Bureau of Standards-C. Engineering and Instrumentation 67(2): 161-187.

Espey, C. and J. Dec (1995). "The Effect of TDC Temperature and Density on the Liquid- Phase Fuel Penetration in a D. I. Diesel Engine." SAE Technical Paper 952456.

Fang, T., R. Coverdill, C. Lee and R. White (2005). "Liquid and Vapour Fuel Distributions within a High Speed Direct Injection (HSDI) Diesel Engine Operating in HCCI and Conventional Combustion Modes." SAE Technical Paper 2005-01-3838.

Fansler, T. D. (1993). "Turbulence Production and Relaxation in Bowl-in-Psition Engines." SAE Paper 930479.

Ferguson, C. R. (1986). Internal Combustion Engines. New York, Wiley.

Fitzgeorge, D. and J. L. Allison (1962-63). "Air Swirl in a Road-Vehicle Diesel

Engine." Proc. Instn. Mech. Engrs(4).

Genzale, C. L., L. M. Pickett and S. Kook (2010). "Liquid penetration of diesel and biodiesel sprays at late-cycle post-injection conditions." SAE Paper 2010-01-0610.

Genzale, C. L., D. D. Wickman and R. D. Reitz (2006). An Advanced Optimization Methodology for Understanding the Effects of Piston Bowl Design in Low-Temperature Diesel Combustion. Thermo- and Fluid Dynamic Processes in Diesel Engines (THIESEL), Valencia, Spain.

Gunabalan, A. and R. Ramaprabhu (2009). "Effect of piston bowl geometry on flow, combustion and emission in D. I. diesel engine: a CFD approach." International Journal of Applied Engineering Research.

Han, J. S., P. H. Lu, X. B. Xie, M. C. Lai and N. A. Henein (2002). "Investigation of diesel spray primary breakup and development for different nozzle geometries." SAE Paper No. 2002-01-2775.

Hecht, E. (2002). Optics, Addison Wesley.

Held, F. R., S. Bornschlegel, S. Riess, T. Vogel and M. Wensing (2013). "Time and Spatially Resolved Measurements of the Interaction between Liquid and Combusting Diesel Spray and Walls in Modern Diesel Engine Conditions." SAE Paper 2013-24-0063.

Hentschel, W. (1996). Modern tools for diesel engine combustion investigtion. Sixth International Sympium on combustion. Naples, Italy.

Heywood, J. B. (1988). Internal Combustion Engine Fundamentals, McGraw-Hill, New York.

Hiroyasu, H. (2000). "Spray breakup mechanism from the hole-type nozzle and its applications." Atomization and Sprays 10: 511-527.

Hiroyasu, H. and M. Arai (1990). "Structure of Fuel Sprays in Diesel Engines." SAE Paper 900475.

Hiroyasu, H., M. Arai and M. Tabata (1989). "Empirical Equations for the Sauter Mean Diameter of a Diesel Spray." SAE Technical Paper 890464.

Hiroyasu, H. and K. Nishida (1989). "Fuel Spray Trajectory and Dispersion in a D.I. Diesel Combustion Chamber," SAE Paper." SAE Paper 890462.

Ishikawa, N. and L. Zhang (1999). "Characteristics of Air-Entrainment in a Diesel Spray." SAE Paper No. 1999-01-0522.

Johnson, J., J. Naber, S.-Y. Lee, G. Hunter, R. Truemner and T. Harcombe (2013). "Correlations of Non-Vaporizing Spray Penetration for 3000 Bar Diesel Spray Injection." SAE paper 2013-24-0033.

Johnson, J. E., S. H. Yoon, J. D. Naber, S. Lee, G. Hunter, R. Truemmer and T. Harcombe (2012). Characteristics of 3000 bar Diesel Spray Injection under Non-Vaporizing and Vaporizing Conditions. 12th Triennial Conference on Liquid Atomization and Spray Systems (ICLASS 2012) Heidelberg, Germany: 2-6.

Kashdan, J., S. Mendez and G. B. G (2007). "On the origin of unburned hydrocarbon emissions in a wall-guided, low NOx diesel combustion system " SAE Paper 2007- 01-1836.

Kashdan, J. T., S. Mendez and G. Bruneaux (2007). "On the origin of unburned hydrocarbon emissions in a wall-guided, low NOx diesel combustion system." SAE Paper 2007- 01-1836.

Kato, T., K. Tsujimura, M. Shintani, T. Minami and I. Yamaguchi (1989). "Spray Characteristics and Combustion Improvements of D.I. Diesel Engine with High-Pressure Fuel Injection." SAE Paper 890265.

Kawanabe, H., C. Kondo, S. Kohori and M. Shioji (2008). "Simultaneous measurements of velocity and scalar fields in a turbulent jet using PIV and LIF." JSME 74(742): 1411- 1418.

Kennard, D. A., C. Crua, J. Lacoste, M. R. Heikal, M. R. Gold and N. S. Jackson (2002). "In- cylinder Penetration and Break-up of Diesel Sprays using a Common-Rail Injection System." SAE Paper 2002-01-1626.

Kennedy, I. M. (1997). "Models of soot formation and oxidation." Prog. Energy Combust. Sci. 23: 92-132. .

Khair, M. K. (2010). "Rate of heat release." Retrieved [10/11/2010], from://www.dieselnet.com/tech/diesel_comb.html.

Khalid' A., T. Yatsufusa, T. Miyamoto, J. Kawakami and Y. Kidoguchi (2009). "Analysis of Relation between Mixture Formation during Ignition Delay Period and Burning Process in Diesel Combustion." SAE Technical Paper 2009-32-0018.

Kim, T. and J. Ghandhi (2003). "Characterization of evaporating diesel sprays using exciplex laser-induced fluorescence measurements." Atomization Sprays 13: 535-559.

Klein-Douwel, R. J. H., P. J. M. Frijters, X. L. Seykens, L. M. T. Somers and R. S. G. Baert (2009). "Gas density and rail pressure effects on diesel spray growth from a heavy- duty common rail injector." Energy Fuels 23: 1832–1842.

Klein-Douwel, R. J. H., P. J. M. Frijters, L. M. T. Somers, W. A. d. Boer and R. S. G. Baert (2007). "Macroscopic diesel fuel spray shadowgraphy using high speed digital imaging in a high pressure cell." Fuel 86: 1994–2007.

Kook, S. and C. Bae (2004). "Combustion Control Using Two-Stage Diesel Fuel Injection in a Single-Cylinder PCCI Engine." SAE Technical Paper 2004-01-0938.

Kook, S. and L. M. Pickett (2012). "Liquid length and vapour penetration of conventional, Fischer–Tropsch, coal-derived, and surrogate fuel sprays at high-temperature and high-pressure ambient conditions." Fuel 93: 539–548.

Lefebvre, A. H. (1980). "Air blast atomization." Prog Energy Combust Sci 6: 233-261.

Lefebvre, A. H. (1989). Atomization and Sprays. Washington, DC, Taylor & Francis.

Lippert, A. M., D. W. Stanton, R. D. Reitz, C. J. Rutland and W.L.H. Hallett (2001). "Investigating the Effect of Spray targeting and Impingement on Diesel Engine Cold Start." SAE paper 2000-01-0269.

Lu, X., D. Han and Z. Huang (2011). "Fuel design and management for the control of advanced compression-ignition combustion modes." Progress in Energy and Combustion Science 37: 741-783.

Luckhchoura, V., F.-X. Robert, N. Peters, M. Rottmann and S. Pischinger (2010). "Investigation of Spray-Bowl Interaction Using Two-part Analysis in a Direct-Injection Diesel Engine." SAE Technical Paper 2010-01-0182.

Lyle, M. P., S. Kook and T. C. Williams (2009b). "Visualization of Diesel Spray Penetration, Cool Flame, Ignition, High temperature Combustion, and Soot Formation using High- Speed Imaging." SAE Paper № : 2009-01-0658.

Lyle, M. P. and S. a. W. Kook, T. C. (2009a). "Transient Liquid Penetration of early-injection Diesel Sprays." SAE Paper № : 2009-01-0839.

Magnusson, A., S. Andersson and S. Jedrzejowski (2006). "Spray-Wall Interaction: Diesel Fuels Impinging on a Tempered Wall." SAE Paper 20001-01-1116.

Majasky, A . (2012). "Diesel emission." Retrieved [09/12/2014], from://www.dieselnet.com/tech/emi_comb.php.

Martin, G., C. Mueller, D. Milam, M. Radovanovic and C. Gehrke (2008). "Early directinjection, low-temperature combustion of diesel fuel in an optical engine utilizing a 15-hole, dual-row, narrow-included-angle nozzle." SAE Paper 2008-01- 2400.

Martin, G. C., C. J. Mueller, D. M. Milam, M. S. Radovanovic and C. R. Gehrke (2008). "Early directinjection, low-temperature combustion of diesel fuel in an optical engine utilizing a 15-hole, dual-row, narrow-included-angle nozzle." SAE Paper 2008-01- 2400.

Minami, T., I. Kamaguchi, M. Shintani, K. Tsujimura and T. Suzuki (1990). "Analysis of Fuel Spray Characteristics and Combustion Phenomena Under High-Pressure Fuel Injection." SAE Paper 900438.

Montanaro, A., L. Allocca, J. Johnson, S.-Y. Lee, J. Naber and A. Zhang (2013). "Influence of the Nozzle Geometry of a Diesel Single-Hole Injector on Liquid and Vapor Phase Distributions at Engine-Like Conditions." SAE paper 2013-24-0038.

Morcos, M., G. Parsons, F. Lauterwasser, M. Boons and W. Hartgers (2009). "Detection methods for accurate measurements of the FAME biodiesel content in used crankcase engine oil." SAE Paper 2009-01-2661).

Morel, T. and R. Keribar (1985). "A Model for Predicting Spatially and Time Resolved Convective Heat Transfer in Bowl-in-Piston Combustion Chambers." SAE Paper 850204.

Morgan, R., J. Wray, D. A. Kennaird, C. Crua and M. R. Heikal (2001). "The Influence of Injector Parameters on the Formation and Break-up of a Diesel Spray." SAE Technical Paper 2001-01-0529.

Mulemane, A., J. S. Han, P. H. Lu, S. J. Yoon and M. C. Lai (2004). "Modeling dynamic behaviour of diesel fuel injection systems." SAE Paper No. 2004-01-0536.

Myong, K., M. Arai, H. Suzuki, J. Senda and H. Fujimoto (2004). "Vaporization characteristics and liquid-phase penetration for multi-component fuels." SAE Paper 2004-01-0529.

Naber JD and S. DL (1996). "Effects of gas density and vaporization on penetration and dispersion of diesel sprays." SAE Paper 960034.

Naber, J. D. and P. Farrell (1993). "Hydrodynamics of droplet impingement on a heated surface." SAE Paper 930919.

Naber, J. D. and D. L. Siebers (1996). "Effects of Gas Density and Vaporization on Penetration and Dispersion of Diesel Sprays." SAE Paper No. 960034.

Ohishi, K., T. Maeda and K. Hummel (2001). "The new common-rail fuel system for the Duramax 6600 V8 diesel engine." SAE Paper 2001-01-2704.

Ohnesorge, W. (1931). "Nozzles, the formation of drops and the resolution of diesel fuel solution using rays." Applied Mathematics and Mechanics 16(6): 355-358.

Oinuma, R., S. Takuma, T. Koyano and M. Takiguchi (2005). "Effects of post injection on piston lubrication in a common rail small bore diesel engine." SAE Paper 2005-01- 2166.

Oppenheim, A. K., P. A. Urtiew and F. J. Weinberg (1966). "On the use of laser light sources in Schlieren-interferometer systems." Proceeding of the Royal Society of London. Series A, containing papers of a mathematical and physical character.

Osuka, I., M. Nishimura, Y. Tanaka and M. Miyaki (1994). "Benefits of New Fuel Injection System Technology on Cold Startability of Diesel Engines – Improvement of Cold Startability and White Smoke Reduction by Means of Multi Injection with Common Rail Fuel System (ECD-12)." SAE Technical Paper 940586.

Park, K., D. M. Wang and A. P. Watkins (1993). "A contribution to the design of a novel direct injection diesel engine combustion system-analysis of pip size." Appl. Math. Modelling 17: 114-124.

Park, S. H., H. J. Kim, H. K. Suh and C. S. Lee (2009). "Experimental and numerical analysis of spray-atomization characteristics of biodiesel fuel in various fuel and ambient temperatures conditions." International Journal of Heat and Fluid Flow 30: 960-970.

Pastor, J. V., R. Payri, J. M. Garcia-Oliver and J. Nerva (2012). "Schlieren Measurements of the ECN-Spray A Penetration under Inert and Reacting conditions." SAE Paper № : 2012-01-0456..

Pasupathy, V. S. and G. Nagarajan (2010). "Effects of the Re-entrant Bowl Geometry on a D.I. Turbocharged Diesel Engine Performance and Emissions: A CFD Approach." Journal of engineering for gas turbines and power 132.

Payri, F., J. Benajes, X. Margot and A. Gil (2004). "CFD Modelling of the in-cylinder flow in direct-injection Diesel engines." Computers & Fluids 33: 995-1021.

Payri, F., V. Bermudez, R. Payri and F. J. Salvador (2004). "The influence of cavitation on the internal flow and the spray characteristics in diesel injection nozzles." Fuel 83: 419-431.

Payri, F., X. Margot, S. Patouna, F. Ravet and M. Funk (2009). "A CFD study of the effect of the needle movement on the cavitation pattern of diesel injectors." SAE Paper No. 2009-24-0025.

Payri, R., J. García-Oliver, M. B. M and J. Manin (2012). "Fuel temperature influence on diesel sprays in inert and reacting conditions." Appl Therm Eng 35: 185-195.

Payri, R., J. M. Garcia, F. J. Salvador and J. Gimeno (2005). "Using spray momentum flux measurements to understand the influence of diesel nozzle geometry on spray characteristics." Fuel 84: 551-561.

Payri, R., J. Gimeno, M. Bardi and A. H. Plazas (2013). "Study liquid length penetration results obtained with a direct acting piezo electric injector." Applied Energy 106: 152- 162.

Payri, R., F. J. Salvador, J. Gimeno and L. D. Zapata (2008). "Diesel nozzle geometry influence on spray liquid-phase fuel penetration in evaporative conditions." Fuel 87: 1165-1176.

Payri, R., F. J. Salvador and J. G. L. D. Zapata (2008). "Diesel nozzle geometry influence on spray liquid-phase fuel penetration in evaporative conditions." Fuel 87: 1165-1176.

Petkar, R. M., C. A. Kardile, P. V. Deshpande, R. Isenburg and R. Soorajith (2004). "Influence of Increased Diesel Fuel Spray Velocities and Improved Spray Penetration in DI Engines." SAE Technical Paper 2004-01-0031.

Pickett, L., C. Genzale, G. Bruneaux, L.-M. Malbec, L. Hermant, C. Christiansen and J. Schramm (2010). "Comparison of diesel spray combustion in different high temperature, high pressure, facilities." SAE Paper 2010-01-2106.

Pickett, L. and J. Lopez (2005). "Jet–wall interaction effects on diesel combustion and soot formation." SAE Paper 2005-01-0921,.

Pickett, L. M., C. L. Genzale, G. Bruneaux, L.-M. Malbec, L. Hermant, C. Christiansen and I. Schramm (2010). "Comparison of Diesel Spray Combustion in Different High- Temperature, High-Pressure Facilities." SAE Technical Paper 2010-01-2106.

Pickett, L. M., S. Kook and Williams (2009). "Transient Liquid Penetration of Early-Injection Diesel Sprays." SAE Technical Paper 2009-01-0839.

Pidwirny, M. (2006). Acid Precipitation. Fundamentals of Physical Geography.

Pierpont, D. A. and R. D. Reitz (1995). "Effects of Injection Pressure and Nozzle Geometry on D.I. Diesel Emissions and Performance." SAE Paper 950604.

Plee, S. L., J. P. Myers and T. Ahmed (1981). "Flame Temperature Correlation for the Effects of Exhaust Gas Recirculation on Diesel Particulate and NOx Emissions." SAE Technical Paper 811195.

Prasad, B. V. V. S. U., T. N. C. Anand, C. S. Sharma and R. V. Ravikrishna (2011). "High swirl-inducing piston bowls in small diesel engines for emission reduction." Applied Energy 88: 2355-2367.

Raj, A. R. G. S., J. M. Mallikarjuna and V. Ganesan (2012). "Energy efficient piston configuration for effective air motion – A CFD study." Applied Energy 30.

Rajalingam, B. V. and P. V. Farrell (1999). "The Effect of Injection Pressure on Air Entrainment Into Transient Diesel Sprays." SAE Paper No. 1999-01-0523.

Rao KK, Winterbone DE and C. E (1992). "Laser illuminated photographic studies of the spray and combustion phenomena in a small high speed DI diesel engine." SAE Paper 922203;.

Reitz, R. D. and F. B. Bracco (1979). "On the Dependence of Spray Angle and Other Spray Parameters on Nozzle Design and Operating Conditions." SAE Technical Paper 790494.

Reitz, R. D. and F. V. Bracco (1982). "Mechanism of Atomization of a Liquid Jet." Physics of Fluids. 25.

Reitz, R. D. and F. V. Bracco (1986). Mechanisms of breakup of round liquids jets. The Encyclopedia of fluid Mechancis. N. P. Ceremisinoff. 3: 223-229.

Rhim, D. R. and P. V. Farrell (2000). "Characteristics of Air Flow Surrounding Non-Evaporating Transient Diesel Sprays." SAE Paper No. 2000-01-2789.

Richard, H. and M. Raffel (2001). "Principle and applications of the background oriented schlieren (BOS) method." Measurement Science and Technology 6: 1576–1585.

Risi, A. d., T. Donateo and D. Laforgia (2003). "Optimization of the Combustion Chamber of Direct Injection Diesel Engines." SAE Technical Paper 2003-01-1064.

Ryan, T. W. and S. M. Shahed (1994). "Injection Pressure and Intake Air Density Effects on Ignition and Combustion in a 4-Valve Diesel Engine." SAE Paper 941919.

Saito, T., Y. Daisho, N. Uchida and N. Ikeya (1986). "Effects of Combustion Chamber Geometry on Diesel Combustion." SAE Technical Paper 861186.

Sasaki, S., H. Akagawa and K. Tsujimura (1998). "A Study on Surrounding Air Flow Induced by Diesel Sprays." SAE Paper No. 980805.

Schünemann, E., S. Fedrow and A. A. Leipertz (1998). "Droplet Size and Velocity Measurements for the Characterization of a DI-Diesel Spray Impinging on a Flat Wall." SAE Technical Paper 982545.

Settles, G. S. (2001). Schlieren and Shadowgraph. Heidelberg, Germany Springer-Verlag.

Settles, G. S. (2006). Schlieren and Shadowgraph Techniques: Visualizing Phenomena in Transparent Media. Springer.

Shenghua, L., J. W. Hwang, M. H. Kim, J. O. Chae and T. Chung (2000). Simulating the effects of Fuel Injection Characteristics on DI Diesel Engine

Emissions. FISITA World Automotive Congress. Seoul.

Shimada, T., T. Shoji and Y. Takeda (1989). "The Effect of Fuel Injection Pressure on Diesel Engine Performance." SAE Paper 891919.

Shimazaki, N., H. Hatanaka, K. Yokota and T. Nakahira (1996). "A Study of Diesel Combustion Process Under the Condition of EGR and High-Pressure Fuel Injection with Gas Sampling Method." SAE Paper 960030.

Shimoda, M., M. Shigemori and S. Tsuruoka (1985). "Effect of Combustion Chamber Configuration on In-Cylinder Air Motion and Combustion Characteristics of D. I. Diesel Engines." SAE Technical Paper.

Shundoh, S., T. Kakegawa, K. Tsujimura and S. Kobayashi (1991). "The Effect of Injection Parameters and Swirl on Diesel Combustion with High Pressure Fuel Injection." SAE Technical Paper 910489.

Shundoh, S., T. Kakegawa and K. Tsujimurwa (1991). "The Effect of Injection Parameters and Swirl on Diesel Combustion with High Pressure Fuel Injection." SAE Paper 910489,.

Siebers, D. (2009). Recent developments on diesel fuel jets under quiescent conditions. Berlin Heidelberg, Springer.

Siebers, D. L. (1998). "Liquid-Phase Fuel Penetration in Diesel Sprays." SAE Paper No.980809.

Siebers, D. L. (1999). "Scaling Liquid-Phase Fuel Penetration in Diesel Sprays Based on Mixing-Limited Vaporization." SAE Paper No. 1999-01-0528.

Siebers, D. L. (1999). "Scaling liquid-phase fuel penetration in diesel sprays based on mixing-limited vaporization." SAE Paper 1999-01-0528.

Smallwood, G. J. and Ö. L. Gülder (2000). "Views on the Structure of transient diesel sprays." Atomization and Sprays 10: 355-386.

Som, S., A. I. Ramirez, S. K. Aggarwal, A. L. Kastengren, E. El-Hannouny, D. E. Longman, C. F. Powell and P. K. Senecal (2009). "Development and Validation of a Primary Breakup Model for Diesel Engine Applications." SAE Technical Paper 2009-01-0838.

Song, B. H. and Y. H. Choi (2008). "Investigation of variations of lubricating oil diluted by post injected fuel for the regeneration of CDPF and its effects on engine wear." Mech Sci Technol 22: 2526–2533.

Song, J., C. Yao, Y. Liu and Z. Jiang (2008). "Investigation on Flow Field in Simplified Piston Bowls for DI Diesel Engine." Engineering Applications of Computational Fluid mechanics 2(3): 354-365.

Song, L. and J. Abraham (2003). "The Structure of Wall-Impinging Jets: Computed vs. Theoretical and Measured Results." Journal of Fluids Engineering 125.

Stanton, D. W., A. M. Lippert, R. D. Reitz and C. J. R. CJ. (1998). "Influence of spray-wall interaction and fuel films on cold starting in direct injection diesel engines." SAE Paper 982584.

Stiesch, G. (2003). Modelling engine spray and combustion process. Berlin Heidelberg, Springer.

Stone, R. (1992). Introduction to Internal Combustion Engines. London, Macmillan.

Suh, H. and C. Lee (2008). "Experimental and analytical study on the spray characteristics of dimethyl ether (DME) and diesel fuels within a common-rail injection system in a diesel engine." Fuel 87: 925-932.

Takahashi, H., K. Tomaru, S. Shiga, T. Karasawa and T. Kurabayashi (1991). "Characteristics of Diesel Spray with Unsteady and Higher Injection Pressure Using a Rapid Compression Machine." SAE Technical Paper 910226.

Takeda, Y., N. Ishikawa, M. Komori and K. Tsujimura (1994). "Diesel Combustion Improvement and Emissions Reduction Using VCO Nozzles with High Pressure Fuel Injection." SAE Technical Paper 940899.

Takeuchi K, Senda J and S. M. (1983). "Transient characteristics of fuel atomization and droplet size distribution in diesel fuel spray." SAE Technical Paper 830449.

Tao, F. and P. Bergstrand (2008). "Effect of Ultra-High Injection Pressure on Diesel Ignition and Flame under High-Boost Conditions." SAE Technical Paper 2008-01-1603.

Timoney. D.J. (1985). "A Simple Technique for Predicting Optimum Fuel-Air Mixing Conditions in a Direct Injection Diesel Engine With Swirl." SAE Paper 851543.

Tindal, M. J., P. G. Brown and S. C. Kyriakides (1982). An Investigation of Swirl and Turbulence in the Cylinders of D. I. Diesel Engines. IMechE Conference on diesel engines for passenger cars and light duty vehicles. London.

Tree, D. R. and K. I. Svensson (2007). "Soot processes in compression ignition engines." Progress in Energy and Combustion Science 33: 272-309.

Verhoeven D, Vanhemelryck JL and B. T. (1998). "Macroscopic and ignition characteristics of high-pressure sprays of single-component fuels." SAE Paper 981069.

Wade, W. R. (1980). "Light-Duty Diesel NOx-HC-Particulate Trade-Off Studies." SAE Technical Paper 800335.

Wang, T.-C., J.-S. Han, X. Xie, M.-C. Lai, N. A. Henein, E. Schwarz and W. Bryzik (1999). "Direct Visualization of High Pressure Diesel Spray and Engine Combustion." SAE Technical Paper 1999-01-3496.

Wickman DD, Senecal PK and R. RD (2001). "Diesel engine combustion chamber optimization using genetic algorithms and multi-dimensional spray and combustion modeling." SAE Paper no. 2001-01-0547.

Winship, M. and W. J. Morgan (1993). "Piston Design for the Nineties." SAE Technical Paper.

Winterbone, D. E., J. Sun and D. A. Yates (1993). "A Study of Diesel Flame Movement in using the Cross Correlation Method." SAE Paper 930979.

Xueliang, H. and L. Shusong (1990). Combustion in an internal combustion engine. Peking, Mechanical Industry Press.

Zhang, L., T. Tsurushima, T. Ueda, Y. Ishii, T. Itou, T. Minami and K. Yokota (1997). "Measurement of Liquid Phase Penetration of Evaporating Spray in a DI Diesel Engine." SAE Technical Paper 971645.

Zhang, L., T. Ueda, T. Takatsuki and K. Yokota (1995). "A Study of the Effect of Chamber Geometries on Flame Behaviour in a D. I. Diesel Engine." SAE Technical Paper, 952515.

Zhang, Y., T. Ito and K. Nishida (2001). "Characterization of Mixture Formation in Split- Injection Diesel Sprays via Laser Absorption Scattering (LAS) Technique." SAE paper 2001-01-3498.

APPENDICES

Appendix A: Diesel fuel sample certificate

This certificate specifies the components of the diesel fuel used for the spray measurements in the present study.

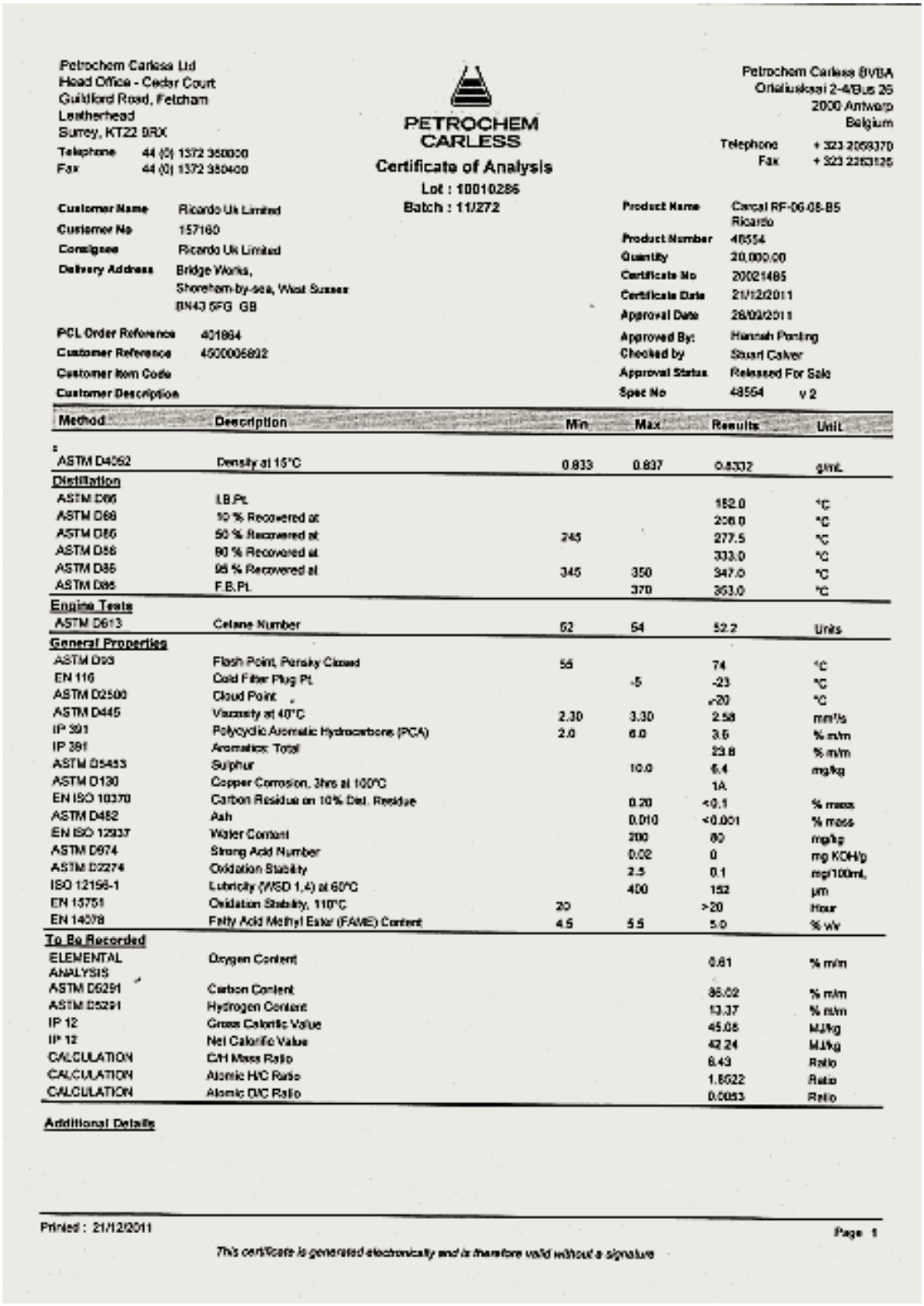

Petrochem Carless Ltd
Head Office - Cedar Court
Guildford Road, Fetcham
Leatherhead
Surrey, KT22 9RX
Telephone 44 (0) 1372 350000
Fax 44 (0) 1372 350400

PETROCHEM CARLESS

Petrochem Carless BVBA
Oriolusiaan 2-4/Bus 26
2000 Antwerp
Belgium
Telephone + 323 2058370
Fax + 323 2353125

Certificate of Analysis

Lot : 10010286
Batch : 11/272

Customer Name	Ricardo Uk Limited	Product Name	Carcal RF-06-03-B5 Ricardo
Customer No	157160	Product Number	48554
Consignee	Ricardo Uk Limited	Quantity	20,000.00
Delivery Address	Bridge Works, Shoreham-by-sea, West Sussex BN43 5FG GB	Certificate No	20021485
		Certificate Date	21/12/2011
		Approval Date	28/09/2011
PCL Order Reference	401864	Approved By:	Hannah Ponting
Customer Reference	4500006802	Checked by	Stuart Calver
Customer Item Code		Approval Status	Released For Sale
Customer Description		Spec No	48554 v 2

Method	Description	Min	Max	Results	Unit
ASTM D4052	Density at 15°C	0.833	0.837	0.8332	g/mL
Distillation					
ASTM D86	I.B.Pt.			182.0	°C
ASTM D86	10 % Recovered at			206.0	°C
ASTM D86	50 % Recovered at	245		277.5	°C
ASTM D86	90 % Recovered at			333.0	°C
ASTM D86	95 % Recovered at	345	350	347.0	°C
ASTM D86	F.B.Pt.		370	353.0	°C
Engine Tests					
ASTM D613	Cetane Number	52	54	52.2	Units
General Properties					
ASTM D93	Flash Point, Pensky Closed	55		74	°C
EN 116	Cold Filter Plug Pt.		-5	-23	°C
ASTM D2500	Cloud Point			<-20	°C
ASTM D445	Viscosity at 40°C	2.30	3.30	2.58	mm²/s
IP 391	Polycyclic Aromatic Hydrocarbons (PCA)	2.0	6.0	3.6	% m/m
IP 391	Aromatics: Total			23.8	% m/m
ASTM D5453	Sulphur		10.0	6.4	mg/kg
ASTM D130	Copper Corrosion, 3hrs at 100°C			1A	
EN ISO 10370	Carbon Residue on 10% Dist. Residue		0.20	<0.1	% mass
ASTM D482	Ash		0.010	<0.001	% mass
EN ISO 12937	Water Content		200	80	mg/kg
ASTM D974	Strong Acid Number		0.02	0	mg KOH/g
ASTM D2274	Oxidation Stability		2.5	0.1	mg/100mL
ISO 12156-1	Lubricity (WSD 1,4) at 60°C		400	152	µm
EN 15751	Oxidation Stability, 110°C	20		>20	Hour
EN 14078	Fatty Acid Methyl Ester (FAME) Content	4.5	5.5	5.0	% v/v
To Be Recorded					
ELEMENTAL ANALYSIS	Oxygen Content			0.61	% m/m
ASTM D5291	Carbon Content			86.02	% m/m
ASTM D5291	Hydrogen Content			13.37	% m/m
IP 12	Gross Calorific Value			45.08	MJ/kg
IP 12	Net Calorific Value			42.24	MJ/kg
CALCULATION	C/H Mass Ratio			6.43	Ratio
CALCULATION	Atomic H/C Ratio			1.8622	Ratio
CALCULATION	Atomic O/C Ratio			0.0053	Ratio

Additional Details

Printed : 21/12/2011

Page 1

This certificate is generated electronically and is therefore valid without a signature

Appendix B: Sample calculation (TP01)

The table below shows the fired conditions for the extracted 50cycles with respect to three parameters (in-cylinder pressure, fuel pressure and intake air temperature) and the statistics calculations thereof, for Test Point 01 of injector A liquid spray measurements.

Fired cycle	TDC ICP (bar)	Fuel pressure (bar)	Intake air temperature (°C)
Cycle1	83.47837293	1940.215665	100.1199245
Cycle11	82.93625399	1997.705383	100.2466073
Cycle21	82.69728953	1940.215665	100.1199245
Cycle31	82.67237672	1969.737412	100.1199245
Cycle41	82.24504709	1974.398741	100.1199245
Cycle51	82.31219538	1966.62986	100.1199245
Cycle61	82.58992128	1955.753427	100.2466073
Cycle71	81.96904711	1988.382726	100.1199245
Cycle81	82.26405128	1932.446784	100.2466073
Cycle91	81.71429621	1979.060069	99.86655899
Cycle101	82.43784808	1954.19965	99.86655899
Cycle111	82.16530789	1920.016575	100.1199245
Cycle121	82.37959047	1951.092098	100.1199245
Cycle131	82.49461387	1954.19965	99.99324176
Cycle141	82.59262166	1940.215665	100.3732901
Cycle151	83.00563447	1988.382726	100.3732901
Cycle161	82.92638568	1952.645874	100.1199245
Cycle171	83.31964283	1934.00056	100.1199245
Cycle181	82.96760547	1943.323217	99.99324176
Cycle191	83.21471866	1989.936502	99.86655899
Cycle201	83.62944946	1958.860979	99.86655899
Cycle211	84.31351858	1940.215665	99.86655899
Cycle221	83.90419964	1972.844964	99.86655899
Cycle231	83.4751536	1972.844964	99.86655899
Cycle241	83.92864108	1913.80147	99.73987622
Cycle251	84.40928624	1946.43077	99.73987622
Cycle261	84.30164741	1991.490278	99.61319345
Cycle271	84.52284479	1949.538322	99.61319345
Cycle281	84.24165753	1924.677903	99.48651067
Cycle291	84.64330069	1935.554337	99.48651067

Cycle301	84.73957938	1947.984546	99.48651067
Cycle311	84.89584161	1958.860979	99.48651067
Cycle321	84.68007989	1921.570351	99.61319345
Cycle331	84.88992665	1918.462799	99.3598279
Cycle341	84.84598903	1930.893008	99.23314513
Cycle351	84.74205359	1935.554337	99.23314513
Cycle361	84.1513049	1958.860979	98.97977958
Cycle371	84.12884728	1934.00056	98.97977958
Cycle381	83.93235082	1946.43077	98.97977958
Cycle391	83.69165409	1934.00056	98.72641404
Cycle401	83.54156312	1943.323217	98.85309681
Cycle411	82.98785153	1923.124127	98.59973127
Cycle421	82.73037645	1907.586366	98.59973127
Cycle431	82.67383206	1940.215665	98.34636572
Cycle441	83.08068313	1946.43077	98.34636572
Cycle451	82.84739636	1876.510842	98.21968295
Cycle461	82.32725098	1941.769441	98.21968295
Cycle471	82.27812131	1949.538322	98.34636572
Cycle481	82.20234657	1918.462799	98.21968295
Cycle491	82.52029877	1893.60238	98.09300017
Median	83.04	1944.88	99.74
Mean	**83.31**	**1946.12**	**99.51**
StDev	**0.926**	**24.963**	**0.687**
Count	50	50	50

Appendix C: Sample calculation (TP06)

The table below shows the fired conditions for the extracted 2cycles with respect to three parameters (in-cylinder pressure, fuel pressure and intake air temperature) and the statistics calculations thereof, for Test Point 06 of injector A liquid spray measurements.

Fired cycle	**TDC ICP (bar)**	**Fuel pressure (bar)**	**Intake air temperature (°C)**
Cycle16	50.48138664	1979.060069	99.10646236
Cycle46	50.41399632	2003.920488	98.97977958
Median	50.44769148	1991.490278	99.04312097
Mean	**50.44769148**	**1991.490278**	**99.04312097**
Stdev	**0.047652156**	**17.57897057**	**0.089578248**
Count	2	2	2

Appendix D: Sample calculation (TP15)

The table below shows the conditions for all the cycles with respect to three parameters (in- cylinder pressure, fuel pressure and intake air temperature) and the statistics calculations thereof, for Test Point 15 of injector A liquid spray measurements.

Cycle	TDC ICP (bar)	Fuel pressure (bar)	Intake air temperature (°C)
Cycle1	41.27788793	591.5379566	98.85309681
Cycle2	41.28430756	585.322852	98.85309681
Cycle3	41.25863536	579.1077473	98.72641404
Cycle4	41.24110713	576.000195	98.72641404
Cycle5	41.44403116	583.7690758	98.72641404
Cycle6	41.13026166	591.5379566	98.85309681
Cycle7	41.41514914	579.1077473	98.85309681
Cycle8	41.34601861	586.8766281	98.72641404
Cycle9	41.34527825	582.2152996	98.72641404
Cycle10	41.20999927	596.1992851	98.72641404
Cycle11	41.35145427	613.2908229	98.85309681
Cycle12	41.47612141	593.0917328	98.85309681
Cycle13	41.28948692	614.844599	98.85309681
Cycle14	41.20185371	588.4304043	98.85309681
Cycle15	41.07767856	610.1832706	98.72641404
Cycle16	41.38107507	588.4304043	98.85309681
Cycle17	41.20777501	593.0917328	98.59973127
Cycle18	41.28874973	586.8766281	98.97977958
Cycle19	41.08977112	600.8606136	98.97977958
Cycle20	41.36157413	599.3068374	98.97977958
Cycle21	40.96757027	586.8766281	98.97977958
Cycle22	41.23147609	589.9841805	98.97977958
Cycle23	41.33639392	599.3068374	98.97977958
Cycle24	41.10582498	579.1077473	98.97977958
Cycle25	41.52006379	589.9841805	98.85309681
Cycle26	41.33071305	610.1832706	98.85309681
Cycle27	41.41810424	582.2152996	98.97977958
Cycle28	41.21617212	594.6455089	98.97977958
Cycle29	41.41687823	602.4143897	98.97977958
Cycle30	41.36231291	599.3068374	98.85309681

Cycle31	41.28430756	610.1832706	98.97977958
Cycle32	41.35910943	603.9681659	98.97977958
Cycle33	41.49488358	597.7530613	98.85309681
Cycle34	41.49562235	588.4304043	98.97977958
Cycle35	41.18555783	597.7530613	98.85309681
Cycle36	41.70348371	586.8766281	98.97977958
Cycle37	41.3608306	596.1992851	98.97977958
Cycle38	41.58424906	599.3068374	98.85309681
Cycle39	41.65608631	582.2152996	98.85309681
Cycle40	41.35046871	607.0757182	98.97977958
Cycle41	41.16136159	603.9681659	98.97977958
Cycle42	41.54154061	605.5219421	98.85309681
Cycle43	41.36206929	591.5379566	98.85309681
Cycle44	41.45538178	607.0757182	98.85309681
Cycle45	41.55635419	611.7370467	98.85309681
Cycle46	41.48994149	603.9681659	98.97977958
Cycle47	41.68718783	613.2908229	98.97977958
Cycle48	41.25986295	579.1077473	98.97977958
Cycle49	41.37268114	579.1077473	98.97977958
Cycle50	41.39341918	603.9681659	98.97977958
Cycle51	41.42131406	603.9681659	98.97977958
Cycle52	41.50426307	583.7690758	98.97977958
Cycle53	41.40057918	579.1077473	98.97977958
Cycle54	41.694351	594.6455089	98.85309681
Cycle55	41.39169009	597.7530613	98.85309681
Cycle56	41.41464446	580.6615235	98.97977958
Cycle57	41.28282208	583.7690758	98.97977958
Cycle58	41.36799377	589.9841805	98.85309681
Cycle59	41.36157096	603.9681659	98.85309681
Cycle60	41.46056589	588.4304043	98.97977958
Cycle61	41.3610758	582.2152996	98.97977958
Cycle62	41.36527594	585.322852	98.85309681
Cycle63	41.27269747	597.7530613	98.97977958
Cycle64	41.46279015	572.8926427	98.85309681
Cycle65	41.38576085	600.8606136	98.97977958
Cycle66	41.56869354	605.5219421	98.97977958
Cycle67	41.38724633	580.6615235	98.97977958
Cycle68	41.41242655	591.5379566	98.97977958
Cycle69	41.62695433	586.8766281	98.97977958
Cycle70	41.44649427	588.4304043	99.10646236
Cycle71	41.40921832	591.5379566	98.97977958
Cycle72	41.38872547	574.4464188	98.97977958
Cycle73	41.36403883	583.7690758	98.97977958
Cycle74	41.56819997	614.844599	98.97977958

Cycle75	41.58942683	580.6615235	99.10646236
Cycle76	41.4499477	600.8606136	98.97977958
Cycle77	41.43365817	605.5219421	98.97977958
Cycle78	41.27220231	596.1992851	98.97977958
Cycle79	41.56893874	577.5539712	98.97977958
Cycle80	41.66348516	585.322852	99.10646236
Cycle81	41.79111851	603.9681659	98.97977958
Cycle82	41.50080329	585.322852	98.97977958
Cycle83	41.51438134	585.322852	99.10646236
Cycle84	41.5412859	608.6294944	98.97977958
Cycle85	41.95898766	577.5539712	98.97977958
Cycle86	41.66447548	585.322852	99.10646236
Cycle87	41.57609874	608.6294944	98.85309681
Cycle88	41.86789626	586.8766281	99.10646236
Cycle89	41.67040155	582.2152996	98.97977958
Cycle90	41.75557006	599.3068374	98.97977958
Cycle91	41.54622957	576.000195	98.97977958
Cycle92	41.7570492	582.2152996	98.97977958
Cycle93	41.52771261	611.7370467	99.10646236
Cycle94	41.53881644	594.6455089	99.10646236
Cycle95	41.51956387	582.2152996	99.10646236
Cycle96	41.70521122	591.5379566	98.97977958
Cycle97	41.61411664	603.9681659	99.10646236
Cycle98	41.29639696	586.8766281	98.97977958
Cycle99	41.41538641	588.4304043	99.10646236
Cycle100	41.59658841	579.1077473	99.10646236
Median	41.4135355	591.5379566	98.97977958
Mean	**41.42993266**	**592.7188265**	**98.9392411**
StDev	**0.176591075**	**10.92926326**	**0.103247814**
Count	100	100	100

Appendix E: Sample calculation (TP01)

The table below shows the fuel tank temperature conditions and the statistics calculations thereof, for Test Point 01 of injector A liquid spray measurements.

Time(s)	Fuel tank T (°C)
1	34.74699887
2	34.93779887
3	35.00139887
4	34.93779887
5	35.70099888
6	35.76459888
7	36.08259888
8	35.95539888
9	36.08259888
10	36.46419888
11	36.40059888
12	35.82819888
13	35.06499887
14	35.89179888
15	35.70099888
16	35.06499887
17	35.44659888
18	36.08259888
19	35.95539888
20	35.57379888
21	35.95539888
22	36.01899888
23	35.51019888
24	35.95539888
25	36.08259888
26	35.89179888
27	36.14619888
28	36.40059888
29	36.78219888
30	36.20979888
31	36.01899888
32	36.33699888
33	36.14619888

34	36.59139888
35	36.65499888
36	37.22739888
37	37.29099888
38	37.41819888
39	36.84579888
40	36.97299888
41	37.29099888
42	37.10019888
43	36.84579888
44	37.10019888
45	37.22739888
46	36.59139888
47	37.48179888
48	38.43579888
49	38.05419888
50	38.49939888
51	38.62659888
52	38.49939888
53	38.30859888
54	38.37219888
55	38.49939888
56	38.75379888
57	38.75379888
58	37.79979888
59	37.60899888
60	38.24499888
Median	36.40059888
Mean	**36.65393888**
StDev	**1.109119746**
Count	60

Appendix F: Spray penetration

results Injector A

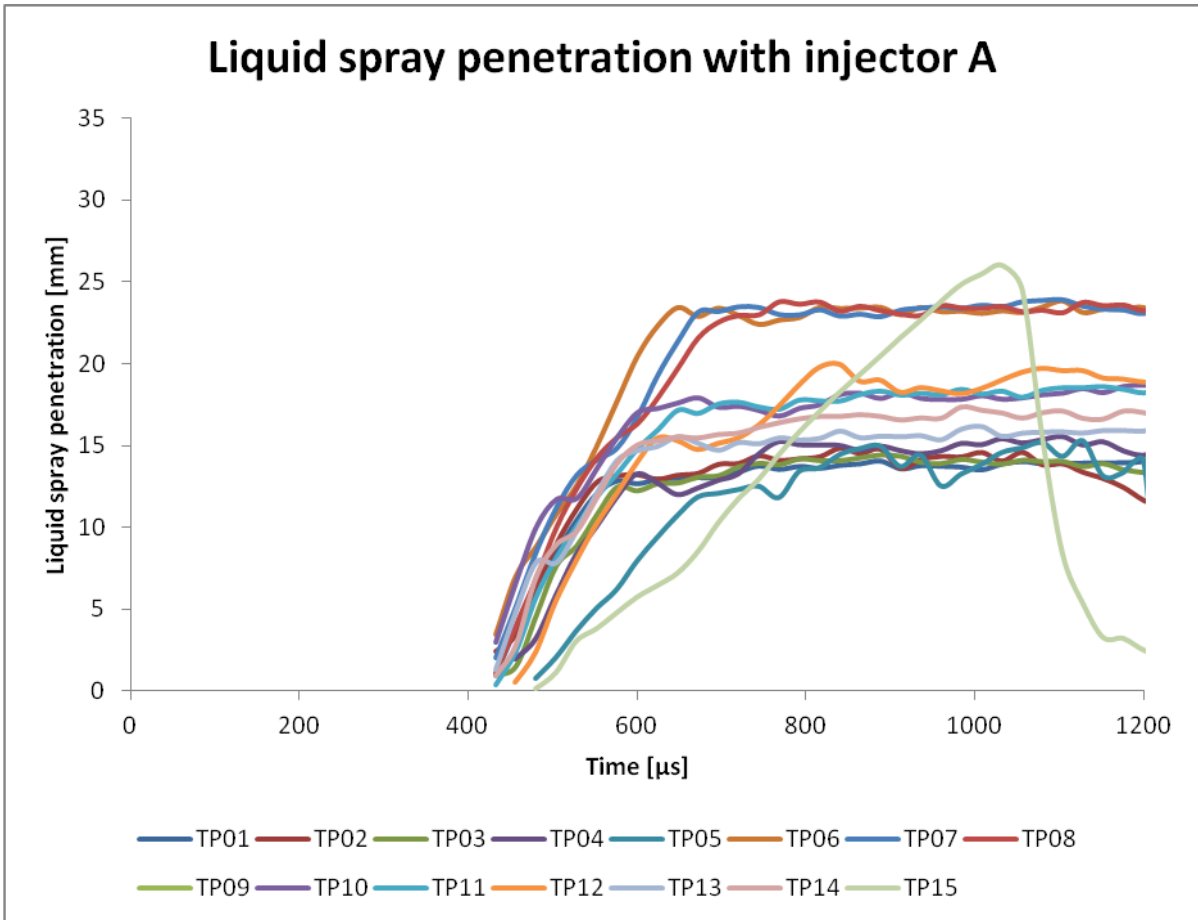

Injector B

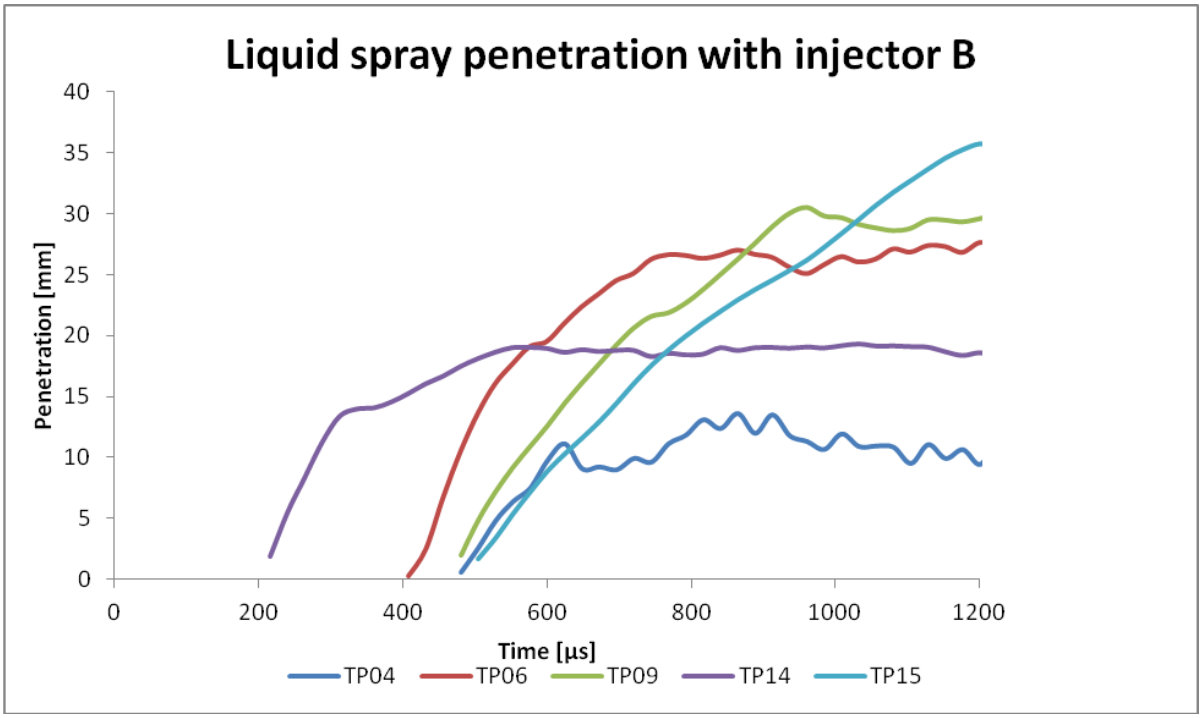
Liquid spray penetration with injector B
Penetration [mm]
0
5
10
15
20
25
30
35
40
0
200
400
600
800
1000
1200
Time [µs]
TP04
TP06
TP09
TP14
TP15

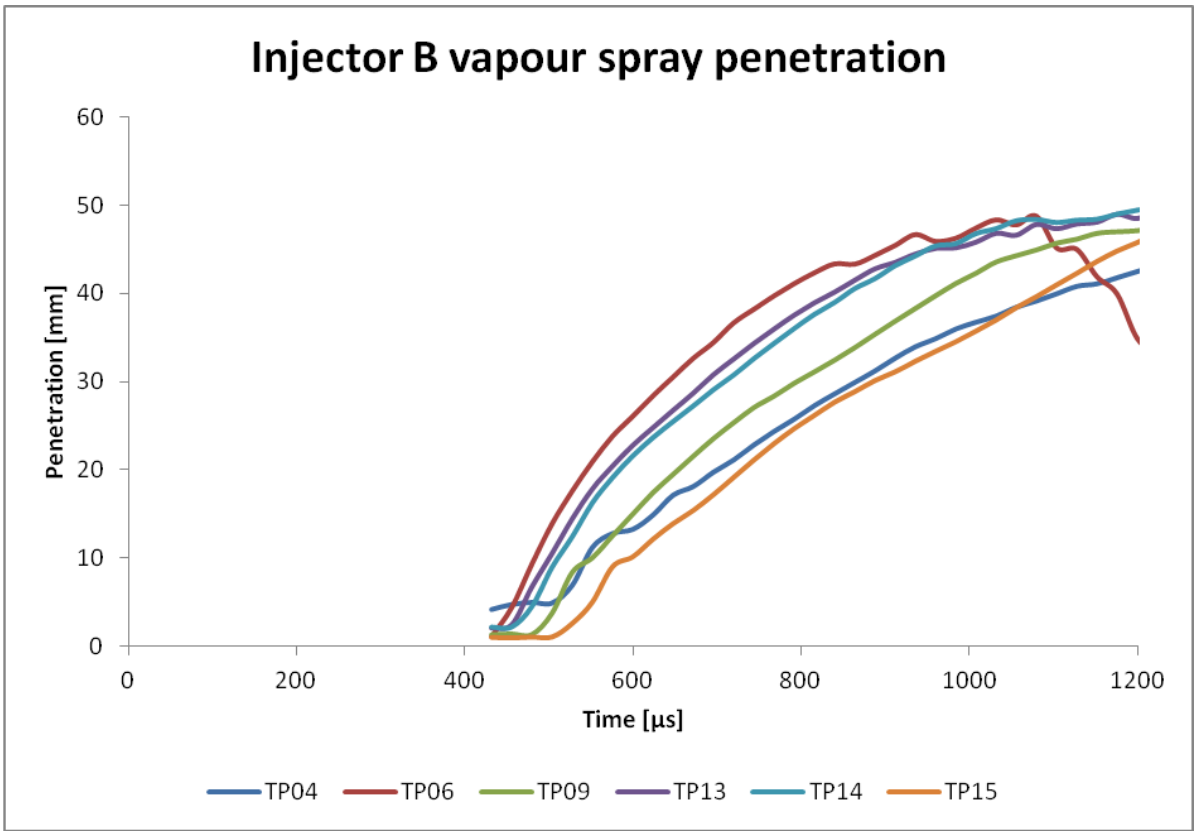
Injector B vapour spray penetration
Penetration [mm]
0
10
20
30
40
50
60
0
200
400
600
800
1000
1200
Time [µs]
TP04
TP06
TP09
TP13
TP14
TP15

Injector C

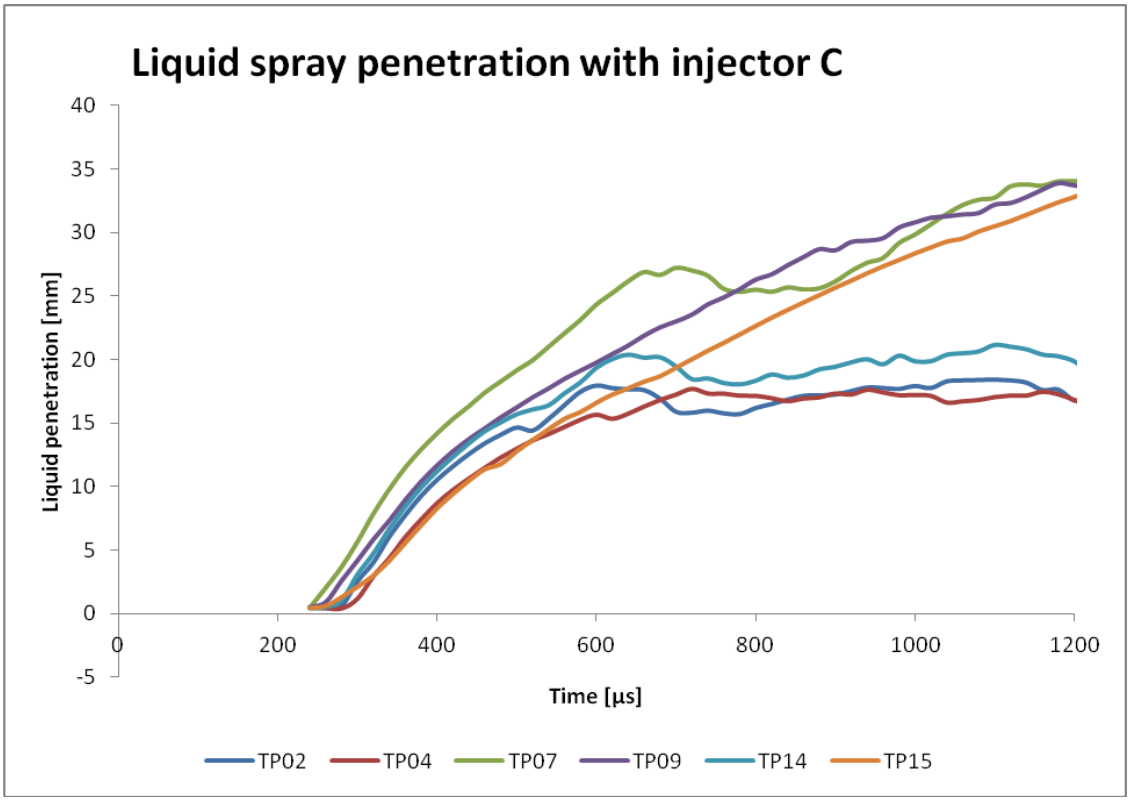
Liquid spray penetration with injector C
Liquid penetration [mm]
40
35
30
25
20
15
10
5
0
-5
0
200
400
600
800
1000
1200
Time [µs]
TP02
TP04
TP07
TP09
TP14
TP15

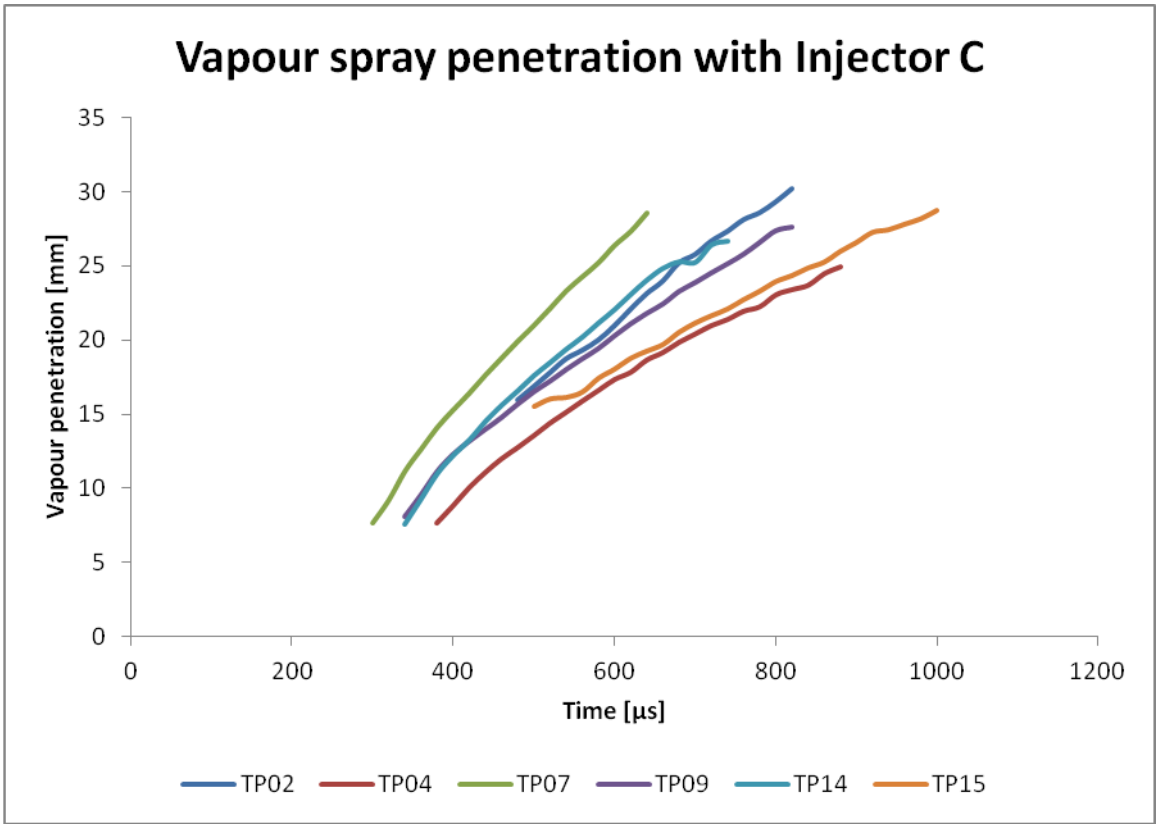
Vapour spray penetration with Injector C
Vapour penetration [mm]
35
30
25
20
15
10
5
0
0
200
400
600
800
1000
1200
Time [µs]
TP02
TP04
TP07
TP09
TP14
TP15

Injector D

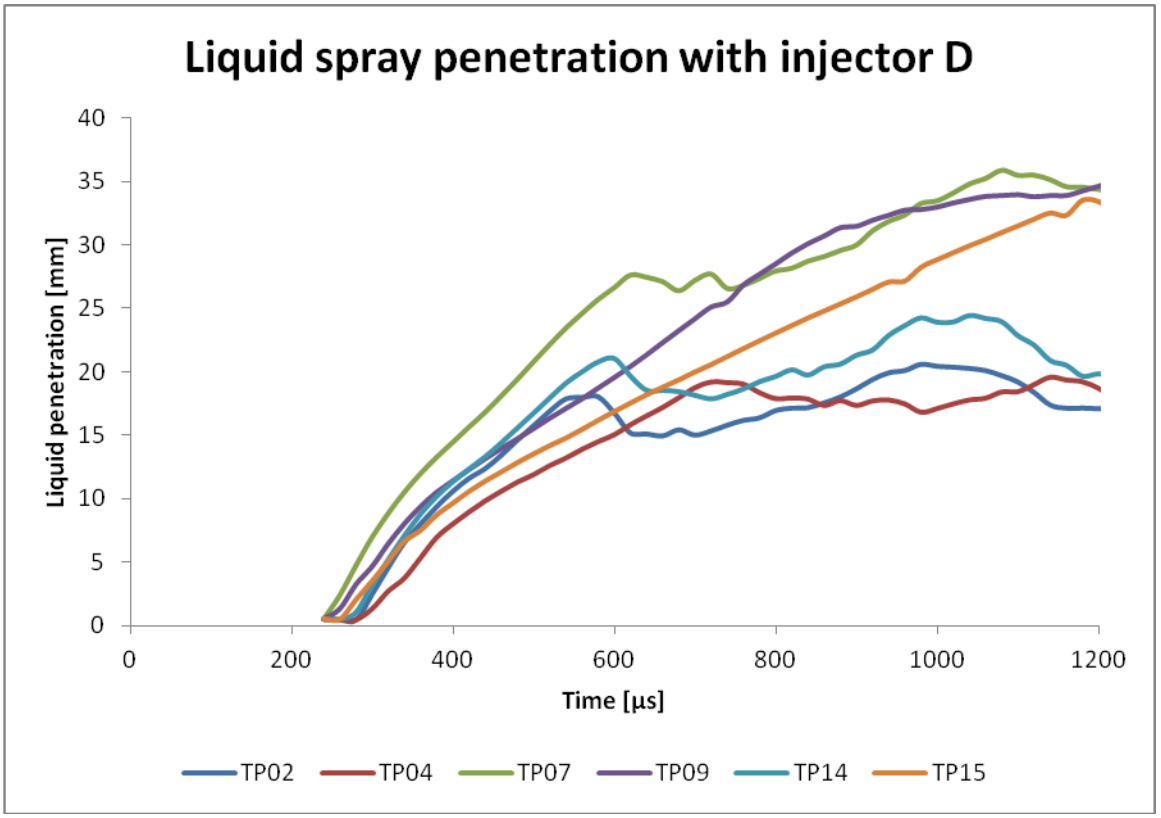
Liquid spray penetration with injector D
Liquid penetration [mm]
0
5
10
15
20
25
30
35
40
0
200
400
600
800
1000
1200
Time [µs]
TP02
TP04
TP07
TP09
TP14
TP15

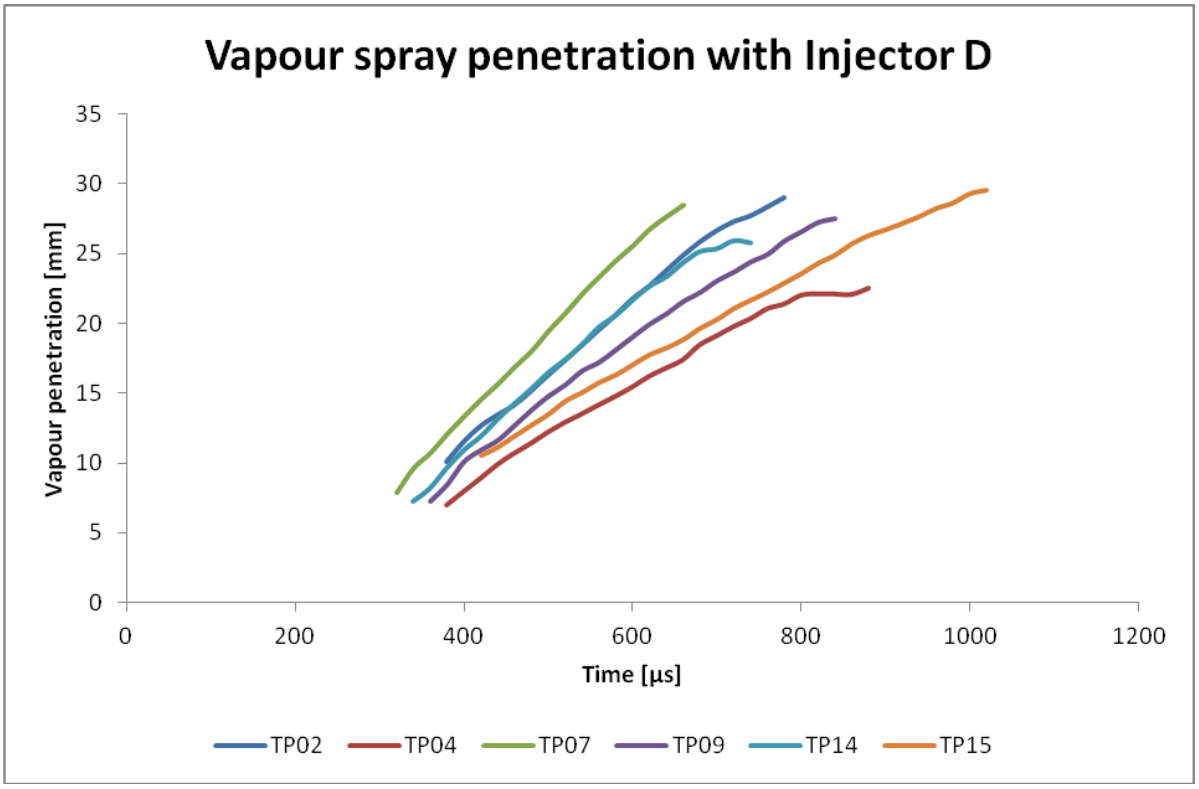
Vapour spray penetration with Injector D
Vapour penetration [mm]
0
5
10
15
20
25
30
35
0
200
400
600
800
1000
1200
Time [µs]
TP02
TP04
TP07
TP09
TP14
TP15

Appendix G: Uncertainty analysis for spray penetration

A sample calculation illustrating how the measurement uncertainty of spray penetration was determined can be found in this section. The measured diesel fuel spray penetration achieved with Injector A under TP06 conditions is presented in the table below.

Time [μs]	Penetration [mm]	% Uncertainty
431.99	3.5	2.38
456	7.09	1.18
479.99	8.87	0.94
504	10.87	0.77
551.99	15.04	0.55
576	17.79	0.47
600	20.51	0.41
623.98	22.36	0.37
647.99	23.47	0.36

The measurement of spray penetration was inaccurate by ±1 pixel. One pixel was found to be equal to 0.08335mm, using the scale factors for Injector A. The degree of uncertainty was then determined as follows

$$\% \text{ Uncertainty} = \frac{uncertainty}{measured\ penetration} \times 100$$

For the penetration at t= 431.99 μs and t= 551.99 μs :

$$\% \text{ Uncertainty} = \frac{0.08335}{3.5} \times 100 = 2.38\ \%$$

$$\% \text{ Uncertainty} = \frac{0.08335}{15.04} \times 100 = 0.55\%$$